Photochimie du bâti : sources et puits de polluants oxydants (Acronyme: photoBAT)

RECAPITULATIF DU PROJET

Titre du projet: Photochimie du bâti : sources et puits de polluants oxydants (Acronyme: photoBAT)

Thème de l'APR: Thème I – Traceurs et parts attribuables

Responsable scientifique :

Christian GEORGE
IRCELYON
Institut de Recherches sur la Catalyse et l'Environnement de Lyon
UMR 5256 CNRS/Université Lyon1
2, avenue Albert Einstein
F-69626 Villeurbanne Cedex
Tel: (33) (0)4 72 43 14 89
Fax: (33) (0)4 72 44 84 38
e-mail: Christian.George@ircelyon.univ-lyon1.fr
http://www.ircelyon.univ-lyon1.fr/

Equipes impliquées dans le projet

DOUSSIN Jean-François
Laboratoire Interuniversitaire des Systèmes Atmosphériques (LISA)
Universités Paris 7 et 12, CNRS (UMR 75 83)
61 av. du Général de Gaulle
94010 CRETEIL cedex
Tel : 01 45 17 15 86
Fax : 01 45 17 15 64
e-mail : doussin@lisa.univ-paris12.fr

MELLOUKI Abdelwahid
ICARE (Institut de Combustion, Aérothermique, Réactivité et Environnement)
CNRS (Centre National de la Recherche Scientifique) - UPR3021
1C, Avenue de la recherche scientifique
45071 Orléans Cedex 02 - FRANCE
Tel: (33) 238 25 76 12
Fax: (33) 238 69 60 04
e-mail : mellouki@cnrs-orleans.fr

Mots Clés: ozone, pic de pollution, sources de radicaux, acide nitreux, mur anti-pollution,

Durée du projet: 24 mois

Photochimie du bâti : sources et puits de polluants oxydants (Acronyme: photoBAT)

Rapport scientifique

Avant propos.

Conformément à la convention signée, ce rapport présente l'ensemble des résultats scientifiques obtenus et est rédigé en anglais, utilisant les tirés à part de publications.

I. Introduction 3
II. Experimental 6
II.a Mineral oxides: Preparation and characterization 6
II.b Minerals for Chamber studies (ICARE and LISA) 6
II.c Experimental set-up 6
II.c.1 Flow Reactor 6
II.c.2 Uptake coefficient 9
II.c.3 CESAM chamber (LISA) 9
II.c.4 Outdoor smog chamber with natural irradiation (ICARE) 11
iii. Results 12
III.1 Nitrogen Oxides 12
III.2 Formaldehyde 17
III.3 0zone formation on titanium dioxide coated glasses 22
III.4 the influence of TiO_2 coating on the chemistry of propene/NO_x/light system under atmospheric conditions 24
IV. CONCLUSIONS 29
VI. References 29
VI. Annex : reprint of published papers 32

Photochimie du bâti : sources et puits de polluants oxydants
(Acronyme: photoBAT)

I. INTRODUCTION

Clean air is essential for people's health and for the quality of the environment. However, since the industrial revolution, the quality of the air that people breathe has deteriorated considerably - mainly as a result of human activities. Rising industrial and energy production, the burning of fossil fuels and the dramatic increase in traffic contribute to air pollution in our towns and cities which, in turn, can lead to serious health problems. For example, air pollution is increasingly being cited as the main cause of lung sickness such as asthma - twice as many people suffer from asthma today compared to 20 years ago.

Air pollution originating from traffic is an important problem in most urban areas. Nitrogen oxides (NO_x), volatile organic compounds (VOCs) and particulate matter (PM) are some of these pollutants. Not only there are strong associations between ambient air pollution levels and adverse health effects[1] but also their transformation within the atmosphere leads to photochemical air pollution.[2] As a result, several regulations have been implemented to reduce emissions from vehicles and also a new approach has been applied in recent years by considering the use of self-cleaning and de-polluting materials to remove these pollutants.

The need to deliver cleaner air has been recognised for several decades with action having been taken at national and EU levels and also through active participation in international conventions. EU action has focused on establishing minimum quality standards for ambient air and tackling the problems of acid rain and ground level ozone. Polluting emissions from large combustion plants and mobile sources have been reduced; fuel quality improved and environmental protection requirements integrated into the transport and energy sectors.

Despite significant improvement, serious air pollution problems remain. Against this backdrop, the Community's Sixth Environmental Action Programme (6th EAP) called for the development of a thematic strategy on air pollution with the objective to attain "levels of air quality that do not give rise to significant negative impacts on, and risks to human health and the environment". Following its communication on the Clean Air For Europe programme (CAFE), the Commission has examined whether current legislation is sufficient to achieve the 6th EAP objectives by 2020. This analysis looked at future emissions and impacts on health and the environment and has used the best available scientific and health knowledge. This analysis showed that significant negative impacts will persist even with an effective implementation of current legislation.

Among the new technical "solutions" designed for large dissemination over the public space, new building and coating materials are being widely proposed to stakeholders as well as public consumers.

Titanium oxide, TiO_2, has become the material of choice in a variety of remediation processes due to its photocatalytic properties[3, 4] and its favourable physical and chemical properties.[3] Besides, it is chemically inert in the dark, not expensive, non toxic and of easy handling. The self-cleaning properties of TiO_2 are ruled by the absorption of band gap light and the production of excited-state conduction-band electrons and valence-band holes, which can react with electron acceptors and electron donors adsorbed on the semiconductor surface.[4] The environmental relevance of TiO_2 is usually related to its overall capacity to deplete organic pollutants from aqueous and gaseous media. Many studies have recently focused on the development of environmental friendly materials by adding TiO_2 to ordinary building materials such as concrete or by preparing TiO_2 film coatings[5-9]. Although various photocatalytic materials are already on the market, very little reliable information is available, except for limited technical data, regarding their impact on air quality considering the potential formation of harmful chemical intermediates. This scenario motivates further studies on the field.[8]

Different works were focused on achieving the removal of NO_x from air by means of de-polluting surfaces containing TiO_2[5,9-22]. However, recent studies showed that UV-illuminated surfaces of pure TiO_2 aerosols can reduce NO_2 to HONO, together with the production of H_2O_2.[23,24] Besides the important impact of nitrous acid (HONO) as a free radical source in the atmosphere,[25] there are several mechanisms by which HONO may be harmful for health. Firstly, HONO is an

acid, which may damage mucous membranes and surfaces of the respiratory tract. Secondly, in the reaction of HONO with amino groups of the nucleotides, the double helix of the DNA can be cross-linked[26-30] leading to mutagenic properties. In addition, in the reaction of HONO with amines, both in the atmosphere but also in-vivo, nitrosamines are formed[31-34] which show carcinogenic and mutagenic properties.[35,36] Langridge *et al.* have recently reported the formation of nitrous acid on a self-cleaning window glass coated by TiO_2.[37] As well, the photo-enhanced NO_2 uptake for real mineral dusts with HONO production was assigned to the chemistry occurring on the TiO_2.[38,39] In this process, nitrate anions are formed as a consequence of the photocatalytic oxidation of NO_2 on UV-illuminated TiO_2 surfaces.[14,23,40-43] Most of these studies argue that nitrate is the innocuous final product of the photocatalytic NO_x removal process. However, the photochemistry of nitrate doped mineral dust samples containing TiO_2 was proved to be a potential renoxification process of the atmosphere.[44] As well, the photochemistry of adsorbed nitrate on aluminium oxide has been proved to give different yields of NO, NO_2 and N_2O according to the presence of water and molecular oxygen.[45,46]

Formaldehyde (HCHO) is an important and highly reactive compound present in all regions of the atmosphere, arising from the oxidation of biogenic and anthropogenic hydrocarbons. HCHO is a key compound in tropospheric chemistry. It is a strong HO_x source (through its photolysis) and is therefore strongly connected to regional O_3 production. The main HCHO removal processes from the atmosphere are currently thought to be its photolysis and the reaction with OH according to [47]:

$$HCHO + h\nu \longrightarrow H_2 + CO \qquad (\lambda < 360\ nm) \qquad (1a)$$

$$HCHO + h\nu \longrightarrow H^{\cdot} + HCO \qquad (\lambda < 325\ nm) \qquad (1b)$$

$$HCHO + OH^{\cdot} \xrightarrow{O_2} HO_2^{\cdot} + H_2O + CO \qquad (2)$$

These removal processes are homogeneous and will happen throughout the troposphere. However, it is known that HCHO is chemically taken up, in the atmosphere, by sulphuric acid aerosols [48]. Therefore, one may question if similar heterogeneous reactions may occur on other surfaces such as mineral surfaces or buildings.

In this project, we studied the efficiency of these photocatalytic materials for air pollution reduction in the urban environment. In the very recent years, photo-catalytic self-cleaning and “de-polluting” materials have been suggested as a remediation technology mainly for NO_x and aromatic VOCs in the polluted urban environment. The associated technologies have been launched on the European market with the aim to have a positive impact on urban air quality. These commercial products are based on the photo-catalytic properties of a thin layer of TiO_2 deposited at the surface of the material (such as glass, pavement, …) or embedded in paints or concrete. The use of TiO_2 photocatalysts as an emerging air pollution control technology has been reported in many European areas. However, it seems that both the effectiveness and the real impact on air quality of these relatively new technologies up to now have been demonstrated only in a very limited manner before going into the European market.

Assessing the effectiveness of these depolluting techniques have a real added value both in terms of policy making (and implementing the EU air quality strategy) and economics (by providing a demonstration of the actual performance of a new technique).

This project aims at evaluating the feasibility of using TiO_2 based products to alleviate the air pollution problem under real atmospheric conditions.

We studied the degradation of nitrogen dioxide and formaldehyde, both key players in urban air pollution, on different substrates containing TiO_2 using dedicated flowtube techniques and atmospheric simulation chambers.

In the next sections we will describe these experimental layouts and show that:

- Nitrogen oxides are efficiently degraded on these photocatalytic surfaces
- Nitrous acid is produced in variable yields, depending on many parameters including surface pH (HONO release may be observed from alkaline surfaces such as cement based products)

The reactivity of NO_2 on irradiated TiO_2 / SiO_2 films was studied, with different TiO_2 contents, as proxies for NO_x de-polluting materials. The influence of the photocatalyst concentration, the role of molecular oxygen and the effect of nitrate

on the reactivity of TiO_2 films were investigated. NO, HONO and nitrate anions are produced as a consequence of the NO_2 loss on UV-illuminated TiO_2 films. A renoxification pathway that involves the photochemistry of the NO_3 radical leads to the release of NO, NO_2 and of HONO from the TiO_2 surface. The presence of O_2 in the carrier gas modifies the NO and HONO production yields in the heterogeneous reaction between NO_2 and TiO_2 as well as the products of the renoxification process.

- Formaldehyde is also efficiently degraded on these photocatalytic surfaces.

  The kinetics of the heterogeneous reaction between gaseous HCHO and TiO_2/SiO_2 mineral coatings have been investigated to mimic HCHO loss on TiO_2 coated depolluting urban surfaces, by means of flow tube studies. The measured uptake kinetics were observed to be strongly enhanced when the surface (or coating) was irradiated in the wavelength range from 340 to 420 nm (with an irradiance of 1.45 mW cm^{-2}). The associated BET uptake coefficient were measured in the range from $(3.00 \pm 0.45) \times 10^{-9}$ to $(2.26 \pm 0.34) \times 10^{-6}$ and were strongly dependent on the HCHO initial concentration in the range 3.5 - 32.5 ppbv, relative humidity from 6 to 70%, temperature from 278 to 303 K and TiO_2 content in the mineral coating from 1 to 100% wt. The measured kinetic was well described using a Langmuir-Hinshelwood type formalism. The estimated uptake coefficients were used to discuss the importance of the heterogeneous HCHO surface loss, in terms of deposition lifetimes, as compared to major homogeneous gas phase losses (OH reaction and photolysis). It is found that deposition may compete with gas phase removal of HCHO in a dense urban environment if more than 10% of urban surface is covered with TiO_2 treated materials.

- TiO_2 coating of urban surfaces may significantly affect the smog production chemical cycles

  The atmospheric degradation of propene in the presence of NOx has been investigated under atmospheric conditions in the presence and absence of materials that contain TiO_2. The experiments have been conducted in different types of atmospheric simulation chambers using lamps and sun as the light sources (indoor and outdoor). The data obtained show that the presence of the TiO_2-doped materials used in this work does have an impact on the chemical processes occurring during the oxidation of propene under atmospheric conditions. Comparison between the concentration profiles of the chemical species (C_3H_6, NO, NO_2 and O_3) versus photolysis time in the presence and absence of the TiO_2 containing materials show that the consumption of propene is enhanced in the presence of TiO_2 with a larger consumption after a time delay. The enhancement seems to occur once the NO_2 maximum concentration is observed. The obtained results are discussed in terms of the possible atmospheric impact of these chemical processes on air quality.

II. EXPERIMENTAL

II.a Mineral oxides: Preparation and characterization

Experiments were performed with different mass mixing ratios of mineral oxides, in the range from 1 to 100 wt%, by diluting titanium dioxide TiO_2 (Degussa-P25, 80% anatase, 20% rutile; P25) in silica SiO_2 (Degussa Aerosil 130). All mixtures were prepared by suspending a total 3 g in 30 mL of ultra pure water (Aquadem milli-Q50). A few milliliters of these sonicated suspensions were dripped uniformly into dried Pyrex tubes (20 cm × 1.1 cm i.d) used as insert for the kinetic measurements (see below), rotated and dried at 373 K. The resulting film covered the entire inner surface of the tube and, to the eye, was fairly uniform in thickness.

However, the knowledge of the film morphology is of great importance for interpreting gas uptake processes. Therefore, scanning electron microscopy (SEM) coupled to Energy Dispersive X-ray spectroscopy (EDX) was used for the characterization of the dried film. For this purpose, the Pyrex inserts were cut in 1 cm long samples (considering finally only both ends and middle parts of the tube), dipped vertically into a mould holding an epoxy resin (araldite epoxy CY 230-ESCIL) and an epoxy resin hardener (HY 956-ESCIL) in a ratio (resin/hardener) equal to 2.5. After 12 hours, the mixture dried and hardened, was forming a polymer at room temperature. The polymer section (holding the tubes inserts) was then polished (ESC 200 GTL polisher from ESCIL) for a better image resolution. Finally, these SEM samples were coated with a thin layer of gold to enable electrons conduction to the observed area. Films at different TiO_2 mixing ratios (1, 5, 50 and 100% wt) have been observed. In addition, the analysis of different zones confirmed the uniformity of the film all along the tube for each sample. Films thickness ranged from 20 to 30 µm. Figure 1 displays both the SEM image of a TiO_2/SiO_2 coating (50wt %) (Part a) and the surface profile of an area scanned from 0 (the Pyrex surface) to 40 µm (polymer matrix) (Part b). It is clear that the film sticks strongly to the Pyrex surface, fitting with any surface defect (see Figure 1.a). Besides, the EDX detection of the yellow line scanned in Figure 1.a corroborates with the film's chemical composition. Indeed, when the probe scanning runs from the Pyrex surface to the polymer matrix, two successive silicon peaks appear. They can be ascribed to the Pyrex composition (higher peak) and to the coating (lower peak). As expected, the titanium peak appears at 11 µm probe scanning and extends on 24 µm (i.e. the film thickness). It reaches the concentration of the lower silicon peak since both TiO_2 and SiO_2 are equally distributed in the film (TiO_2 50%wt / SiO_2 50%wt coating). Note that the Ti and Si concentrations are estimated to 15% wt of the coating as the gold deposited at the SEM sample is also detected. The cartography of another 50%wt TiO_2 sample scanned from the Pyrex glass tube (right) to the film (left) (shown with a 4000 magnification in Figure 1c) proves that the Ti and Si atoms are equally and homogeneously distributed in a 50% TiO_2 film.

II.b Minerals for Chamber studies (ICARE and LISA)

The non treated glass is a standard window glass while the treated glass is a Pilkington™ Activ© self cleaning glass. As comparison of results obtained from complementary chambers as the basis of our strategy, all samples used among the consortium were from the same type and producer. Moreover, experiments were conducted using glass from the same production lot. The conditioning procedure was homogenized among partners consisting in a washing procedure based in a full rinsing with ultra pure water.

II.c Experimental set-up

II.c.1 Flow Reactor

The uptake experiments were conducted in a horizontal cylindrical coated-wall flow tube reactor made of Pyrex. The Pyrex tube containing the TiO_2/SiO_2 film was placed in the reactor, which was surrounded by 3 fluorescent lamps (OSRAM Sylvania TLD15W/08) having a continuous emission in the 340–420 nm range with a total irradiance of 1.5×10^{15} photons cm^2 s^{-1}. NO_2 was introduced in

the flow tube by means of a movable injector with radius 0.3 cm. Synthetic air as well as pure nitrogen were used as carrier gases with a total flow rate of 200 sccm in the flow tube reactor, ensuring a laminar regime. The NO_2 and NO concentrations were measured at the reactor exit as a function of the injector position along the tube. This position determined the exposure time of the film surface towards the gas. A THERMO 42C chemiluminescent analyzer was used for NO and NO_2 detection. The latter is based on the reaction between NO and O_3, which produces a characteristic luminescence with an intensity that is linearly proportional to the NO concentration. NO_2 is transformed into NO by means of a molybdenum converter in order to be measured with the chemiluminescent reaction. As HONO is detected by the same instrument as NO_2, a denuder tube (9 cm × 0.95 cm i.d.) containing a mixture of K_2CO_3 / Na_2CO_3 (Fluka) was introduced between the exit of the flow cell reactor and the detector. The denuder was either bypassed, leading to the detection of NO and NO_2 together with HONO; or it was switched into the sample line along the experiment, so that only NO and NO_2 species were measured after HONO removal from the gas stream. Therefore, HONO concentration was obtained as the difference of the detector signal without and with the carbonate denuder in the sampling line.[49]

Gas phase NO_2 concentration used in the experiments was fixed in 150 ppbv (3.8×10^{12} molec cm^{-3}). The experiments were conducted at 298 ± 1 K by circulating temperature-controlled water through the outer jacket of the flow tube reactor and were performed under atmospheric pressure and 30% of relative humidity. The temperature of the gas streams and the humidity were measured by using an SP UFT75 sensor (Partners BV). All gases were taken directly from cylinders without further purification prior to use. High purity synthetic air (99.999%), N_2 (99.0%) and NO_2 (1 ppmv in N_2; 99.0%) were purchased from Air Liquide. The gas flows were monitored before entering the reactor by mass flow controllers (Brooks).

Periodical calibrations of the NO_2 from the cylinder were performed using the carbonate denuder. Only 3% of the total NO_2 (and possible contaminants) was trapped in the denuder, this value was then considered in the calculation of the uptake coefficients and products yield.

NO_2 may photodissociate with unit quantum yield in the wavelength region emitted by the lamps (300-420nm), but its loss in the gas phase is negligible for the residence time of 6 seconds used in our experiments. An estimation of the photolysis rate constant, $J = 6.52 \times 10^{-4}$ s^{-1} gives rise to a loss of 0.4% of the total NO_2 (g). Control experiments were performed to confirm the chemical inactivity of the Pyrex flow tube surfaces, and to evaluate the contribution of NO_2 photolysis. The empty tube (with no film) was filled with NO_2 and exposed to light. NO_2 photodissociation and loss at the Pyrex surface were negligible (below 3% of the total NO_2 loss) in comparison to the NO_2 loss observed in the presence of the TiO_2 / SiO_2 film.

Gaseous formaldehyde was swept out from the reactor with Nitrogen from a home-made silicon permeation tube immerged in a 3.7 wt% HCHO solution at 298 K. The resulting gas mixtures were monitored at the reactor outlet with a portable HCHO analyzer fully developed at IRCELYON [50]. The relative humidity released from this permeation source of HCHO is ca. 6%.
Formaldehyde is stripped out of the gas flow via a glass tube sampler, followed by a derivatization with 3-methyl-2-benzothiazolinone hydrazone (MBTH) in two successive steps in order to form a strongly absorbing chromophore [51]. The detection, in solution, of the converted HCHO was realized by means of a combination of a spectrograph (Andor technology / Shamrock SR - 163 i) coupled to a CCD camera (Andor Technology / iDus DV-420). Teflon AF2400 tubing (Biogeneral) were used as UV-visible long path cell [52]. Combining the strongly absorbing chromophore with a 100 cm long optical path led to a detection limit of ca. 3 pptv with 15 to 30 minutes resolution time depending on the first step conversion time. These formaldehyde measurements were validated against optical and chromatographic methods. Calibrations with Differential Optical Absorption Spectroscopy (DOAS) and Fourier Transformer Infrared spectroscopy (FTIR) showed less than 6% deviation. Similar results were obtained comparing to HCHO measurements by means of liquid chromatography coupled to UV-DAD detection subsequent to DNPH titration whether with Sepack cartridges [53] or with Radiello passive tubes trapping techniques [54].

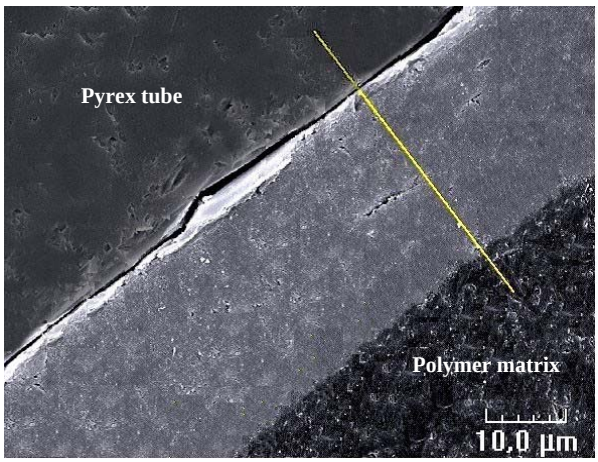

(a)

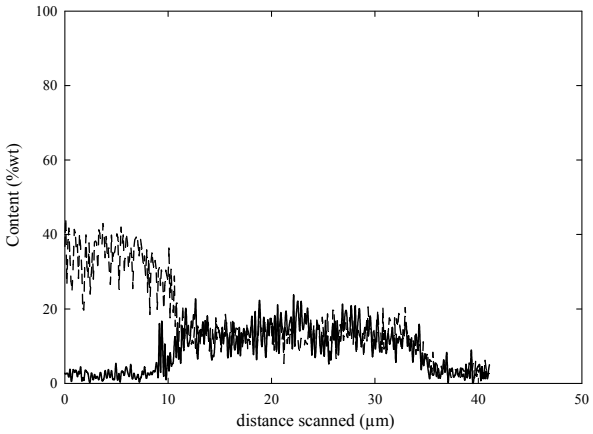

(b)

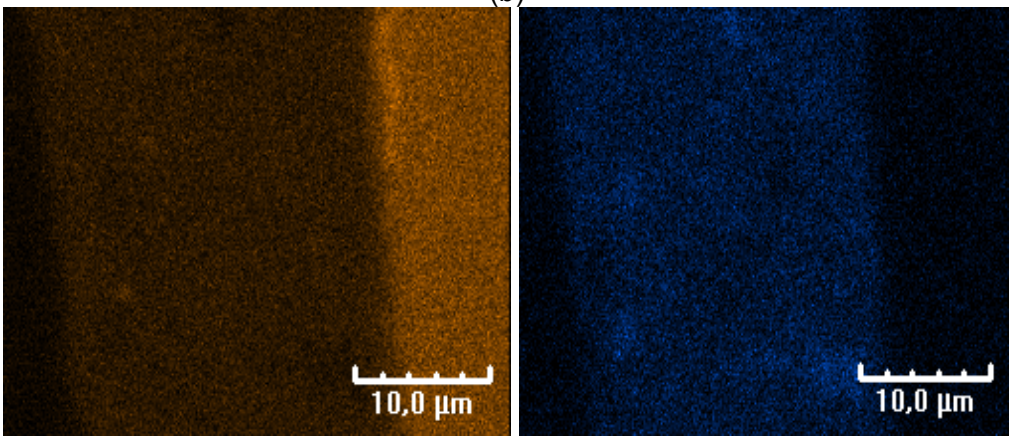

(c)

Figure 1: (a) SEM image showing the interface of 50%wt TiO_2 / SiO_2 coating, (b) Surface profile of the yellow line scanned in part (a) displaying Ti (full line) and Si (dashed-line) concentrations (c) Cartography of another 50%wt TiO_2 coating showing Ti (blue) and Si (yellow) distribution in the film.

II.c.2 Uptake coefficient

The kinetic behaviour of the heterogeneous reaction between NO_2 and TiO_2/SiO_2 films under irradiation can be well described by assuming a pseudo first-order reaction with respect to the gas-phase NO_2 concentration. The derived first-order rate constant, k_{obs}, is related to the geometric uptake coefficient (γ_g) by:

$$\frac{d}{dt}\ln\frac{C_0}{C_i} = k_{obs} = \frac{\gamma_g < c_{NO_2} >}{2r_{tube}} \quad (3)$$

where r_{tube}, γ_g, t, and $< c_{NO_2} >$ are the flow-tube radius (0.547 cm), the geometric uptake coefficient, the exposure time, and the NO_2 average molecular velocity, respectively. C_0 is the NO_2 concentration when there is no contact between the film and the reagent; whereas C_i is the trace gas concentration when the contact with NO_2 is allowed. The uptake coefficient is defined as the fraction of effective collisions between a gas phase reagent and a reactive surface that lead to the loss of the gas phase reagent due to chemical reaction. γ_g is a mass dependent parameter for these substrates as diffusions and reaction of the trace gas take place at the internal surface of the films.[41] For that reason, a mass-independent uptake was derived by taking into account the entire BET surface area of the TiO_2 / SiO_2 films[38,55].

Equation (3) does not contemplate possible diffusion limitations caused by the formation of a radial concentration gradient in the gas phase, which would occur if the loss at the surface is too fast to be recovered with the reagent supply. As a consequence, the uptake coefficient was calculated by using the Cooney-Kim-Davis (CKD) method[56], which takes into account axial and lateral diffusion combined with a first order loss at the inner surface of a cylindrical tube under laminar flow conditions. An implementation of this method has been previously used.[57] The diffusion coefficient D was calculated using the formula proposed by Fuller *et al.*[58]

II.c.3 CESAM chamber (LISA)

The experiments were carried out using a new Multiphase Atmospheric Experimental Simulation Chamber (CESAM, Figure 2) which has been constructed at LISA laboratory .[59] It consists of a 4.2 m^3 stainless steel vessel which can be roughly described as a vertical cylinder in which 6 glass plates (120 cm × 40 cm) are vertically hung offering a geometrical surface of 2.88 m². A set of stainless steel magnetic torque mixing fans are installed inside the chamber reactor which allows to mix the gas phase compounds in less than 100 s. The chamber is equipped with a powerful solar simulator system which comprises 3 Xenon arc lamps of 4 kW each. This set-up provides an irradiation inside the chamber very close to the sun spectrum at the ground level (Figure 3). The lamps are symmetrically located above the chamber on a rigid framework. By optimizing the focal point of the light beam, it is possible to obtain a converging or diverging light beam with a maximum intensity inside the reactor; meanwhile the light spots projected at bottom level are as large as possible for minimizing the local overheating effects.

The photolysis frequency of NO_2 may vary in CESAM chamber by several physical parameters, such as the modifications of the Xenon lamps position and the irradiation sources aging. J_{NO2} is thereby quantified periodically in the chamber before carrying out any experiment. For this study, J_{NO2} was determined directly by measuring the actinic flux in the chamber (using a spectroradiometer LICOR LI1800) and indirectly by simulating the NO_x/air/light chemical system during dedicated experiments[60-61]. The chemical actinometry determination of J_{NO2} in CESAM chamber is described in detail by Wang et al., 2010. J_{NO2} can be calculated experimentally by considering the equation arising from the photostationary state hypothesis[62],

$$J_{NO2} = k_{(NO+O3)}[NO][O_3]/[NO_2]$$

or determined by adjusting the observation curves and the numeric models (Wang, J.; Doussin, J. F. et al., 2010). The obtained values for J_{NO2} and $J_{O(1D)}$ were respectively found equal to $(3.5\pm0.5)\times10^{-3}$ s^{-1} and $(1.2\pm0.2)\times10^{-5}$ s^{-1} in CESAM which is roughly one third of those measured in the boundary layer on a sunny day at mid latitude, in June at noon.

The chamber was evacuated to 10^{-4} mbar before each experiment. Synthetic air was produced from the mixture of ca. 200 mbar of O_2 (AIRLIQUIDE, ALPHAGAZ™ class 1) and ca. 800 mbar of N_2 produced from the evaporation of a pressurized liquid N_2 tank. NO was purchased from

AIRLIQUIDE (ALPHAGAZ™ purity Class 2 UN1956). Experiments were carried out at atmospheric pressure and a temperature of 293±2 K.
The simulation chamber is equipped with in-situ long path FITR system (192 m) and with environmental analyzer. A Horiba™ APOA® 370 monitor was used for O_3 detection by means of a cross flow modulated ultraviolet absorption method while NOx measurements were performed using a Horiba™ APNA® chemiluminescence monitor. Nitrous acid was quantified using the NitroMac instrument[63] with a detection limit of 3 ppt for a time period of 10 minutes. Several experiments were performed in the absence of glass, in the presence of non treated surfaces and with TiO_2 treated surfaces inside the chamber. NO initial concentration ranged from 20 to 100 ppb and relative humidity was varied from 0 to 40%.

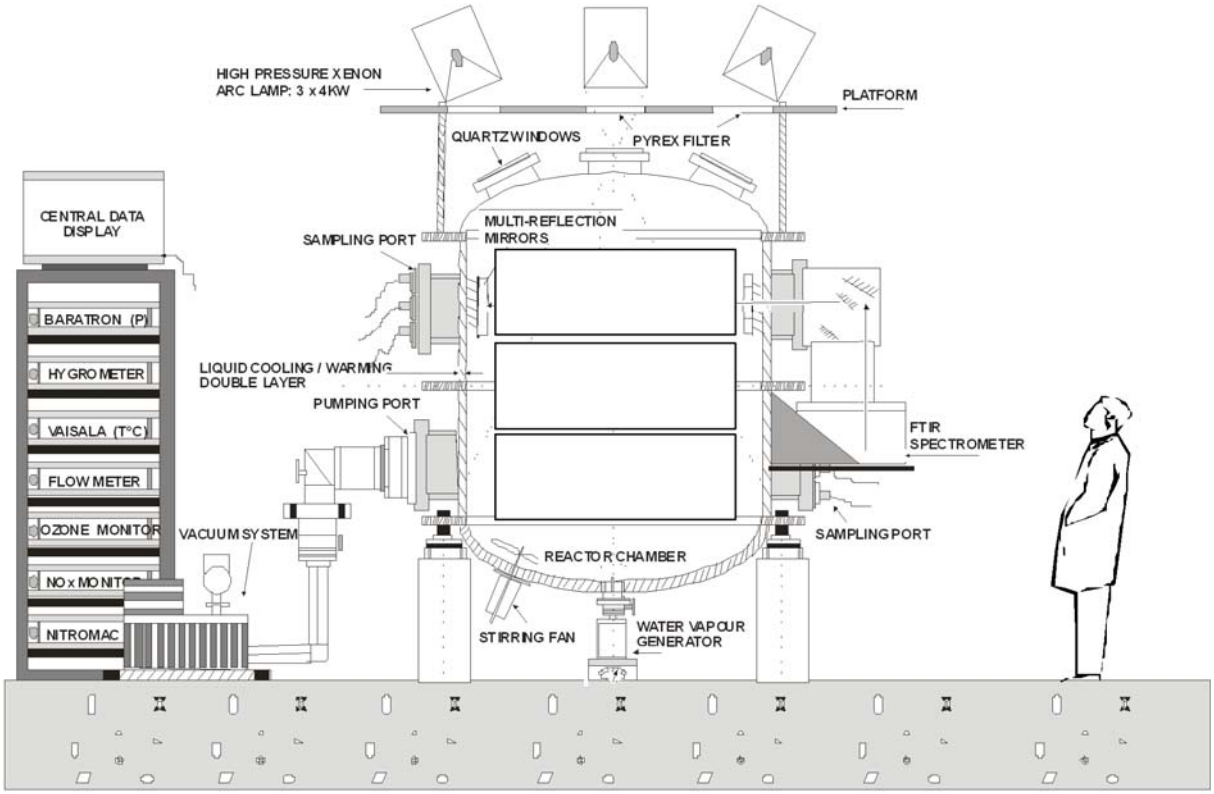

Figure 2. Scheme of the CESAM reactor. The three rectangles in bold represent the 6 plates of material set back to back in the chamber.

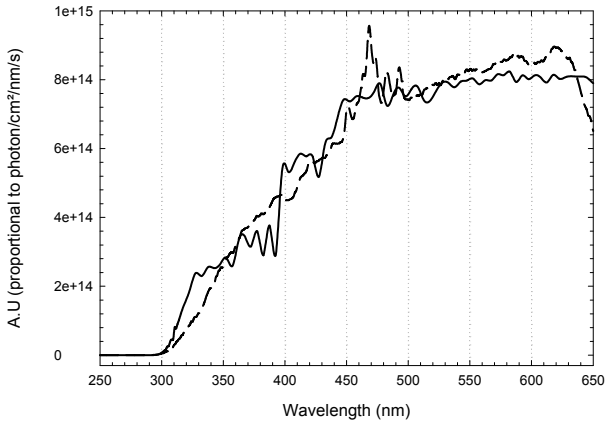

Figure 3 Comparison of irradiation spectra. The thin black curve is the solar spectrum calculated from TUV NCAR, 12h, 45°N, 21 June. The dashed line curve is the spectra taken from inside the chamber with a Li1800 LiCOR spectroradiometer.

II.c.4 Outdoor smog chamber with natural irradiation (ICARE)

The newly built Teflon chamber of 3.4 m^3 volume (Figure S4) was installed on the roof of the laboratory (ICARE – Orléans) for natural irradiation exposure. The chemical analysis were performed using commercial monitors (O_3, NO, NO_2 and NO_x). The physical parameters (pressure, temperature, relative humidity, light intensity (J_{NO2})) were continuously monitored using specific captors. In particular, J_{NO2} was continuously measured using a 4 pi-sr J_{NO2} filter radiometer (from meteorology consult Gmbh) positioned inside the chamber. J_{NO2} typical values were in the range $(0.5\text{-}1)\times10^{-2}$ s^{-1}. The ratio $k_{(NO+O3)}$ $[O_3][NO]$ / J_{NO2} $[NO_2]$ was calculated using J values and NO, NO_2 and O_3 concentrations. For experiments conducted in absence of TiO_2 coated glass the ratio was 1, as predicted by the Leighton relationship. However, deviations from that value were observed when a TiO_2 coated glass was placed inside the chamber, indicating the occurrence of other efficient chemical processes.

A Teflon fan inside the chamber ensures the homogenisation of the gas mixture in less than 1 minute. Along the experiment, a slight air stream flowing into the chamber enables to compensate the sampling volumes and maintains a slight overpressure to prevent any possible contamination from outside air. A series of tests has been performed on the setup to ensure its reliability, such as leaks and homogenisation tests. The experiments were performed in the temperature range 293-301 K with a variation of 7 to 8 °C over the course of the runs. Several experiments were performed with the empty chamber, with non treated glass surfaces inside the chamber and in the presence of glass surfaces treated with TiO_2. The relative humidity was maintained below 5%.

Figure 4. Picture of the ICARE outdoor chamber used in this work.

III. RESULTS

III.1 Nitrogen Oxides

Figure 5 illustrates the behaviour of TiO_2 (10%) / SiO_2 films exposed to a continuous flow of 150 ppbv of NO_2 in the dark and under irradiation for a fixed length of the flow tube. Figures 1a and 1b show the results obtained in pure N_2 and in the mixture of O_2 and N_2, respectively.

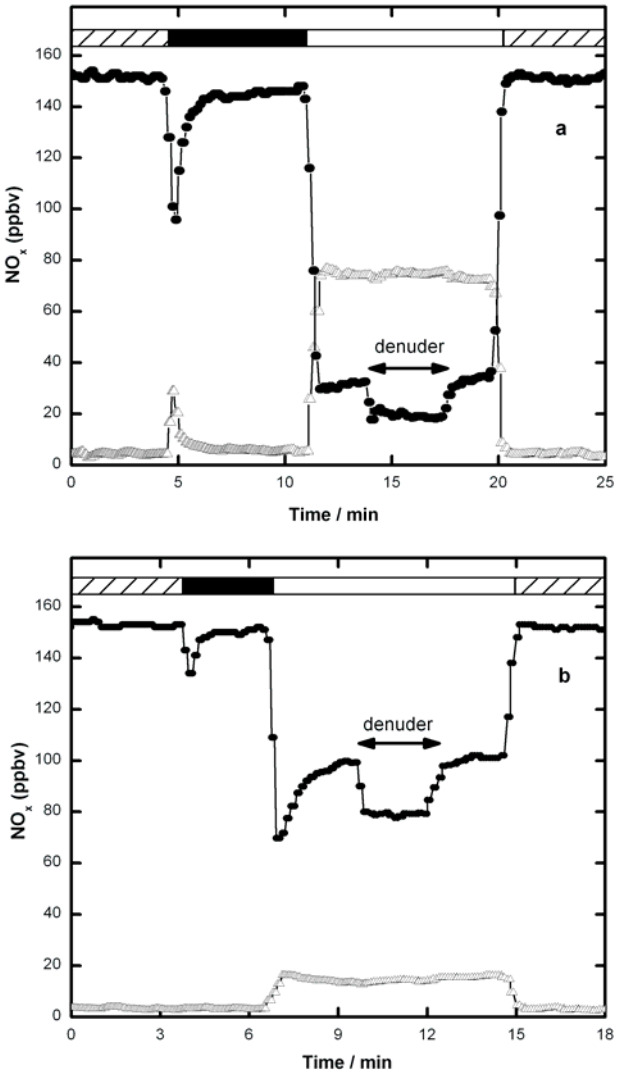

Figure 5: NO_2 loss under irradiation of a TiO_2 (10%) /SiO_2 film when (a) only N_2 was used as carrier gas, and (b) when the mixture O_2 (15%); N_2 (85%) was used as carrier gas. (●): NO_2 signal; (△): NO signal. The dashed bars correspond to the initial concentration of NO_2 which is not in contact with the film. The black and the white bars indicate the contact time between the NO_2 flow and a certain length of the film in the dark and under irradiation, respectively. The inclusion of the denuder into the sample line is indicated in the figure (see Experimental).

A NO_2 concentration of 150 ppbv was chosen for these studies because it can be found during intense photochemical pollution events in urban environments.[23,64] As well, it allowed varying the TiO_2 content from 10 to 100% (as the observed rate is slower at higher gas phase concentrations). Once a constant initial NO_2 concentration was established, the injector was withdrawn to a certain distance to expose some fraction of the film to NO_2, indicated in the top of the figure with a black bar. The NO_2 was allowed to stabilize until it reached a *plateau*, before recovering the initial concentration with time. The uptake in the dark was more important in absence of O_2 in the carrier gas for all residence times and for films with 10% and 100% of TiO_2. This behaviour may be related to the competition between NO_2 and O_2 for the adsorption sites on the film surface. When the lamps were turned on, a strong decrease of the NO_2 signal was observed (it must be remembered that without the alkaline denuder this signal corresponds to the

sum of the NO_2 and HONO species) highlighting a strong light induced uptake on these surfaces. The production of HONO was then verified under both conditions by passing the sample line through an alkaline denuder which trapped acidic species before detection. NO was produced both in absence and presence of O_2 in the carrier gas, the latter being in agreement with previous results.[43] When the lamps were turned off and the injector was moved forward to its original position, the initial NO_2 concentration was recovered. Figure 5 clearly shows that the NO_2 uptake on the samples as well as the NO and HONO formation were considerably enhanced under irradiation, both in presence and absence of molecular oxygen in the carrier gas for films with 10% wt. TiO_2. The HONO yield was higher in presence of O_2 whereas the NO formation was favoured in the absence of O_2 (see Table 1).

Table 1: Effect of the carrier on the uptake coefficients, HONO and NO yields when exposing the films towards 150 ppbv of NO_2. Errors are 2σ precision.

carrier	TiO_2 (x%)/SiO_2	γ_{BET}	HONO / %	NO / %
N_2	10	$(2.0 \pm 0.6)\times10^{-7}$	8 ± 2	50 ± 10
O_2 (15%) / N_2 (85%)	10	$(2.2 \pm 0.8)\times10^{-9}$	14 ± 4	26 ± 8
N_2	100	$(1.5 \pm 0.4)\times10^{-6}$	3 ± 1	71 ± 8
O_2 (15%) / N_2 (85%)	100	$(1.1 \pm 0.2)\times10^{-7}$	12 ± 4	-

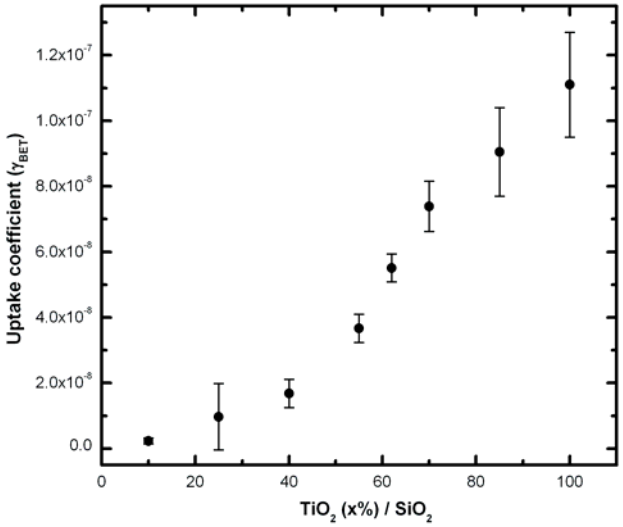

Figure 6: Effect of TiO_2 content on the uptake coefficient when the films were exposed to155 ppbv of gas phase NO_2 under irradiation using O_2 (15%) and N_2 (85%) as carrier. Error bars are 2σ precision.

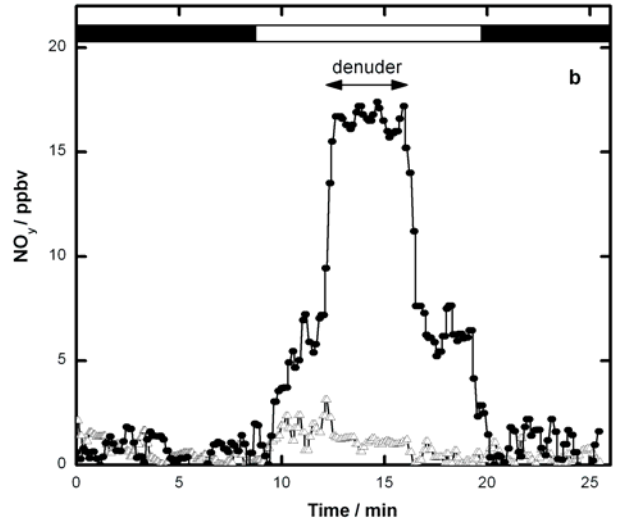

Figure 7: Effect of light on pure TiO_2 films which were previously exposed to NO_2 and light using: synthetic air as carrier gas. The black and the white bars indicate the contact time between the carrier flow and the total length of the film in the

dark and under irradiation, respectively. The inclusion of the denuder into the sample line is signalled in the figure. (●): NO_2 signal; (△): NO signal.

Table 2: Effect of the TiO_2 content on the gas phase product yields when exposing the films to 150 ppbv of NO_2 under irradiation. Errors are 2σ precision.

TiO_2 (x%)/SiO_2	HONO / %	NO / %
10	14 ± 4	26 ± 8
25	35 ± 2	16 ± 4
40	28 ± 7	42 ± 9
55	36 ± 20	49 ± 20
62	11 ± 5	3 ± 1
70	10 ± 6	2 ± 1
85	27 ± 7	-
100	12 ± 4	-

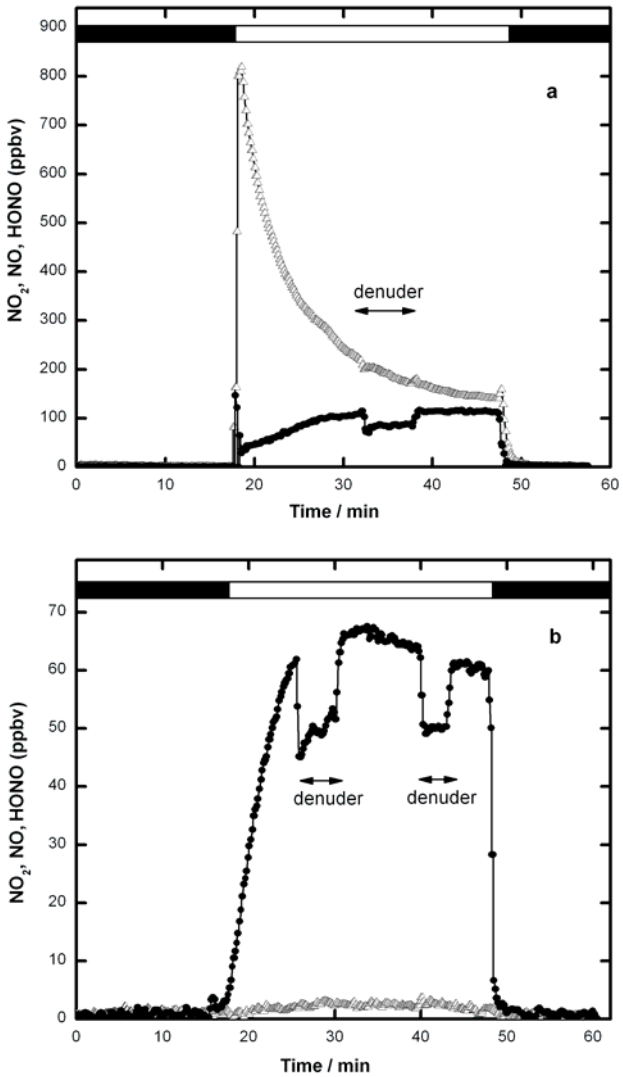

Figure 8: Effect of light on a TiO_2 / KNO_3 50 % w film when (a): it is exposed to a flow of N_2; and (b): it is exposed to a flow of synthetic air. The black and the white bars indicate the contact time between the carrier flow and the film in the dark and under irradiation, respectively. The inclusion of the denuder into the sample line is signalled in the figure. (●): NO_2 signal; (△): NO signal.

The effect of the TiO_2 content on the NO_2 loss was determined for illuminated TiO_2 / SiO_2 films (Figure 6). As it was expected, the uptake coefficients increased with increasing TiO_2 content

in the films, which *a priori* would indicate that the higher the content of TiO_2 at the surface, the more efficient it should be as a de-polluting material.[5] As shown in Table 2, HONO was produced for all TiO_2 concentrations tested under irradiation, while NO was produced only on films containing between 10 and 55 % of TiO_2. Furthermore, the HONO + NO yields on the different TiO_2 / SiO_2 films were always lower than 100 %. This result may be explained by the formation of nitrate during the heterogeneous reaction between TiO_2 and NO_2 under irradiation.[14,23,40-43] Rodriguez *et al.*[65] have proved by photoemission data and DF (Density Functional) calculations that surface NO_3 is formed through the disproportionation of NO_2 on Ti sites.

After exposure to NO_2 under irradiation the films were flushed by a constant flow of synthetic air or pure N_2 (depending on the carrier gas used on each case) in order to promote molecules desorption from the surface. Once no further traces of NO and NO_2 were observed, lamps were turned on again and emission of different NO_y species from the surface was observed. Figure 7 shows the formation of NO and NO_2 under irradiation for both carrier gases. In agreement with the results presented in Figure 5, NO was the major product in pure nitrogen (Figure 7a). However, not only NO_2 was the major product when air was used as carrier gas but also the production of another volatile compound was observed when passing the effluent flow through the carbonate denuder (Figure 7b). This product was observed for films which had previously been exposed to NO_2 under illumination and contained between 40 and 100% TiO_2, and it was not observed when N_2 was used as carrier gas. We hypothesise that the signal observed switching the carbonate denuder into the sample line may be due to N_2O formation, as previously observed by Rubasinghege and Grassian on aluminium oxide particle surfaces containing adsorbed nitrate.[45] These results may suggest that nitrate ions produced during the heterogeneous reaction of NO_2 and illuminated TiO_2 films may be involved in a renoxification process as previously discussed by Ndour *et al.* for mineral dusts containing TiO_2.[44]

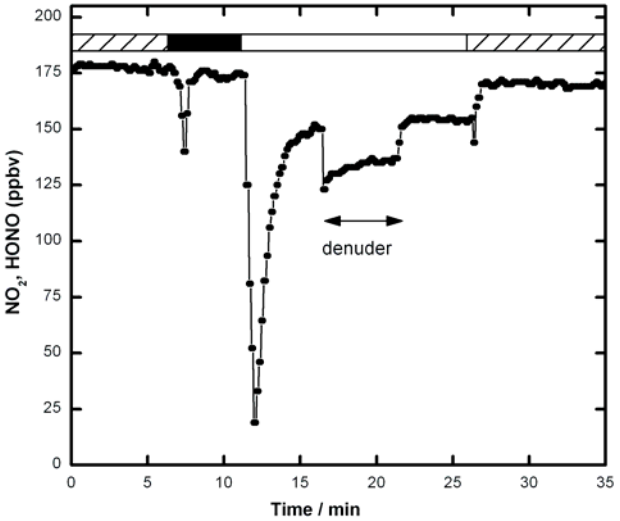

Figure 9: Effect of the NO_2 exposure under irradiation after the renoxification process on the same film of TiO_2 / KNO_3 50 % w presented in Fig. 4b. The dashed bars correspond to the initial concentration of NO_2 which is not in contact with the film. The black and the white bars indicate the contact time between the NO_2 flow and the film in the dark and under irradiation, respectively. (●): NO_2 signal.

The proposed mechanism for the obtained gas phase products, which is consistent with that reported by Ohko *et al.*[43] is the following:

$TiO_2 + h\nu \rightarrow h^+_{vb} + e^-_{cb}$	(4)
$H_2O + h^+_{vb} \rightarrow H^+ + HO^\bullet$	(5)
$NO_2 + e^- \rightarrow NO_2^-$	(6)
$NO_2 + HO^\bullet \rightarrow HNO_3$	(7)
$NO_2^- + H^+ \rightarrow HONO$	(8)
$NO_2^- + h\nu \rightarrow NO + O^-$	(9)

In the presence of molecular oxygen, there is an electron transfer to O_2 that acts as the primary electron acceptor, leading to oxygen activated species[4,66,67] which can participate in the previous mechanism as follows:

$O_2 + e^- \rightarrow O_2^{\bullet -}$	(10)
$NO_2 + O_2^{\bullet -} \rightarrow NO_2^{\bullet -} + O_2$	(11)
$H^+ + O_2^{\bullet -} \rightarrow HO_2^{\bullet}$	(12)
$HO_2^{\bullet} + NO \rightarrow NO_2 + HO^{\bullet}$	(13)

These pathways explain the higher HONO yield and the lower NO yield obtained from the heterogeneous reaction between NO_2 and illuminated TiO_2 films in presence of O_2 in the carrier gas. The production of $HO_2^{\bullet}$ by reaction (12) leads to the formation of H_2O_2, which has been observed by Beaumont *et al*.[23] Indeed, no H_2O_2 is detected in absence of O_2.[4] Gerischer and Heller[68] have suggested that electron transfer to O_2 may be the rate-limiting step in semiconductor photocatalysis. Hirakawa *et al*. have proved that $O_2^{\bullet -}$ participates in the decomposition of alcohols.[69]

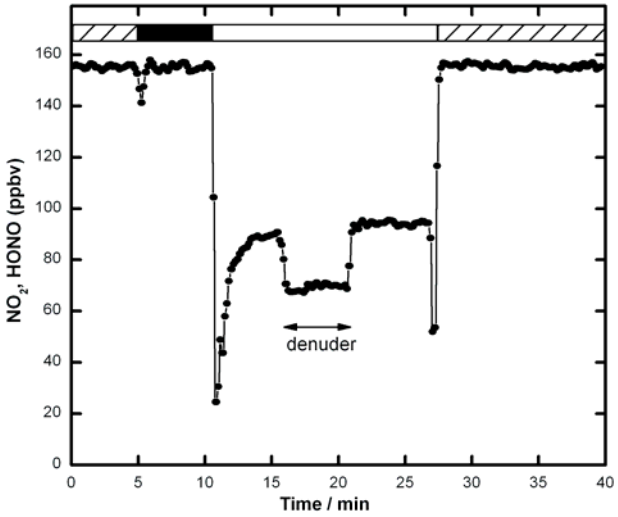

Figure 10: Effect of the NO_2 exposure under irradiation on a film of TiO_2 (55%) / SiO_2. The dashed bars correspond to the initial concentration of NO_2 which is not in contact with the film. The black and the white bars indicate the contact time between the NO_2 flow and the film in the dark and under irradiation, respectively. (●): NO_2 signal.

A second set of experiments was performed to verify the role of nitrate anions in the renoxification process, using TiO_2 films prepared with 50 % wt of KNO_3. Again, the role of molecular oxygen in the carrier gas was investigated. Figure 8a shows that NO was the major product when pure N_2 was used as carrier gas, in agreement with the results from Figure 7, while NO_2 and HONO were the main products in the presence of O_2 in the carrier gas. Similarly, Schuttlefield *et al.*[46] observed high NO_2 and low NO emission during the renoxification process of nitrate adsorbed on alumina surfaces in an atmosphere with oxygen. Rubasinghege and Grassian[45] suggested that oxygen vacancy sites may play a role in the photochemical process of adsorbed nitrate or on the chemistry of the photoproducts, as these sites may be binding sites for molecular O_2. Figure 8 also shows that NO release in pure N_2 is faster than the release of NO_2 in air, which is also in agreement with the results shown in Figure 7. This difference can also be explained considering the affinity of O_2 for the adsorption sites of TiO_2. Control experiments were carried out to determine whether nitrate photolysis was involved in the release of NO, HONO and NO_2. None of these products were observed on films without TiO_2; indeed irradiation of a SiO_2 / KNO_3 50 % w and KNO_3 film did not lead to any NO_y release; at least over our limit of detection. These control experiments indicate that nitrate photolysis was a negligible pathway in our experiments, in contrast with the mechanism proposed by Grassian and co-workers[45,46] on adsorbed nitrate on aluminium oxide particles. The proposed mechanism for the renoxification process has already been discussed by Ndour *et al.*[44] for dust samples irradiated in pure N_2.

$NO_3^- + h_{vb}^+ \rightarrow NO_3^\bullet$	(12)
$NO_3^\bullet + h\nu \rightarrow NO + O_2$	(13)
$NO_3^\bullet + h\nu \rightarrow NO_2 + O$	(14)

The ability of a TiO_2 / KNO_3 50 %w film to remove NO_2 (~170 ppbv) under irradiation in an atmosphere with O_2 was also investigated. Figure 9 evidences that the TiO_2 surface is active towards NO_2 removal with HONO production under irradiation even when the film was prepared with a high content of nitrate. The observed NO_2 loss (~35 ppbv) approximately balance the release of NO_2 (~50 ppbv) from the renoxification process (Figure 8b) and the NO_2 loss (~85 ppbv) observed on a film of TiO_2 (55%) / SiO_2 shown in Figure 10. These results are in disagreement with previous studies,[42,43] where the photocatalyst was deactivated by the nitrate ions produced during the photo-oxidation. But these previous investigations did not considered the renoxification process occurring at the surface of the TiO_2 film when nitrate ions are deposited. This result suggests that HONO would not only be produced during the heterogeneous reaction between NO_2 and a clean irradiated TiO_2 surface but also on a TiO_2 surface containing nitrate. As a consequence, special care should be taken in the development of an environmental friendly material which contains TiO_2 in its matrix as undesired products may be also formed under irradiation.

III.2 Formaldehyde

For all mineral coatings used in this study, the derived BET uptake coefficients measured in the dark were very low (of the order of 3×10^{-9}). This indicates a weak loss of HCHO on the surface, which is, within our sensitivity, independent of the TiO_2/SiO_2 mixing ratio. Similar to Carlos-Cueller et al (2003) we have observed low reactivity of HCHO onto SiO_2 films.. Both dark and UV light conditions, led to uptake coefficients of ca. $(3.1 \pm 0.5) \times 10^{-9}$ i.e., no photoenhancement was observed.

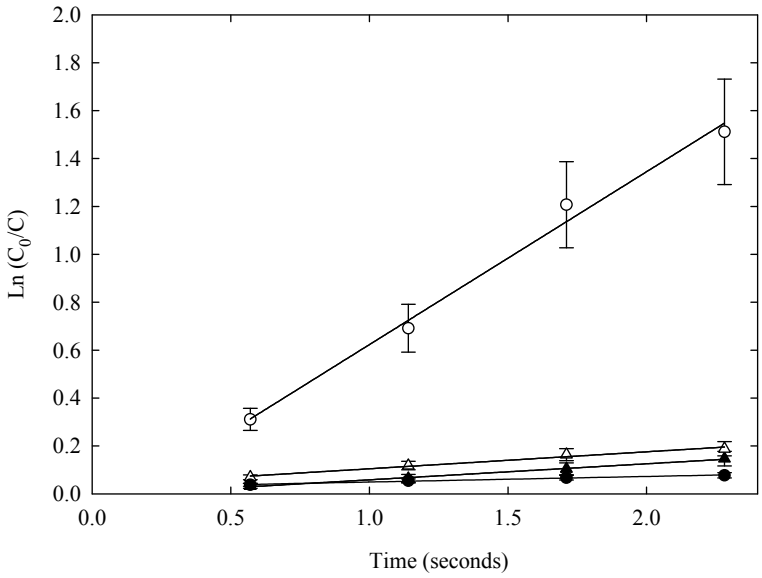

Figure 11 Kinetic of logarithmic HCHO decay as a function of residence time for 11 ppb of HCHO, at 298 K at 6% of RH on different films mixing ratios. Circles and triangles correspond to measurements performed with pure TiO_2 and pure SiO_2 coatings respectively. Open and dark symbols are assigned to illuminated and dark conditions.

A very different behavior is observed for HCHO uptake onto TiO_2 doped surface under illumination with weak near UV irradiation (irradiance of 2.7×10^{15} photons cm^{-2} s^{-1} in the 340-420 nm range). In this case the uptake is markedly photoenhanced (nearly 40 times greater than under dark conditions (see figure 11)). Under steady-state conditions, these findings underline the importance of the photocatalytic HCHO removal at the surface of the film containing traces of TiO_2. HCHO degradation by photocatalytic engineered systems was already described in the literature [70-72]. It is suggested that the photocatalytic oxidation of HCHO is due to surface reaction with OH radicals, produced by the reaction of the hole, created once TiO_2 is irradiated with UV light, and

adsorbed water. However, to our knowledge there are no data available for the HCHO uptake coefficient on irradiated mineral dust films or proxy of them to be used for atmospheric purposes.

The irradiance used in this study, is approximately 5 times less than the solar irradiance between 340 and 420 nm reaching the Earth surface [73]. Therefore, we investigated the dependence of the BET steady-state uptake coefficient on the irradiance at 293 K, 30% RH and 2 ppbv of HCHO. As shown in Figure 12, the BET uptake coefficient is linearly dependent on the irradiance, which varied from 1.9 × 10^{15} to 2.7 × 10^{15} photons cm^{-2} s^{-1} confirming the heterogeneous photochemical nature of the HCHO loss. If the linearity observed in Figure 12 is extrapolated to the irradiance reaching the Earth ground in the same wavelength range at fixed HCHO mixing ratio and humidity, it is then possible to estimate an atmospherically relevant uptake coefficient. The BET uptake coefficients are normalized to the measured irradiance I reaching the film during the experimental determination, according to:

$$\Gamma_{phot} = \frac{\gamma_{BET}}{I} \quad (15)$$

where I is the irradiance reaching the film during the experimental determination. The obtained normalized coefficient, Γ_{phot}, has units of $(mW\ cm^{-2})^{-1}$. For the majority of the experiments, I was equal to 1.45 mW cm^{-2}. Then Γ_{phot} can be then multiplied by the irradiance reaching the Earth ground or the troposphere, making possible a rough assessment of the impact of light on the heterogeneous HCHO chemistry on SiO_2-TiO_2 oxides; provided that all other parameters are kept constant.

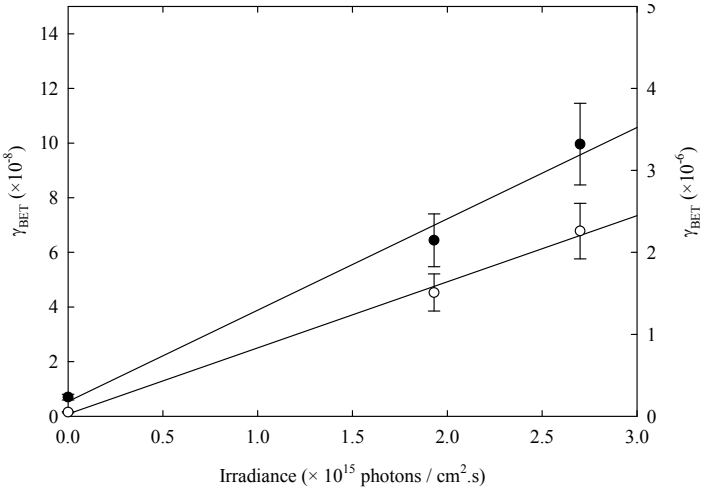

Figure 12: Dependence of the uptake coefficient as a function of UV light irradiance. Experiments were conducted with 2 ppbV of HCHO at 30% of RH and 293 K. Filled and open circles are raw data carried with 5% wt of TiO_2 diluted in SiO_2 and pure TiO_2 coatings respectively. The latter data are related to the right hand scale.

Another important atmospheric variable parameter is the HCHO initial mixing ratio. The uptake coefficients were observed to be inversely dependent on the initial gaseous HCHO concentration. Figure 13 shows the uptake coefficient decreasing from (6.0 ± 0.9) × 10^{-7} to (2.0 ± 0.3) × 10^{-7} for pure TiO_2 coatings and from (3.0 ± 0.5) × 10^{-8} to (1.5 ± 0.2) × 10^{-8} for 5%wt TiO_2 films with increasing HCHO concentration in the range from 3.5 to 32.5 ppbv, with a plateau being attained around 10 ppbv. Our data clearly show that the rate is inversely proportional to the HCHO concentration, as previously observed in many heterogeneous studies onto different solid and liquid surfaces, both organic and inorganic [74-79]. More specifically, the inverse of the uptake rate has been observed to dependent linearly with the inverse of the HCHO inlet concentration, in agreement with a Langmuir-Hinshelwood formalism.

The effect of water vapor on the uptake process was also investigated between 6 and 70% relative humidity (RH) for both 5 and 100%wt of TiO_2. As shown in Figure 14, γ_{BET} decreases at low (below 20%) and high humidity level (over 50-60%) and reaches a maximum at around 30% of RH. This, indicates that higher amount of water inhibits the surface loss. Such a dependence on the relative humidity has already been reported [70,71,80,81] and was explained by the competitive adsorption of water and the volatile organic compound (VOC) at the surface along with modifying

the amount of OH radicals produced at the TiO_2 surface, which is the driving force for the HCHO uptake. Similar conclusions certainly hold in the present study.

The results shown in Figure 15, indicate that the HCHO uptake coefficient increases from $(1.8 \pm 0.3) \times 10^{-7}$ to $(3.2 \pm 0.5) \times 10^{-7}$ for pure TiO_2 coatings and from $(4.8 \pm 0.8) \times 10^{-9}$ to $(2.0 \pm 0.3) \times 10^{-8}$ for SiO_2/TiO_2 (5 %wt) with increasing temperature in the range from 278 to 298 K. As adsorption and chemical reactivity have opposite temperature trends, these observations indicate that the surface reaction controls the observed positive dependence on the temperature.

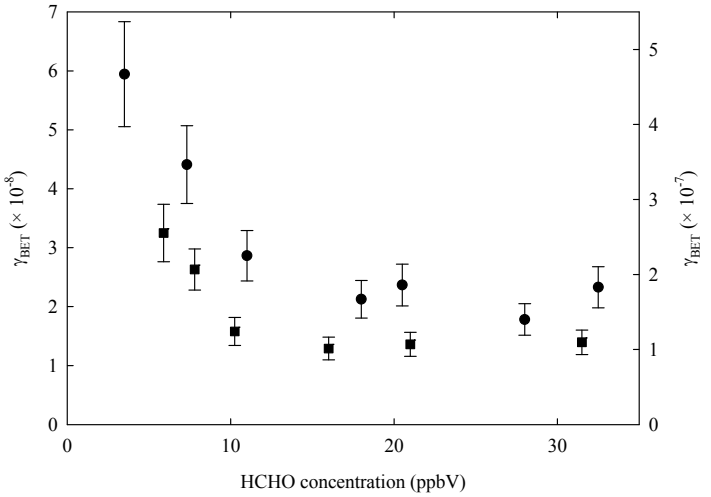

Figure 13: Trend of uptake coefficient as a function of the introduced HCHO concentration ranging from 3.5 to 32.5 ppbv. Experiments were performed with 6% of RH, at 293 K in UV-light conditions (lamps irradiance = 2.7×10^{15} photons cm^{-2} s^{-1}). Squares (■) and circles (●) correspond to measurements performed with 5% wt of TiO_2 diluted in SiO_2 and pure TiO_2 coatings respectively. The latter data are related to the right hand scale.

In the real environment, exposed surfaces may have variable TiO_2 content. We therefore tested mixing ratios between 1 and 100 wt % of TiO_2 in a SiO_2 matrix and the experimental results are presented in Figure 16, showing again a linear dependence of the uptake coefficient with respect to the wt % of TiO_2.

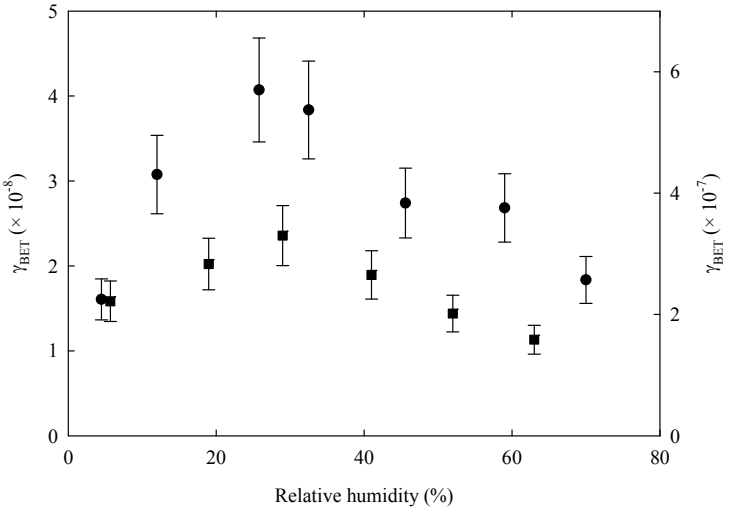

Figure 14: Effect of RH onto uptake coefficients. Experiments were carried out onto illuminated coatings with 2.7×10^{15} photons cm^{-2} s^{-1} and exposed to 11 ppb of HCHO at 293 K. Squares (■) and circles (●) correspond to measurements performed with 5% wt of TiO_2 diluted in SiO_2 and pure TiO_2 coatings respectively. The latter data are related to the right hand scale.

The present data show a strongly enhanced reactivity of synthetic surfaces containing TiO_2 and SiO_2, taken as proxies for atmospheric dust particles when irradiated with weak near UV irradiation using a coated flow tube reactor. Under dark conditions, the steady-state uptake BET coefficient (determined after 30 min of HCHO exposure time to the surface) is estimated as $(2.97 \pm 0.45) \times 10^{-9}$ onto SiO_2/TiO_2 (5% wt) films and to $(3.18 \pm 0.5) \times 10^{-9}$ onto pure TiO_2 coatings. Our results, compared to Xu et al. (2006) data conducted onto α-Al_2O_3 particles at 293 K ($\gamma_{BET} = (9.4 \pm 1.7) \times 10^{-9}$), are smaller [82]. Initial dark uptake kinetics of formaldehyde, onto pure mineral oxide

surfaces (i.e. SiO_2, α-Fe_2O_3, α-Al_2O_3) measured by Grassian and co-workers at 295 K in a Knudsen-cell reactor operating at low pressure and under dry conditions [83,84] were showed to be much greater (in the range of 3×10^{-7} to 1×10^{-4}) than our values (in the order of 2×10^{-6} for pure illuminated TiO_2 coatings). One difference lies in the low time resolution of the present series compared with quasi instantaneous response in the molecular flow reactor. Another difference lies in the rapid surface deactivation they observed, in contrast to the sustained HCHO uptake for 3.5 hours exposure time measured in our work. Actually, water molecules and other trace gases can strongly interact with mineral oxide surfaces affecting the adsorption and reaction kinetics and so the HCHO uptake onto the surface. The photochemistry of mineral aerosols could be an important sink for HCHO in a dust plume. The global impact of such dust photochemistry is now facilitated by the photoinduced uptake coefficients reported in this study.

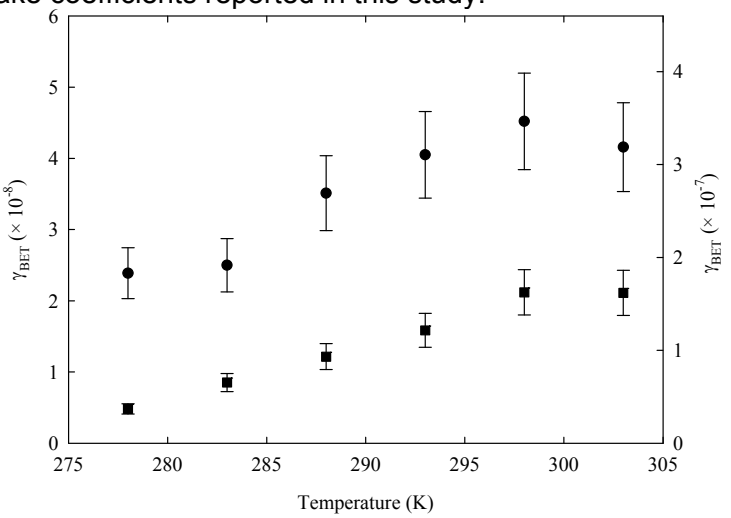

Figure 15: Effect of temperature on uptake coefficient. Experiments were driven with coatings illuminated with 2.7×10^{15} photons cm^{-2} s^{-1} and exposed to 11 ppb of HCHO at 30% of RH. Squares (■) and circles (●) correspond to measurements performed with 5% wt of TiO_2 diluted in SiO_2 and pure TiO_2 coatings respectively. The latter data are related to the right hand scale.

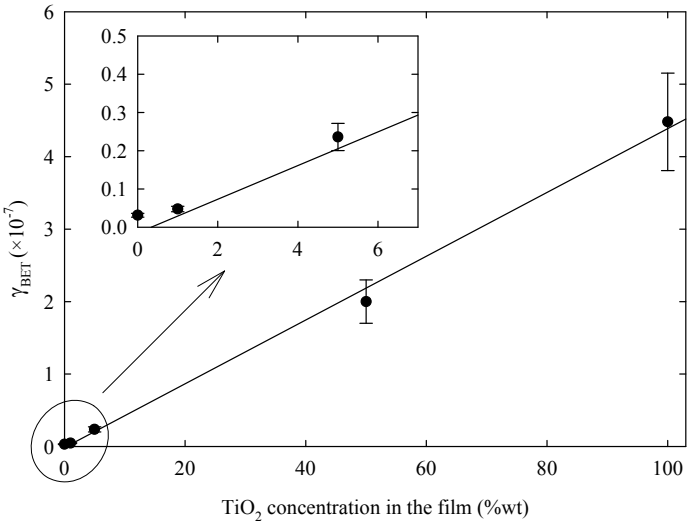

Figure 16: Dependence of uptake coefficient with respect to TiO_2 content in the coatings. Experiments were performed with coatings irradiated with 2.7×10^{15} photons cm^{-2} s^{-1} and exhibited to 11 ppb of HCHO at 30% of RH and at 293 K.

The dry deposition of HCHO is generally not suggested to be an efficient removal pathway. This has also been observed here as the HCHO uptake rate on pure SiO_2 was very slow. However, adding TiO_2 to construction materials may add a new removal pathway close to the ground. In fact, such materials, through the TiO_2 photocatalytic properties, are suggested to be a sink for various organic pollutants. The kinetic information obtained in this study can be used to assess whether and under which conditions, HCHO removal through TiO_2 based construction materials may be significant. For performing such an evaluation let us assume a city in which such materials are deployed at a large scale i.e., a city in which buildings are coated by a thin layer of TiO_2 (as

already made in some locations). Let us assume that this TiO_2 layer covers between 0% (i.e., the case of most current cities) and 100% (a hypothetical futuristic case where all building are made with these TiO_2 based construction materials). Using previous modelling studies for dense urban areas [85-87], which consider both the rates of occupied surface at the ground and shaped constructed surface, we estimate that the building surface exposed to HCHO deposition is 2.25 times the city surface at the ground. Current commercial TiO_2 based construction materials are covered by an approximately 10 nm thick active TiO_2 layer [88] having an internal (BET) surface as the films explored in this study. This would expose a total chemically active surface of 1.04×10^8 m^2 taking into consideration a ground surface of 46×10^6 m^2 (which would be Lyon's city surface[89]).

To assess if these processes may represent a significant HCHO sink, an easy way would be to compare the lifetimes associated to its main removal processes i.e., photolysis or reaction with OH to photoinduced uptake on the buildings. The first two lifetimes are readily available from the literature. Assuming an average OH concentration of 10^6 molecules cm^{-3}, the OH channel lifetime is calculated to be almost 26 hours [90]. Considering a solar zenith angle of 30° and therefore an irradiance of 1.92×10^{17} photons cm^{-2} s^{-1} [91,92], HCHO is photolysed with a lifetime of 6 hours. The heterogeneous pathway (i.e., degradation at the surface of TiO_2 based construction materials) is evaluated by using the uptake coefficient derived in this study.

To a first approximation, equation (4) can still be used to calculate the HCHO lifetime just by replacing the volume of the tube by the volume of air in the urban environment (simply defined as the ground surface times the mixing height) and the surface by the total surface of photocatalytical active material deployed in this virtual city. For these calculations, we used the uptake coefficient measured at 2 ppbv at 30% relative humidity and 293 K linearly extrapolated to real solar conditions ($I = 1.21 \times 10^{16}$ photons cm^{-2} s^{-1}) in the UV region (340 to 420 nm), we can estimate that, the associated uptake coefficient onto pure TiO_2 films, is $(9.7 \pm 1.4) \times 10^{-6}$.

Assuming a mixing height (h) between 50 and 500 m, the HCHO lifetime can be approximated to:

$$\tau_d(\text{hours}) = \frac{5.47 \times 10^6 \times h(\text{m})}{S(\text{m}^2)} \qquad (16)$$

Figure 17 compares all three estimated lifetimes as a function of the urban TiO_2 coverage. Obviously, it can be seen that HCHO loss increases significantly from high to low mixing heights where the deposition process is forced. Compared to HCHO loss by means of OH reaction, deposition process onto urban surfaces from heights ranging from 100 to 200 m is significant if 20 and 40 % of constructed surface is covered by pure TiO_2, respectively. Besides, we note that for the upper mixing heights, HCHO concentrations are estimated to be smaller which contribute, according to Figure 14, to faster kinetics deposition. In this case, one may reconsider uptake coefficients values in the calculation of HCHO lifetime.

Hence, for low mixing heights i.e. 50 m (or in other words for close vicinity of buildings), the removal by active depolluting material can compete with the other homogeneous removal pathways if 10% or more of the building are covered with TiO_2. Moreover, if 40% of urban surfaces or more is activated then the heterogeneous removal may dominate over OH reaction and photolysis. Therefore this hypothetical exercise showed that implementing TiO_2 based construction materials, can for the specific case of HCHO be a significant sink term potentially improving urban air quality.

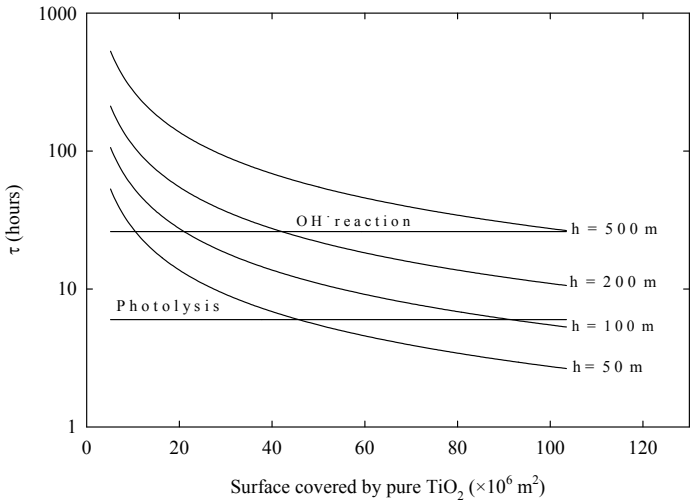

Figure 17: Lifetimes of HCHO due to photolysis, reaction with $OH^{\cdot}$ and deposition process onto mineral surfaces. The latter trends are represented as a function of surface covered by TiO_2 coatings for different air mixing heights (ranging from 50 m to 500 m).

III.3 Ozone formation on titanium dioxide coated glasses

After introduction of synthetic air and NO into the CESAM chamber, the concentrations of NO, NO_2, HNO_2 and O_3 are monitored in the dark for one hour. Then the artificial illumination is turned on and the chemical system is again monitored for 90 minutes. A similar procedure is adopted for the Teflon outdoor chamber using natural illumination. After flushing dry purified air, known amounts of NO and NO_2 are injected and the NO, NO_2 and O_3 concentrations are monitored for 30 minutes in the dark. The reactor is then exposed to natural light and the gas mixture evolution is followed for 4 hours. The results for a TiO_2 coated glass and for a standard glass studied with the CESAM and the outdoor chamber are displayed in Figures 18 and 19, respectively.

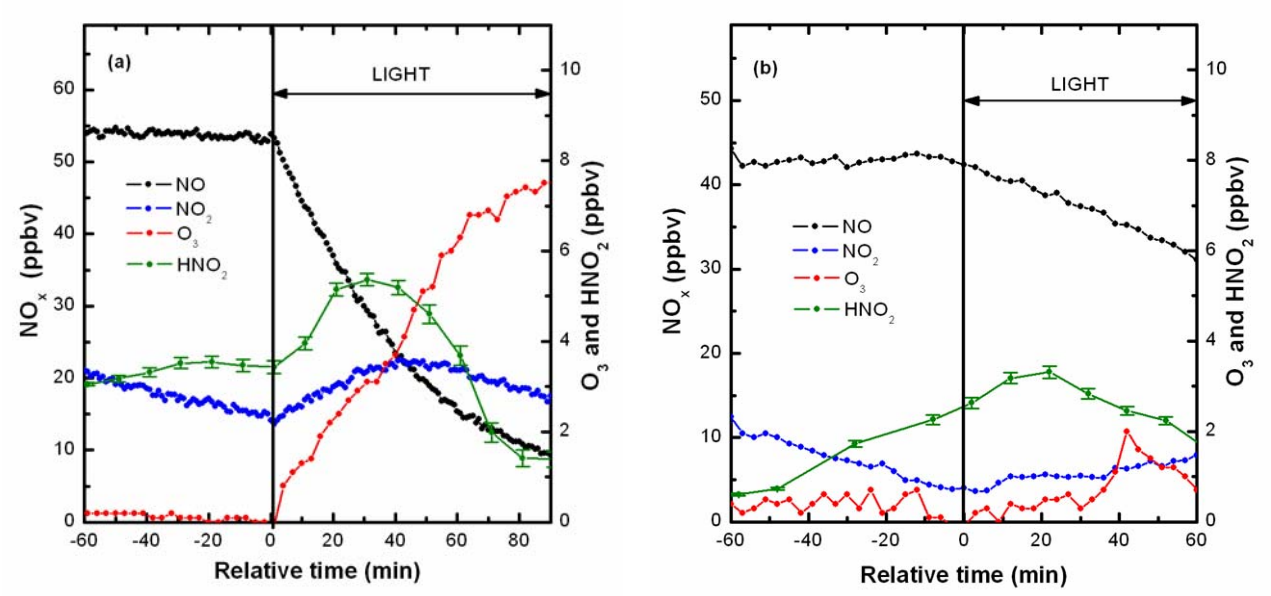

Figure 18. NO, NO_2, HNO_2 and O_3 profiles recorded in the presence of (a) a TiO_2 coated glass and (b) a standard glass in the CESAM chamber. The vertical line indicates the moment when the light was turned on.

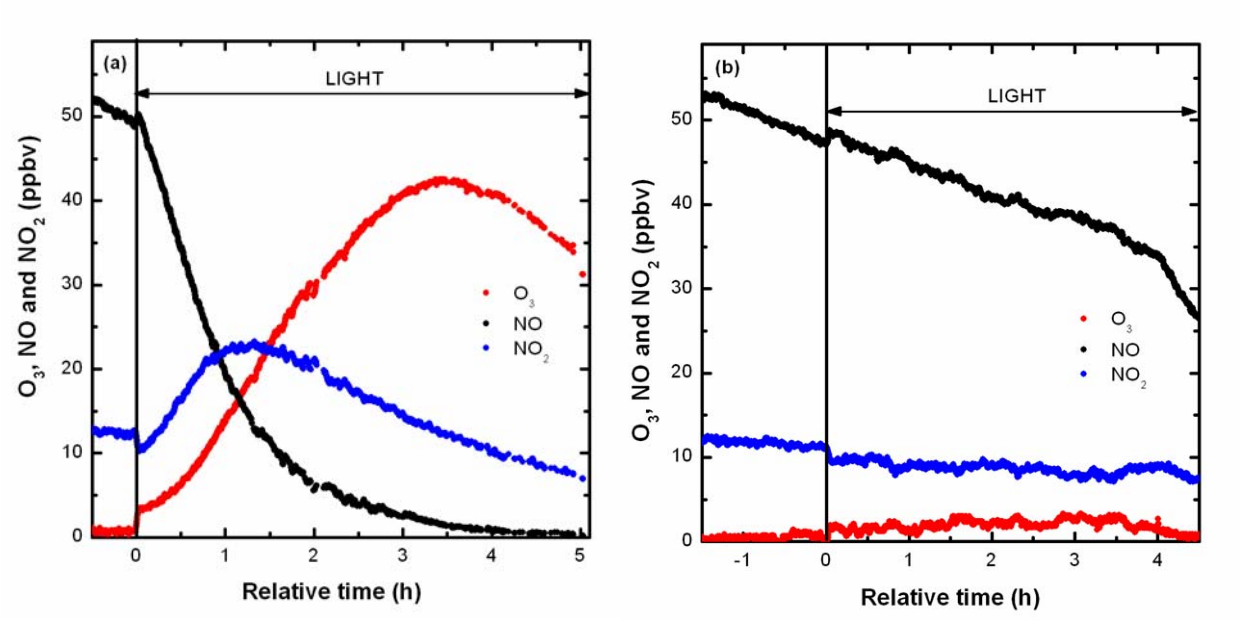

Figure 19. NO, NO_2 and O_3 profiles under natural irradiation in the presence of (a) a TiO_2 coated glass and (b) a standard glass in the outdoor chamber. The vertical line indicates the moment when the chamber was exposed to natural illumination.

Despite the different time scales, illumination type and chambers building material, the observed trace gases evolution is similar. In agreement with previous studies,[93] NO uptake on the TiO_2 coated glass is enhanced under irradiation decreasing with time in both experiments. The NO_2 concentration profile exhibits a maximum under illumination, suggesting that it is formed from NO photocatalytic oxidation and then converted into HNO_3 and HNO_2 at the surface.[24,37-39,43] At the same time a significant accumulation of ozone is observed. In agreement with previous studies,[24,37,38,94] HNO_2 production is enhanced under irradiation in presence of TiO_2 (Figure 19). However, when a standard glass is analyzed in both chambers, no ozone formation is detected (Figures 18b and 19b). As well the NO_2 and NO concentration profiles are similar for the standard glass and the empty outdoor chamber with no evidence of a light effect (Figures 19b). These results indicate that O_3 formation can not be explained by the gas phase chemistry occurring in the chambers. The differences between the O_3 profiles obtained for the blank experiments and the coated glass suggested that TiO_2 should be involved in the reaction mechanism leading to O_3 formation via heterogeneous reaction. But simulation chamber experiments are not concluding about the processes that lead to the results obtained.

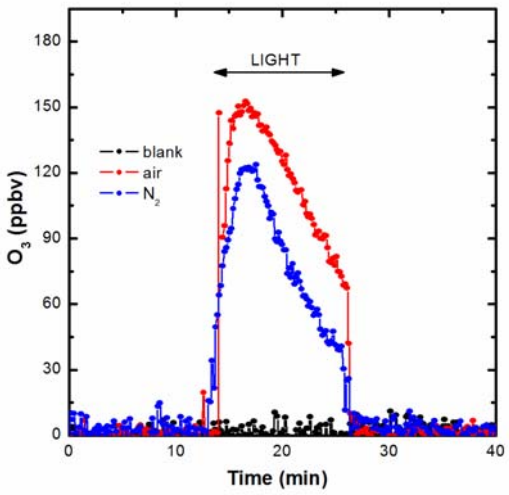

Figure 20. Effect of light (8 near-UV emitting lamps in the 300-420 nm wavelength range) on a TiO_2 / KNO_3 (50 % w/w) film using synthetic air and pure N_2 as carriers. The same blank signal was given by an empty tube and by a tube with a KNO_3 deposit using both carriers.

To investigate the origin of the observed O_3 increase a second type of experiment has been carried out using a flow tube reactor. It is well known that nitrate anions are formed as a consequence of the photocatalytic oxidation of NO_2 on UV-illuminated TiO_2 surfaces,[14,23,40-43]. Therefore, film of TiO_2 / KNO_3 50 % w/w has been exposed to near-UV irradiation using synthetic air or pure N_2 as carrier gases (Figure 20). As described previously, a renoxification process occurs on illuminated TiO_2 films mixed with nitrate[44,94]. In contrast with the mechanism proposed by Grassian and co-workers[45,95] for a film composed by nitrate and aluminium oxide, under the experimental condition used (weak UV radiation) nitrate photolysis is negligible (Figure 20). An alternative renoxification pathway (1-3) including the photochemistry of the NO_3 radical can explain the release of NO and NO_2 from the illuminated TiO_2 surfaces,[44] and the further formation of O_3. The following mechanism can also explain the relative higher concentration of O_3 produced with O_2 as carrier gas:

$NO_3^- + h_{vb}^+ \rightarrow NO_3^\bullet$	(17)
$NO_3^\bullet + h\nu \rightarrow NO + O_2$	(18)
$NO_3^\bullet + h\nu \rightarrow NO_2 + O^\bullet$	(19)
$O^\bullet + O_2 \rightarrow O_3$	(20)
$NO_3^\bullet + O_2 \rightarrow NO_2 + O_3^\bullet$	(21)

Although O_3 has been recently proved to decompose on illuminated TiO_2 surfaces;[96] its formation is observed when TiO_2 treated surfaces are exposed to NO_x under illumination. This difference can be explained by a renoxification process involving the photochemistry of the NO_3 radical. Even if majority of the studies[14,23,40-43] argue that nitrate is an innocuous final product of the photocatalytic NO_x removal process, the present work demonstrates for the first time that O_3 can actually been formed on TiO_2 glasses coated by nitrate. The heterogeneous reactions carried out on the surface of TiO_2 containing materials indicate that new remediation technologies based on these materials may not have the desired impact on the environment and human health.

III.4 the influence of TiO_2 coating on the chemistry of propene/NO_x/light system under atmospheric conditions

Two series of experiments have been conducted: At ICARE relatively high concentration were used (i.e around 1.3 ppm of propene and 700 ppb of NOx) while at LISA the initial concentrations were ranging from 150 to 400 ppb in VOC and from 50 to 100 ppb in NOx. In total 15 experiments were carried out.

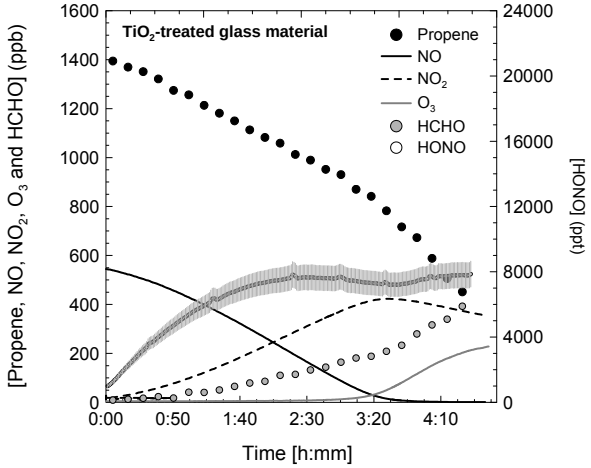

Figure 21 : Concentration-time profiles of reactants and oxidation products in the propene/NO/air/light system in the presence of TiO_2 treated glass. (runs performed at ICARE).

Test runs were first conducted to check the behaviour of NO and/or propene in absence of glass plates with and without irradiation. The decrease of the concentrations of these species versus time was found to be similar to that due to dilution. Figures 21 and 22 show examples of the experimental concentration-time profiles of the reactants (NO and propene) and the observed products, respectively, with the non-TiO_2-treated and with the TiO_2-treated glass plates when initial concentrations were $[propene]_0$=1294-1394 ppb and $[NO]_0$=545-561 ppb.

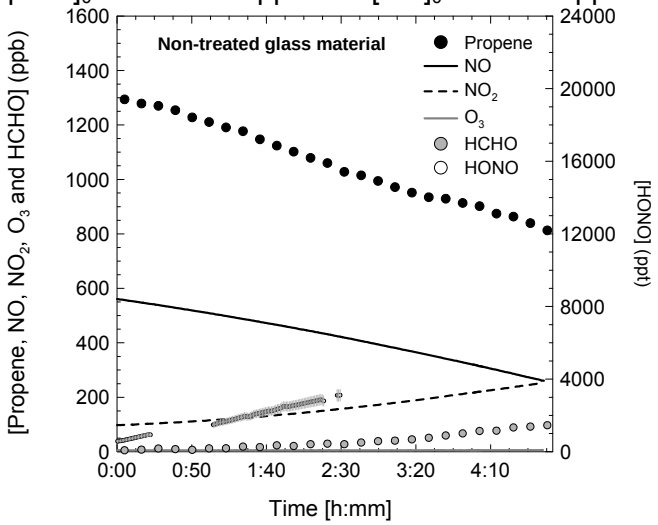

Figure 22 : Concentration-time profiles of reactants and oxidation products in the propene/NO/air/light system in the presence of non-TiO_2-treated glass (runs performed at ICARE).

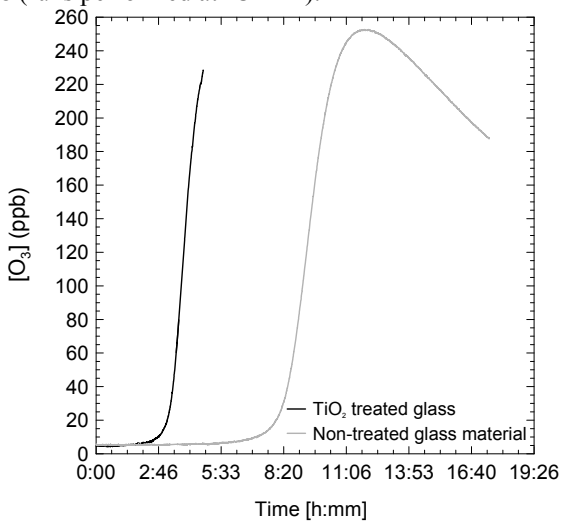

Figure 23 : Concentration-time profiles of O_3 under different conditions during photo-oxidation propene/NO experiment (runs performed at ICARE).

These results indicate that there is a significant additional loss of propene and NO in the presence of TiO_2-treated glass materials in comparison with their loss in the presence of non treated glass materials. In the first two and a half hour of the run (i.e before any significant production of ozone) only 250 ppb of propene is consumed for the non-treated glass while around 400 ppb have been consumed for the TiO_2-containing material. For NO concentration-photolysis time profiles, photocatalytic effect is even more pronounced where 99% has disappeared for the treated-glass material and only 43% for the non-treated glass materials in the first four hours. In a second part of the experiment, one can notice a significant ozone production which lead to an additional loss of propene due to ozonolysis in the case of TiO_2-treated material. In the case of non-treated glass, the ozone formation is significantly delayed as shown in Figure 23 due to the fact that a much longer reaction time is necessary in such a system to reach a low NO level. Nevertheless, as soon as ozone accumulation starts, it shows very similar efficiencies in both systems.

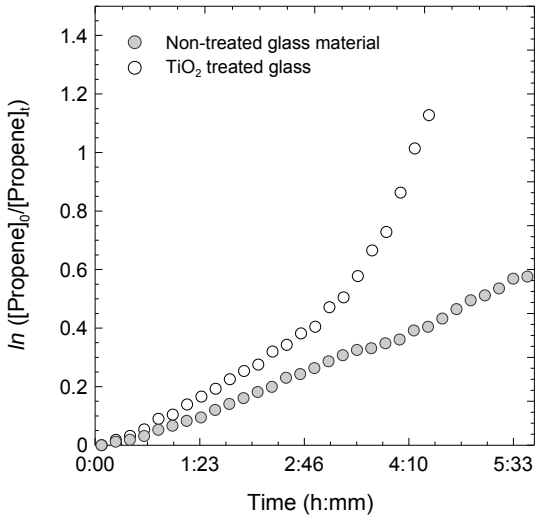

Figure 24 : The loss of propene under different conditions during photo-oxidation propene/NO experiment.

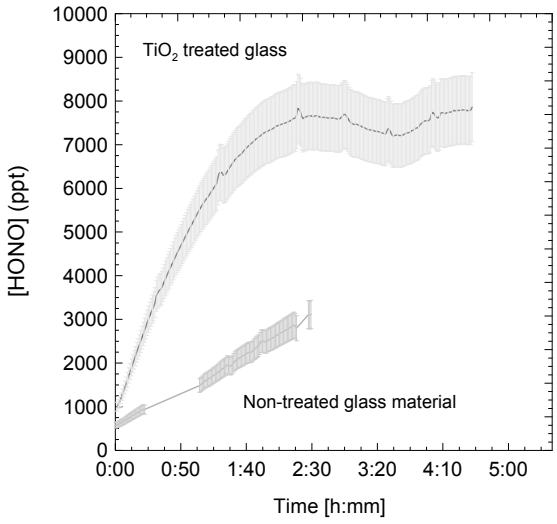

Figure 25 : Concentration-time profiles of HONO under different conditions during photo-oxidation propene/NO experiment.

Test experiments have been carried out with propene alone irradiated in the presence of TiO_2 treated glass. They have shown that no significant additional propene losses could be observed. This support the fact that, in such chemical system, the two main propene loss processes are reaction with OH and with ozone. Figure 25 shows a rough analysis of the propene loss during the experiments. Assuming a pseudo first order behaviour (i.e constant radical concentration), ln([propene]$_0$/[propene] was plotted as a function of the irradiation time. The figure shows a linear increase in the consumption of the propene as the reaction goes with a larger slope in the presence of the treated surfaces compared to the non-treated ones. The time-concentration profile deviates from the linearity for longer reaction time in the case of the treated surfaces. This can be attributed to the increase of ozone concentration as the reaction goes.. The slope of the first part of the curve when TiO_2 treated glass was used is 50% larger than with normal glass which indicates that OH levels were 50% higher in the case of photocatalytically active glass. This observation might be correlated with the fact that nitrous acid (HONO) was also formed (Figure 25), reaching a concentration which was 2.5 times higher for the TiO_2-material than for the non-treated glass material, leading to a final concentration around 8 ppb in the presence of treated material.

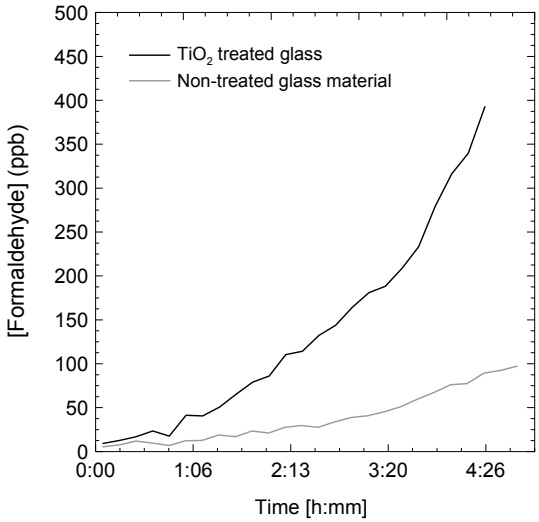

Figure 26 : Concentration-time profiles of Formaldehyde under different conditions during photo-oxidation Propene/NO experiment.

Formaldehyde was also observed as oxidation product where 72 ppb was formed in the presence of non-treated material while higher concentration was obtained for the treated material, reaching 309 ppb for 4 hours reaction time scale (Figure 26).

Several experiments were carried out at lower concentration. At this much atmospherically relevant levels, the effect were found less obvious. Nevertheless, similar conclusion than those arising from ICARE experiment can be drawn. As shown on figure 27, when 50 ppb of NO was initially used the pseudo-first order of the propene loss was two time larger in the presence of TiO_2 coated glass that with normal glass.

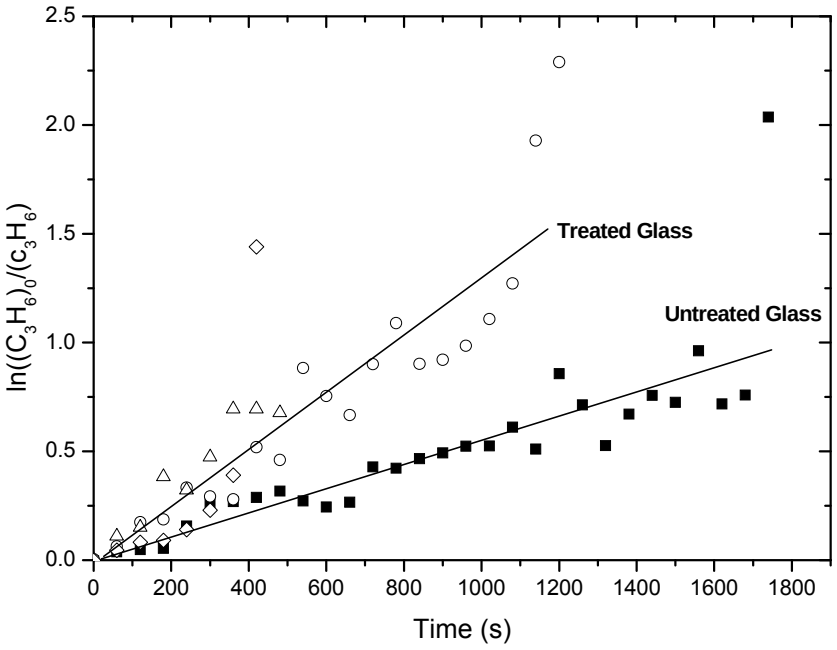

Figure 27 : Pseudo-fist order plot of the propene loss in the presence of non-treated and treated material

The comparison of concentration-time profiles recorded for both materials given in figure 28 shows that under these conditions the two conditions lead to very similar observations. This can be easy explained by the fact that the effect of TiO_2 material on nitrogen oxides is a function of NOx levels itself. It is hence not surprising that a lower NOx conditions the effect were smaller. Nevertheless, a very interesting additional effect was recorded during these experiments. Indeed, even if the ozone production rate is very similar during the first 40 minutes of the experiment, a

unexpected plateau is reach with treated glass while the ozone production remain in the case of non-treated materials. The reason for this behaviour is not clear and further investigations are needed. Nevertheless one can make the hypothesis that secondary products involved in ozone production when propene concentration become low are trapped by photocatalytic surfaces and no more available in the gas phase.

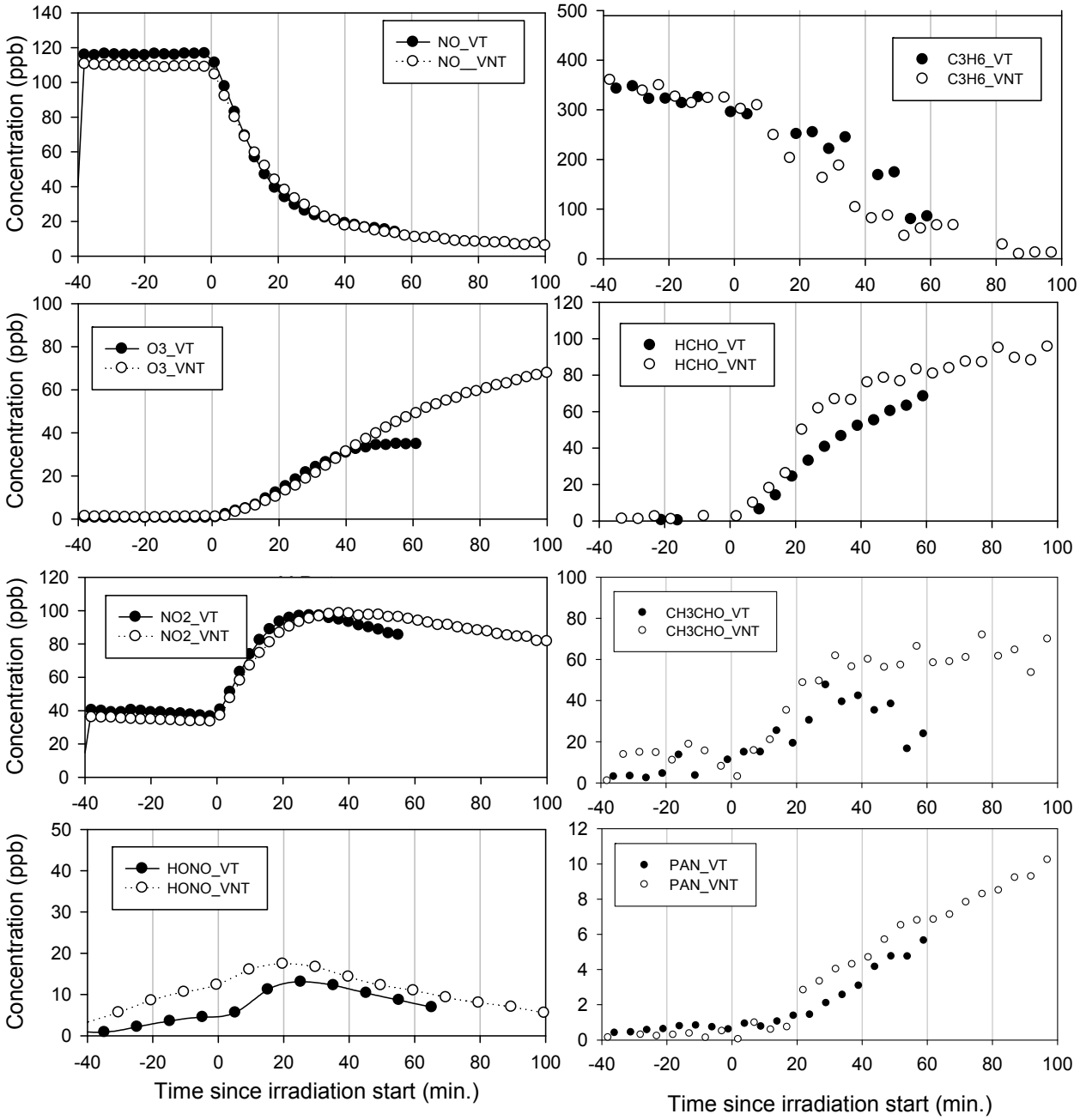

Figure 28 : Concentration-time profiles of reactants and products during a low concentration simulation experiment performed at LISA in the presence of treated glass (black symbols) or non-treated glass (empty symbols). Time origin is taken when light was turned on.

IV. CONCLUSIONS

The reactivity of NO_2 on irradiated TiO_2 / SiO_2 films was studied, with different TiO_2 contents, as proxies for NOx de-polluting materials. The influence of the photocatalyst concentration, the role of molecular oxygen and the effect of nitrate on the reactivity of TiO_2 films were investigated. NO, HONO and nitrate anions are produced as a consequence of the NO_2 loss on UV-illuminated TiO_2 films. A renoxification pathway that involves the photochemistry of the NO_3 radical leads to the release of NO, NO_2 and of HONO from the TiO_2 surface. The presence of O_2 in the carrier gas modifies the NO and HONO production yields in the heterogeneous reaction between NO_2 and TiO_2 as well as the products of the renoxification process.

The kinetics of the heterogeneous reaction between gaseous HCHO and TiO_2/SiO_2 mineral coatings have been investigated to mimic HCHO loss on TiO_2 coated depolluting urban surfaces, by means of flow tube studies. The measured uptake kinetics were observed to be strongly enhanced when the surface (or coating) was irradiated in the wavelength range from 340 to 420 nm (with an irradiance of 1.45 mW cm^{-2}). The associated BET uptake coefficients were measured in the range from $(3.00 \pm 0.45) \times 10^{-9}$ to $(2.26 \pm 0.34) \times 10^{-6}$ and were strongly dependent on the HCHO initial concentration in the range from 3.5 to 32.5 ppbv, relative humidity from 6 to 70%, temperature from 278 to 303 K and TiO_2 content in the mineral coating from 1 to 100% wt. The measured kinetics were well described using a Langmuir-Hinshelwood type formalism. The estimated uptake coefficients were used to discuss the importance of the heterogeneous HCHO surface loss, in terms of deposition lifetimes, as compared to major homogeneous gas phase losses (OH reaction and photolysis). It is found that deposition may compete with gas phase removal of HCHO in a dense urban environment if more than 10% of urban surface is covered with TiO_2 treated materials.

Experiments were conducted at high and low concentrations on the photooxidation of gas mixture propene/NO chosen as a model for VOCs atmospheric oxidation. These results show that the photocatalytic effect of TiO_2 can affect the oxidative capacity of the gas phase composition. They also show that these effects are non linear and ambiguous as they affect strongly the NO/NO_2/HONO system which is the heart of the ozone production scheme. In order to assess an affect at larger scale on photo-oxidant concentration, additional experiments coupled with computer simulations are needed.

Indeed, this project has produced the basic physico-chemical parameters required to build consistent mechanism taking into account the complex interaction of photo-catalytical surfaces with their atmospheric environment. It is now possible and necessary to draw models which will help to quantify the effect of the competition or the synergy between these new processes and the fluid dynamic at street or urban scale.

VI. REFERENCES

(1) Brunekreef, B.; Holgate, S. T. *Lancet* **2002**, *360*, 1233

(2) Finlayson-Pitts, B. J.; Pitts, J. N., Jr. *Science* **1997**, *276*, 1045.

(3) Parkin, I. P.; Palgrave, R. G. *Journal of Materials Chemistry* **2005**, *15*, 1689.

(4) Hoffmann, M. R.; Martin, S. T.; Choi, W. Y.; Bahnemann, D. W. *Chemical Reviews* **1995**, *95*, 69.

(5) Beeldens, A.; Van Gemert, D. *RILEM Proceedings pro041 (RILEM International Symposium on Environment-Conscious Materials and Systems for Sustainable Development)* **2004**, 353.

(6) Dehn, F.; Bahnemann, D.; Bilger, B. *RILEM Proceedings pro041 (RILEM International Symposium on Environment-Conscious Materials and Systems for Sustainable Development)* **2004**, 347.

(7) Kasanen, J.; Suvanto, M.; Pakkanen, T. T. *Journal of Applied Polymer Science* **2009**, *111*, 2597.

(8) Motohashi, K.; Inukai, T.; Toshimasa, K. *RILEM Proceedings pro041 (RILEM International Symposium on Environment-Conscious Materials and Systems for Sustainable Development)* **2004**, 27.

(9) Vallée, F.; Ruot, B.; Bonafous, L.; Guillot, L.; Pimpinelli, N.; Cassar, L.; Strini, A.; Mapelli, E.; Schiavi, L.; Gobin, C.; André, H.; Moussiopoulos, N.; Papadopoulos, A.; Bartzis, J.; Maggos, T.; McIntyre, R.; Lehaut-Burnouf, C.; Henrichsen, A.; Laugesen, P.; Amadelli, R.; Kotzias, D.; Pichat, P. *RILEM Proceedings pro041 (RILEM International Symposium on Environment-Conscious Materials and Systems for Sustainable Development)* **2004**, 337.

(10) Ao, C. H.; Lee, S. C.; Mak, C. L.; Chan, L. Y. *Applied Catalysis B: Environmental* **2003**, *42*, 119.

(11) Devahasdin, S.; Fan, C.; Li, K.; Chen, D. H. *Journal of Photochemistry and Photobiology A: Chemistry* **2003**, *156*, 161.

(12) Frazer, L. *Environmental Health Perspectives* **2001**, *109*, A174.

(13) Hamada, H.; Komure, K.; Takahashi, R.; Yamaji, T. *RILEM Proceedings pro041 (RILEM International Symposium on Environment-Conscious Materials and Systems for Sustainable Development)* **2004**, 361.
(14) Ibusuki, T.; Takeuchi, K. *Journal of Molecular Catalysis* **1994**, *88*, 93.
(15) Maggos, T.; Bartzis, J. G.; Leva, P.; Kotzias, D. *Applied Physics a-Materials Science & Processing* **2007**, *89*, 81.
(16) Maggos, T.; Bartzis, J. G.; Liakou, M.; Gobin, C. *Journal of Hazardous Materials* **2007**, *146*, 668.
(17) Maggos, T.; Plassais, A.; Bartzis, J. G.; Vasilakos, C.; Moussiopoulos, N.; Bonafous, L. *Environmental Monitoring and Assessment* **2008**, *136*, 35.
(18) Moussiopoulos, N.; Barmpas, P.; Ossanlis, I.; Bartzis, J. *Environmental Modeling & Assessment* **2008**, *13*, 357.
(19) Nakajima, F.; Hamada, I. *Catalysis Today* **1996**, *29*, 109.
(20) Wang, H.; Wu, Z.; Zhao, W.; Guan, B. *Chemosphere* **2007**, *66*, 185.
(21) Yumoto, H.; Matsudo, S.; Akashi, K. "Photocatalytic decomposition of NO2 on TiO2 films prepared by arc ion plating"; 3rd International Symposium on Applied Plasma Science (ISAPS 01), 2001, Fairbanks, Alaska.
(22) Arsac, F.; Bianchi, D.; Chovelon, J. M.; Ferronato, C.; Herrmann, J. M. *The Journal of Physical Chemistry A* **2006**, *110*, 4213.
(23) Beaumont, S. K.; Gustafsson, R. J.; Lambert, R. M. *ChemPhysChem* **2009**, *10*, 331.
(24) Gustafsson, R. J.; Orlov, A.; Griffiths, P. T.; Cox, R. A.; Lambert, R. M. *Chemical Communications* **2006**, 3936.
(25) Kleffmann, J. *ChemPhysChem* **2007**, *8*, 1137.
(26) Becker, E. F.; Zimmerma.Bk; Geiduschek, E. P. *Journal of Molecular Biology* **1964**, *8*, 377.
(27) Harwood, E. A.; Hopkins, P. B.; Sigurdsson, S. T. *Journal of Organic Chemistry* **2000**, *65*, 2959.
(28) Kirchner, J. J.; Hopkins, P. B. *Journal of the American Chemical Society* **1991**, *113*, 4681.
(29) Kirchner, J. J.; Sigurdsson, S. T.; Hopkins, P. B. *Journal of the American Chemical Society* **1992**, *114*, 4021.
(30) Shapiro, R.; Dubelman, S.; Feinberg, A. M.; Crain, P. F.; McCloskey, J. A. *Journal of the American Chemical Society* **1977**, *99*, 302.
(31) Grosjean, D. *Journal of the Air & Waste Management Association* **1991**, *41*, 306.
(32) Hanst, P. L.; Spence, J. W.; Miller, M. *Environmental Science & Technology* **1977**, *11*, 403.
(33) Pitts, J. N. *Environmental Health Perspectives* **1983**, *47*, 115.
(34) Pitts, J. N.; Grosjean, D.; Vancauwenberghe, K.; Schmid, J. P.; Fitz, D. R. *Environmental Science & Technology* **1978**, *12*, 946.
(35) Fahmy, O. G.; Fahmy, M. J. *Cancer Res* **1976**, *36*, 5404.
(36) Shapley, D. *Science* **1975**, *191*, 268.
(37) Langridge, J. M.; Gustafsson, R. J.; Griffiths, P. T.; Cox, R. A.; Lambert, R. M.; Jones, R. L. *Atmospheric Environment* **2009**, *43*, 5128.
(38) Ndour, M.; D'Anna, B.; George, C.; Ka, O.; Balkanski, Y.; Kleffmann, J.; Stemmler, K.; Ammann, M. *Geophysical Research Letters* **2008**, *35*, 5.
(39) Ndour, M.; Nicolas, M.; D'Anna, B.; Ka, O.; George, C. *Physical Chemistry Chemical Physics* **2009**, *11*, 1312.
(40) Dalton, J. S.; Janes, P. A.; Jones, N. G.; Nicholson, J. A.; Hallam, K. R.; Allen, G. C. *Environmental Pollution* **2002**, *120*, 415.
(41) Grassian, V. H. *International Reviews in Physical Chemistry* **2001**, *20*, 467.
(42) Lin, Y. M.; Tseng, Y. H.; Huang, J. H.; Chao, C. C.; Chen, C. C.; Wang, I. *Environmental Science & Technology* **2006**, *40*, 1616.
(43) Ohko, Y.; Nakamura, Y.; Fukuda, A.; Matsuzawa, S.; Takeuchi, K. *The Journal of Physical Chemistry C* **2008**, *112*, 10502.
(44) Ndour, M.; Conchon, P.; D'Anna, B.; Ka, O.; George, C. *Geophysical Research Letters* **2009**, *36*, 4.
(45) Rubasinghege, G.; Grassian, V. H. *Journal of Physical Chemistry A* **2009**, *113*, 7818.
(46) Schuttlefield, J.; Rubasinghege, G.; El-Maazawi, M.; Bone, J.; Grassian, V. H. *Journal of the American Chemical Society* **2008**, *130*, 12210.
(47) Atkinson, R. "Atmospheric chemistry of VOCs and NOx," Air Pollution Research Center, Department of Environmental Sciences, and Department of Chemistry,University of California,Riverside,CA,USA., 2000.
(48) Iraci, L. T.; Tolbert, M. A. *J. Geophys. Res., [Atmos.]* **1997**, *102*, 16099.
(49) Gutzwiller, L.; George, C.; Rossler, E.; Ammann, M. *J. Phys. Chem. A* **2002**, *106*, 12045.
(50) Sassine. M, D. A. B., Picquet-Varrault. B, Perraudin. E, Doussin. F, George. C, . *under preparation* **2009**.
(51) Sawicki, E.; Hauser, T. R.; Stanley, T. W.; Elbert, W. *Anal. Chem.* **1961**, *33*, 93.
(52) Dasgupta, P. K.; Zhang, G.; Poruthoor, S. K.; Caldwell, S.; Dong, S.; Liu, S.-Y. *Anal. Chem.* **1998**, *70*, 4661.
(53) Grosjean, D. *Environ. Sci. Technol.* **1991**, *25*, 710.
(54) Clarisse, B.; Laurent, A. M.; Seta, N.; Le Moullec, Y.; El Hasnaoui, A.; Momas, I. *Environ. Res.* **2003**, *92*, 245.
(55) Nicolas, M.; Ndour, M.; Ka, O.; D'Anna, B.; George, C. *Environmental Science & Technology* **2009**, *43*, 7437.
(56) Cooney, D. O.; Kim, S. S.; Davis, E. J. *Chem. Eng. Sci.* **1974**, *29*, 1731.
(57) Ammann, M.; Roessler, E.; Strekowski, R.; George, C. *Phys. Chem. Chem. Phys.* **2005**, *7*, 2513.
(58) Fuller, E. N.; Ensley, K.; Giddings, J. C. *J. Phys. Chem.* **1969**, *73*, 3679.
(59) Wang, J.; Doussin, J. F.; Perrier, S.; Perraudin, E.; Katrib, Y.; Pangui, E.; Picquet-Varrault, B. *In preparation* **2010**.
(60) Akimoto, H.; Sakamaki, F.; Hoshino, M.; Inoue, G.; Okuda, M. *Environmental Science & Technology* **1979**, *13*, 53.
(61) Metzger, A.; Dommen, J.; Gaeggeler, K.; Duplissy, J.; Prevot, A. S. H.; Kleffmann, J.; Elshorbany, Y.; Wisthaler, A.; Baltensperger, U. *Atmospheric Chemistry and Physics* **2008**, *8*, 6453.
(62) Hynes, R. G.; Angove, D. E.; Saunders, S. M.; Haverd, V.; Azzi, M. *Atmospheric Environment* **2005**, *39*, 7251.
(63) Afif, C.; Jambert, C.; Colomb, A.; Eyglunent, G.; Abboud, B. A., M. ; Daele, V.; Perros, P. E. *Environ. Sci. Technol.* **2009**, *in preparation*.
(64) Pandey, S. K.; Kim, K.-H.; Chung, S.-Y.; Cho, S. J.; Kim, M. Y.; Shon, Z.-H. *Atmospheric Environment* **2008**, *42*, 607.

(65) Rodriguez, J. A.; Jirsak, T.; Liu, G.; Hrbek, J.; Dvorak, J.; Maiti, A. *Journal of the American Chemical Society* **2001**, *123*, 9597.
(66) Hashimoto, K.; Wasada, K.; Toukai, N.; Kominami, H.; Kera, Y. *Journal of Photochemistry and Photobiology a-Chemistry* **2000**, *136*, 103.
(67) Shang, J.; Du, Y.; Xu, Z. *Chemosphere* **2002**, *46*, 93.
(68) Gerischer, H.; Heller, A. *Journal of the Electrochemical Society* **1992**, *139*, 113.
(69) Hirakawa, T.; Daimon, T.; Kitazawa, M.; Ohguri, N.; Koga, C.; Negishi, N.; Matsuzawa, S.; Nosaka, Y. *Journal of Photochemistry and Photobiology A: Chemistry* **2007**, *190*, 58.
(70) Obee, T. N. *Environ. Sci. Technol.* **1996**, *30*, 3578.
(71) Obee, T. N.; Brown, R. T. *Environ. Sci. Technol.* **1995**, *29*, 1223.
(72) Liu, H.; Lian, Z.; Ye, X.; Shangguan, W. *Chemosphere* **2005**, *60*, 630.
(73) Gueymard, C. A., Myers, D., and Emery, K.: . *Solar Energy, 73, 443-467, http://rredc.nrel.gov/solar/spectra/am1.5/#Gueymard2* **2002**.
(74) Clifford, D.; Donaldson, D. J.; Brigante, M.; D'Anna, B.; George, C. *Environmental Science & Technology* **2008**, *42*, 1138.
(75) Hanisch, F.; Crowley, J. N. *J. Phys. Chem. A* **2001**, *105*, 3096.
(76) Jammoul, A.; Gligorovski, S.; George, C.; D'Anna, B. *J. Phys. Chem. A* **2008**, *112*, 1268.
(77) McNeill, V. F.; Wolfe, G. M.; Thornton, J. A. *J. Phys. Chem. A* **2007**, *111*, 1073.
(78) Mmereki, B. T.; Donaldson, D. J. *J. Phys. Chem. A* **2003**, *107*, 11038.
(79) Poeschl, U.; Letzel, T.; Schauer, C.; Niessner, R. *J. Phys. Chem. A* **2001**, *105*, 4029.
(80) Dibble, L. A.; Raupp, G. B. *Catal. Lett.* **1990**, *4*, 345.
(81) Zhang, C.; He, H.; Tanaka, K.-i. *Applied Catalysis B: Environmental* **2006**, *65*, 37.
(82) Xu, B.-Y.; Zhu, T.; Tang, X.-Y.; Ding, J.; Li, H.-J. *Gaodeng Xuexiao Huaxue Xuebao* **2006**, *27*, 1912.
(83) Li, P.; Perreau, K.; Covington, A.; Song, E.; Carmichael, C. H.; G. R. Grassian, V. H. *J. Geophys. Res., [Atmos.]* **2001**, *106*, 5517.
(84) Carlos-Cuellar, S.; Li, P.; Christensen, A. P.; Krueger, B. J.; Burrichter, C.; Grassian, V. H. *The Journal of Physical Chemistry A* **2003**, *107*, 4250.
(85) Theurer, W. *Atmos. Environ.* **1999**, *33*, 4057.
(86) Diamond, M. L.; Priemer, D. A.; Law, N. L. *Chemosphere* **2001**, *44*, 1655.
(87) Kwamena, N.-O. A.; Clarke, J. P.; Kahan, T. F.; Diamond, M. L.; Donaldson, D. J. *Atmos. Environ.* **2007**, *41*, 37.
(88) Abdullah, H. Z.; Taib, H.; Sorrell, C. C. *Adv. Appl. Ceram.* **2007**, *106*, 105.
(89)
(90) Stief, L. J.; Nava, D. F.; Payne, W. A.; Michael, J. V. *The Journal of Chemical Physics* **1980**, *73*, 2254.
(91) Calvert, J. G. "The homogeneous chemistry of formaldehyde generation and destruction within the atmosphere," Chemistry Department, Ohio State University, 1980.
(92) Finalyson-Pitts, B. J.; Pitts, J. N. *Academic press* **2000**, 2.
(93) Lim, T. H.; Jeong, S. M.; Kim, S. D.; Gyenis, J. *Journal of Photochemistry and Photobiology A: Chemistry* **2000**, *134*, 209.
(94) Monge, M.; D'Anna, B.; George, C. *Submitted to Physical Chemistry Chemical Physics*.
(95) Schuttlefield, J.; Rubasinghege, G.; El-Maazawi, M.; Bone, J.; Grassian, V. H. *Journal of the American Chemical Society* **2008**, *130*, 12210.
(96) Nicolas, M. l.; Ndour, M.; Ka, O.; D'Anna, B.; George, C. *Environmental Science & Technology* **2009**, *43*, 7437.

VI. ANNEX : REPRINT OF PUBLISHED PAPERS

Atmospheric Environment xxx (2009) 1–8

Contents lists available at ScienceDirect

Atmospheric Environment

journal homepage: www.elsevier.com/locate/atmosenv

Kinetics of the tropospheric formaldehyde loss onto mineral dust and urban surfaces

Maria Sassine [a,b], Laurence Burel [a,b], Barbara D'Anna [a,b], Christian George [a,b,*]

[a] Université de Lyon, Lyon F-69626, France
[b] CNRS, UMR5256, IRCELYON, Institut de recherches sur la catalyse et l'environnement de Lyon, Villeurbanne F-69626, France

ARTICLE INFO

Article history:
Received 20 March 2009
Received in revised form
23 July 2009
Accepted 24 July 2009

Keywords:
Heterogeneous reaction
HCHO
TiO_2 mineral coatings
Dust
Urban surfaces

ABSTRACT

The kinetics of the heterogeneous reaction between gaseous HCHO and TiO_2/SiO_2 mineral coatings were investigated using a coated-wall flow tube to mimic HCHO loss on mineral aerosol and TiO_2 coated depolluting urban surfaces. The measured uptake kinetics were strongly enhanced when the flow tube was irradiated with 340–420 nm UV light with an irradiance of 1.45 mW cm^{-2}. The associated BET uptake coefficients ranged from $(3.00 \pm 0.45) \times 10^{-9}$ to $(2.26 \pm 0.34) \times 10^{-6}$ and were strongly dependent on HCHO initial concentration, relative humidity, temperature, and TiO_2 content in the mineral coating, which ranged from 3.5 to 32.5 ppbv, 6–70%, 278–303 K, and 1–100 %wt, respectively. The measured kinetics were well described using a Langmuir–Hinshelwood type formalism. The estimated uptake coefficients were used to discuss the importance of heterogeneous HCHO surface loss, in terms of deposition lifetimes, as compared to major homogeneous gas-phase losses such as OH reaction and photolysis. It is found that deposition may compete with gas-phase removal of HCHO in a dense urban environment if more than 10% of the urban surface is covered with TiO_2 treated material.

1. Introduction

Formaldehyde (HCHO) is an important and highly reactive compound present in all regions of the atmosphere, arising from the oxidation of biogenic and anthropogenic hydrocarbons, and is a key compound in tropospheric chemistry. It is a strong HO_x source (through its photolysis) and is therefore strongly connected to regional O_3 production. The main HCHO removal processes from the atmosphere are currently thought to be its photolysis and the reaction with OH according to (Atkinson, 2000):

$$HCHO + h\nu \rightarrow H_2 + CO \quad (\lambda < 360\ nm) \tag{1a}$$

$$HCHO + h\nu \rightarrow H^{\cdot} + HCO \quad (\lambda < 325\ nm) \tag{1b}$$

$$HCHO + OH^{\cdot} \xrightarrow{O_2} HO_2^{\cdot} + H_2O + CO \tag{2}$$

These removal processes are homogeneous and will happen throughout the troposphere. However, it is also known that HCHO is chemically taken up in the atmosphere by sulphuric acid aerosols (Iraci and Tolbert, 1997). Therefore, it is worth investigating whether similar heterogeneous reactions may occur on other surfaces such as mineral surfaces or buildings.

At the global scale, mineral dust aerosol relates to climate, biogeochemical cycles (Andy, 2002), human health (Derbyshire, 2007) as well as atmospheric chemistry (Dentener et al., 1996). In fact, dust surfaces exposed to trace gases may promote chemical reactions that do not occur in purely homogeneous media. Recently, we showed that the uptake of otherwise unreactive gases (i.e., O_3 and NO_2) is strongly enhanced on mineral oxide surfaces (Ndour et al., 2008a,b) and may be related to traces of TiO_2 present in dust particles irradiated with UV light. A similar enhancement could exist for HCHO conversion on mineral dust surfaces.

At the local scale, air pollution and NO_x levels due to traffic is one of the most pressing problems in urban areas. In order to adhere to regulations requiring a reduction in emissions, the use of photocatalytic self-cleaning and "depolluting" materials has been suggested in recent years as a remediation technique in polluted urban environments (Fujishima and Hashimoto, 1996). Some of these commercial products are based on the photocatalytic

* Corresponding author at: CNRS, UMR5256, IRCELYON, Institut de recherches sur la catalyse et l'environnement de Lyon, Villeurbanne F-69626, France. Tel.: +33 (0) 472431489.
E-mail address: christian.george@ircelyon.univ-lyon1.fr (C. George).

1352-2310/$ – see front matter © 2009 Elsevier Ltd. All rights reserved.
doi:10.1016/j.atmosenv.2009.07.044

properties of TiO_2, which when exposed to sunlight may help in the abatement of atmospheric NO_x. The use of TiO_2 photocatalysis as an environmentally friendly pollution control technology has been reported in many European areas; specifically, a thin layer of TiO_2 can be either deposited at the surface of a material (such as glass or pavement) or embedded in paints constituents and concrete (Beeldens and Van Gemert, 2005; Fujishima and Hashimoto, 1996; Stephan and Wilhelm, 2006), and its applications include not only depollution but also surface maintenance (Van and Montgomery, 1998; Basel, 2008).

Despite the importance of HCHO interactions with TiO_2 surfaces under atmospheric conditions, the details of these reactions are not yet documented. Several previous studies have described the reaction in the dark between HCHO and metals (such as aluminium) (Kieu et al., 2001; Saleh and Hussain, 1986) or some inorganic oxides (such as aluminium oxide Al_2O_3 and ferric oxide Fe_2O_3) (Lur'e and Mikhno, 1999; Xu et al., 2006), as proceeding quite slowly due to weak adsorption of HCHO on such surfaces at ambient temperature. Similar experiments have demonstrated that HCHO reacts with some mineral oxides at 295 K with high initial uptake coefficients that rapidly decreases on the time scale of a few minutes (Carlos-Cuellar et al., 2003; Grassian, 2001; Li et al., 2001; Usher et al., 2003). Other studies (Liu et al., 2005; Obee and Brown, 1995) focused on the photocatalytic degradation of HCHO on pure TiO_2 coatings or TiO_2–Fe_2O_3 mixtures (Yang et al., 2000) at high HCHO concentrations (0.5–100 ppmv), which are not representative of atmospheric conditions or dust composition. Hence, to our knowledge, little is known about the heterogeneous chemistry of HCHO on mineral oxide surfaces or its overall significance in the atmosphere.

Accordingly, the objective of this work was to investigate whether surface reactions on mineral coatings containing variables amount of TiO_2 could be a significant tropospheric sink of HCHO in both the free troposphere (mineral dust containing traces up to 5 %wt of TiO_2) and urban environments (almost pure TiO_2). In this study, we used a coated-wall flow tube to investigate the uptake kinetics of HCHO onto coatings composed of TiO_2/SiO_2 mixtures. We also examined the effect of temperature, relative humidity, HCHO concentration and TiO_2 content on the uptake coefficient. The measured uptake coefficients at pure TiO_2 surfaces were used to assess the case of HCHO loss in an urban environment through dry deposition processes. In this manner, HCHO deposition lifetimes were calculated and compared to major photochemical HCHO removal pathways.

2. Experimental section

2.1. Mineral oxides: preparation and characterization

Experiments were performed with different mass mixing ratios of mineral oxides, in the range from 1 to 100 %wt, by diluting titanium dioxide TiO_2 (Degussa-P25, 80% anatase, 20% rutile; P25) in silica SiO_2 (Degussa Aerosil 130). All mixtures were prepared by suspending 3 g of the mineral oxides in 30 mL of ultra pure water (Aquadem milli-Q50). A few milliliters of the sonicated suspensions were dripped uniformly into dry Pyrex tubes (20 cm × 1.1 cm i.d.) that were then rotated and dried at 373 K. The resulting film covered the entire inner surface of the tube and, to the eye, was fairly uniform in thickness.

Characterization of the dried film was performed using scanning electron microscopy (SEM) coupled to energy dispersive X-ray spectroscopy (EDX). For this purpose, the Pyrex tubes were cut into 1-cm long samples (considering finally only both ends and middle parts of the tube) and dipped vertically into a mould containing an epoxy resin (araldite epoxy CY 230-ESCIL) and an epoxy resin hardener (HY 956-ESCIL) in a ratio of 2.5:1 (resin:hardener). After 12 h, the mixture dried and hardened, forming a polymer at room temperature. The polymer section (holding the tubes) was then polished (ESC 200 GTL polisher from ESCIL) for better image resolution. Finally, these SEM samples were coated with a thin layer of gold to enable electron conduction to the observed area. Films with different TiO_2 mixing ratios (1, 5, 50 and 100 %wt) were observed. In addition, the analysis of different zones confirmed the uniformity of the film along the length of the tube for each sample. Film thicknesses ranged from 20 to 30 μm. Fig. 1 shows both the SEM image of a TiO_2/SiO_2 coating (50 %wt) (part a) and the surface profile of an area scanned from 0 (the Pyrex surface) to 40 μm (polymer matrix) (part b). It is clear that the film adheres strongly to the Pyrex surface, fitting with any surface defect (see Fig. 1a). The EDX detection of the yellow line scanned in Fig. 1a corroborates the film's chemical composition. More specifically, there are two successive silicon signal in the scanning profile from the Pyrex surface to the polymer matrix, which are due to the Pyrex composition (higher peak) and to the coating (lower peak). The titanium signal begins at a distance of 11 μm and extends to 35 μm (Fig. 1), thus indicating a film thickness of 24 μm. It reaches the concentration of the lower silicon peak since both TiO_2 and SiO_2 are equally distributed in the film (TiO_2 50 %wt/SiO_2 50 %wt coating). Note that the Ti and Si concentrations are estimated to 15 %wt of the coating as the gold deposited at the SEM sample is also detected. The cartography of another 50 %wt TiO_2 sample scanned from the Pyrex glass tube (right) to the film (left) (shown with a 4000 magnification in Fig. 1c) proves that the Ti and Si atoms are equally and homogeneously distributed in a 50 % TiO_2 film.

2.2. Flow tube reactor

The heterogeneous interactions between formaldehyde and mineral surfaces were studied by exposing films of TiO_2/SiO_2 mixtures to known HCHO concentrations. All experiments were performed under atmospheric pressure and at constant temperature in a reactor described elsewhere (Jammoul et al., 2008). A cylindrical Pyrex tube coated with the reactive surface and not used for imaging was introduced into the constant-temperature reactor, which was surrounded with fluorescent lamps (UV Black-Light-Blue OSRAM Sylvania TLD 15W/08) emitting in the spectral range between 340 and 420 nm with $\lambda_{MAx} = 365$ nm. The spectral irradiance $E(\lambda)$ reaching the inner surface of the reactor has been quantified previously (Jammoul et al., 2008). The gas flows (N_2) were controlled by mass flow controllers (Brooks electronic). All gases were introduced into the reactor via a tubular movable injector (0.3 cm outer radius ending with a porous section). Using a total gas flow of 500 mL min^{-1}, no gas-phase photodissociation of HCHO was observed, and laminar flow conditions were established within the first centimetre of the flow tube ($Re < 100$).

2.3. HCHO generator and analyzer

Gaseous formaldehyde was introduced into the reactor in a flow of nitrogen through a home-made silicon permeation tube immersed in a 3.7 %wt HCHO solution. The temperature was held at 298 K, and the relative humidity exiting the permeation tube was ca. 6%.

The gas flow exiting the reactor was monitored with a portable HCHO analyzer developed at IRCELYON (Sassine et al., in preparation). In this novel analyzer, formaldehyde is stripped out of the gas flow via a glass tube sampler and undergoes derivatization with 3-Methyl-2-benzothiazolinone hydrazone (MBTH) in two successive steps in order to form a strongly absorbing chromophore

Please cite this article in press as: Sassine, M., et al., Kinetics of the tropospheric formaldehyde loss onto mineral dust and urban surfaces, Atmospheric Environment (2009), doi:10.1016/j.atmosenv.2009.07.044

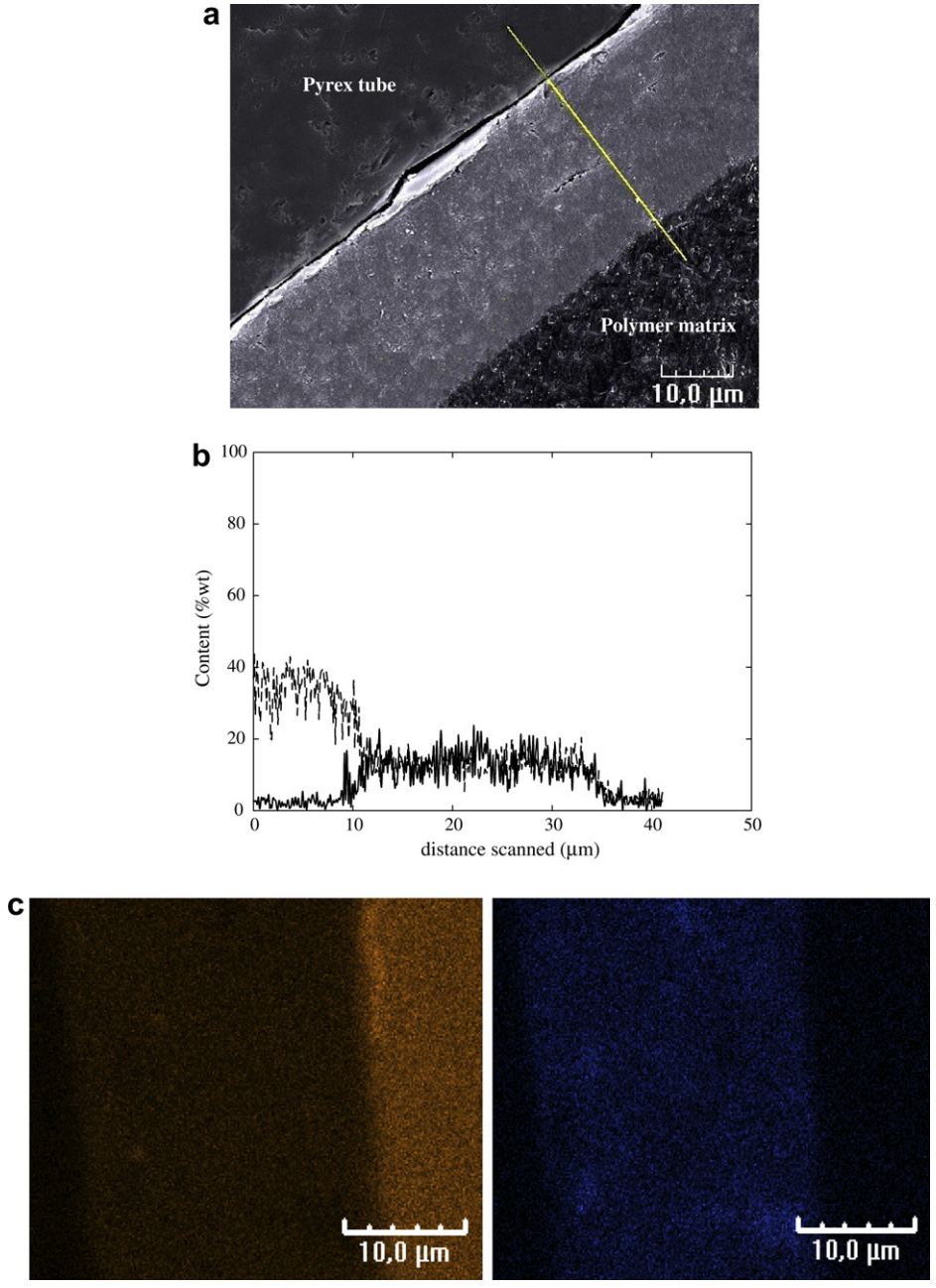

Fig. 1. (a) SEM image showing the interface of 50 %wt TiO_2/SiO_2 coating, (b) Surface profile of the yellow line scanned in part (a) displaying Ti (full line) and Si (dashed-line) concentrations (c) Cartography of another 50 %wt TiO_2 coating showing Ti (blue) and Si (yellow) distribution in the film.

(Sawicki et al., 1961). The detection, in solution, of the converted HCHO was realized by means of a combination of a spectrograph (Andor technology/Shamrock SR – 163 i) coupled to a CCD camera (Andor Technology/iDus DV-420). Teflon AF2400 tubing (Biogeneral) was used as the UV–vis long path cell (Dasgupta et al., 1998). Combining the strongly absorbing chromophore with a 100-cm long optical path led to a detection limit of ca. 3 pptv with a resolution time of 15–30 min. These formaldehyde measurements were validated against optical and chromatographic methods. Calibrations with Differential Optical Absorption Spectroscopy (DOAS) and Fourier transform infrared spectroscopy (FTIR) showed less than 6% deviation. Similar results were found when HCHO measurements were compared with those obtained using liquid chromatography coupled to UV-DAD detection subsequent to DNPH titration, and were independent of the method between Sepack cartridges (Grosjean, 1991) and Radiello passive tubes trapping techniques (Clarisse et al., 2003).

2.4. Kinetic analysis

The uptake rate of HCHO on the mineral surfaces was determined by monitoring its loss in the gas phase as a function of the position of the movable injector, i.e., as a function of the exposure time of the oxide surface to the gas. The linear fit (Fig. 2) of the measured HCHO concentrations at different exposure times is typically used to derive an apparent pseudo-first-order coefficient (k_{obs}) for HCHO decay.

Please cite this article in press as: Sassine, M., et al., Kinetics of the tropospheric formaldehyde loss onto mineral dust and urban surfaces, Atmospheric Environment (2009), doi:10.1016/j.atmosenv.2009.07.044

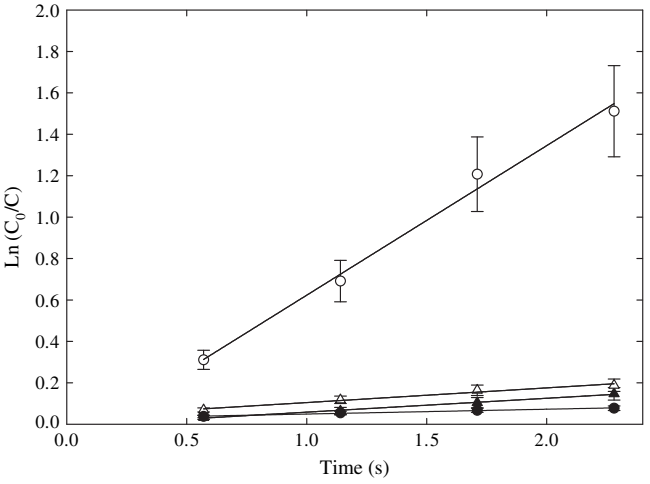

Fig. 2. Kinetic of logarithmic HCHO decay as a function of residence time for 11 ppb of HCHO, at 298 K at 6% of RH on different films mixing ratios. Circles and triangles correspond to measurements performed with pure TiO_2 and pure SiO_2 coatings respectively. Open and dark symbols are assigned to illuminated and dark conditions.

$$k_{obs} = \frac{1}{4}\gamma_{BET} \times < c > \times \left(\frac{S_{BET}}{V_{tube}}\right) \quad (3)$$

Consequently, HCHO lifetime can be approximated as follows:

$$\tau = \frac{1}{k_{obs}} = \left(\frac{V_{tube}}{S_{BET}}\right) \times \frac{4}{\gamma_{BET} \times < c >} \quad (4)$$

where k_{obs} is the observed rate constant of the reaction, $<c>$ is the mean molecular speed of gaseous HCHO, and V_{tube} is the volume of the flow tube. S_{BET} is the BET area of the entire inorganic sample exposed to gas interaction and γ_{BET} is the mass-independent uptake coefficient taking into account the entire sample surface (not just the geometric upper-most surface) (Grassian, 2001; Michel et al., 2003; Underwood et al., 2000, 2001). A linear dependence of the observed uptake rate on sample mass was observed, indicating that the use of BET sample area is appropriate in the calculation of the uptake coefficient.

The experimental data presented in the paper have been corrected for diffusion limitation using the Cooney–Kim–Davis (CKD) method, (Behnke et al., 1997; Cooney et al., 1974), which takes into account axial and lateral diffusion combined with a first-order loss at the inner surface of a cylindrical tube under laminar flow conditions. The diffusion coefficient was calculated using the formula proposed by Fuller et al. (Fuller et al., 1969). At atmospheric pressure and 273 K, the calculated ozone diffusion coefficient was 0.22 cm^2 s^{-1}. Under most experimental conditions, the radial diffusion correction was negligible for geometric uptake coefficients below 4×10^{-6} (less than 10% of the experimental value), and it increased progressively with increasing geometric uptake coefficient to a maximum of 50% correction for geometric uptake coefficients of 4×10^{-5}.

The kinetic parameters were determined after 30 min of exposure to the film. This delay corresponds to the response time of the HCHO analyzer, which is based on the time needed for the HCHO concentration to reach a plateau and at which point the steady-state uptake coefficient (γ_{ss}) can be determined. However, kinetics tests performed with an exposure time of 3.5 h showed no HCHO saturation at the TiO_2-doped surface, suggesting that HCHO uptake was sustained for the entire exposure period.

The experiments were conducted with an HCHO mixing ratio between 3.5 and 32.5 ppbv, a TiO_2 content from 1 to 100 %wt, a film mass range between 6 and 40 mg and a relative humidity between 6 and 70%.

3. Results

For all mineral coatings used in this study, the BET uptake coefficients derived from dark experiments were very low (of the order of 3×10^{-9}). This indicates a weak loss of HCHO on the surface, which is, within our sensitivity, independent of the TiO_2/SiO_2 mixing ratio.

In the case of pure SiO_2 films, our observations were similar to those of Carlos-Cuellar et al. (2003), who reported low reactivity of HCHO. Under both dark and UV-light conditions, uptake coefficients of $(3.1 \pm 0.5) \times 10^{-9}$ were measured, suggesting that no photoenhancement occurred.

A very different behavior is observed for HCHO uptake onto a TiO_2-doped surface that is exposed to weak near-UV irradiation (irradiance of 2.7×10^{15} photons cm^{-2} s^{-1} in the 340–420 nm range). In this case, the uptake is markedly photoenhanced (nearly 40 times greater than under dark conditions (see Fig. 2)). Under steady-state conditions, these findings underline the importance of photocatalytic HCHO removal at the surface of a film containing traces of TiO_2. HCHO degradation by photocatalytic engineered systems has been described in the literature (Liu et al., 2005; Obee and Brown, 1995). It is suggested that the photocatalytic oxidation of HCHO is due to surface reaction with OH radicals that are produced from the interaction between adsorbed water and the electron holes that are created when TiO_2 is irradiated with UV light. However, to our knowledge, there are no data available for the HCHO uptake coefficient on irradiated mineral dust films or any proxy of them to be used for atmospheric purposes.

The irradiance used in this study is approximately 5 times less than the solar irradiance between 340 and 420 nm reaching the Earth surface (Gueymard et al., 2002). We therefore investigated the dependence of the BET steady-state uptake coefficient on irradiance under conditions of 293 K, 30% RH and 2 ppbv of HCHO. As shown in Fig. 3, the BET uptake coefficient is linearly dependent on the irradiance, which varied from 1.9×10^{15} to 2.7×10^{15} photons cm^{-2} s^{-1}, thus confirming the heterogeneous photochemical nature of the HCHO loss. If the linearity observed in Fig. 3 is extrapolated to the irradiance reaching the surface of the Earth in the same wavelength range at fixed HCHO mixing ratio and

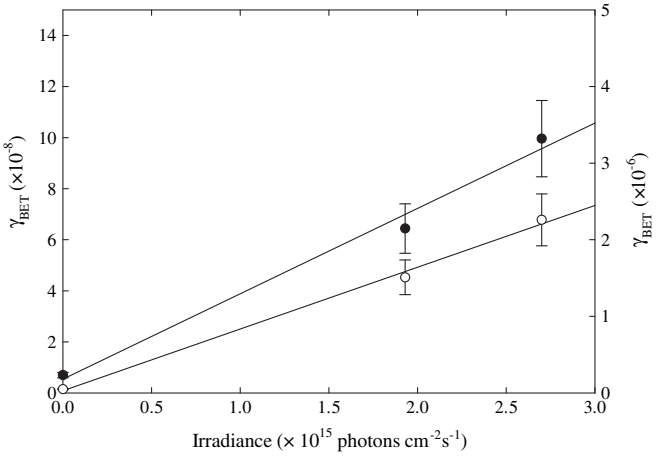

Fig. 3. Dependence of the uptake coefficient as a function of UV light irradiance. Experiments were conducted with 2 ppbV of HCHO at 30% of RH and 293 K. Filled and open circles are raw data carried with 5 %wt of TiO_2 diluted in SiO_2 and pure TiO_2 coatings respectively. The latter data are related to the right hand scale.

Please cite this article in press as: Sassine, M., et al., Kinetics of the tropospheric formaldehyde loss onto mineral dust and urban surfaces, Atmospheric Environment (2009), doi:10.1016/j.atmosenv.2009.07.044

humidity, then it is possible to estimate an atmospherically relevant uptake coefficient. The BET uptake coefficients are normalized to the measured irradiance I reaching the film during the experiments, according to:

$$\Gamma_{\text{phot}} = \frac{\gamma_{\text{BET}}}{I} \quad (5)$$

where the obtained normalized coefficient, Γ_{phot}, has units of $(\text{mW cm}^{-2})^{-1}$. For the majority of the experiments, I was equal to 1.45 mW cm^{-2} Γ_{phot} can be multiplied by the irradiance reaching the Earth's surface or the troposphere, thus facilitating a rough assessment of the impact of light on the heterogeneous HCHO chemistry on SiO_2–TiO_2 oxides, provided that all other parameters are kept constant (see discussion).

Another important atmospheric variable parameter is the initial HCHO mixing ratio. The uptake coefficients were observed to be inversely dependent on the initial gaseous HCHO concentration. Fig. 4 shows the uptake coefficient decreasing from $(6.0 \pm 0.9) \times 10^{-7}$ to $(2.0 \pm 0.3) \times 10^{-7}$ for pure TiO_2 coatings and from $(3.0 \pm 0.5) \times 10^{-8}$ to $(1.5 \pm 0.2) \times 10^{-8}$ for 5 %wt TiO_2 films with increasing HCHO concentration in the range from 3.5 to 32.5 ppbv, with a plateau being attained around 10 ppbv. Our results agree with those reported in many other heterogeneous studies of uptake onto different solid and liquid surfaces, both organic and inorganic (Clifford et al., 2008; Hanisch and Crowley, 2001; Jammoul et al., 2008; McNeill et al., 2007; Mmereki and Donaldson, 2003; Poeschl et al., 2001). More specifically, the inverse of the uptake rate has been observed to depend linearly with the inverse of the HCHO inlet concentration, in agreement with a Langmuir–Hinshelwood formalism.

The effect of water vapor on the uptake process was also investigated between 6 and 70% relative humidity (RH) for both 5 and 100 %wt of TiO_2. As shown in Fig. 5, γ_{BET} decreases at low (below 20%) and high RH (over 50–60%) and reaches a maximum at approximately 30% RH. This indicates that higher amounts of water inhibit surface loss. Such a dependence on the relative humidity has already been reported (Dibble and Raupp, 1990; Obee and Brown, 1995; Zhang et al., 2006) and can be explained by the competitive adsorption of water and the volatile organic compound (VOC) at the surface as well as the decrease in the amount of OH radicals produced at the TiO_2 surface, which is the driving force for HCHO uptake.

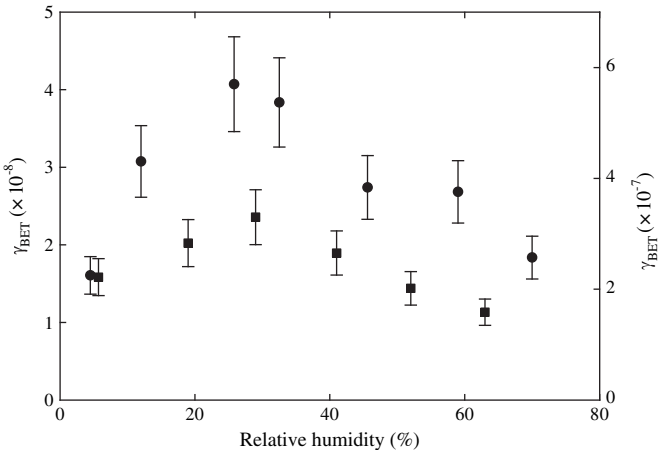

Fig. 5. Effect of RH onto uptake coefficients. Experiments were carried out onto illuminated coatings with 2.7×10^{15} photons cm^{-2} s^{-1} and exposed to 11 ppb of HCHO at 293 K. Squares (■) and circles (●) correspond to measurements performed with 5 %wt of TiO_2 diluted in SiO_2 and pure TiO_2 coatings respectively. The latter data are related to the right hand scale.

The results shown in Fig. 6 indicate that the HCHO uptake coefficient increases with increasing temperature, which were varied between 278 and 298 K. Specifically, the uptake coefficient increased from $(1.8 \pm 0.3) \times 10^{-7}$ to $(3.2 \pm 0.5) \times 10^{-7}$ for pure TiO_2 coatings and from $(4.8 \pm 0.8) \times 10^{-9}$ to $(2.0 \pm 0.3) \times 10^{-8}$ for 5 %wt TiO_2/SiO_2 coatings. As adsorption and chemical reactivity have opposite temperature trends, these observations indicate that surface reactions are dominant in the observed positive dependence on the temperature.

In the real environment, exposed surfaces may have variable TiO_2 content. We therefore tested mixing ratios between 1 and 100 %wt of TiO_2 in a SiO_2 matrix and the experimental results are presented in Fig. 7, showing again a linear dependence of the uptake coefficient with respect to the %wt of TiO_2.

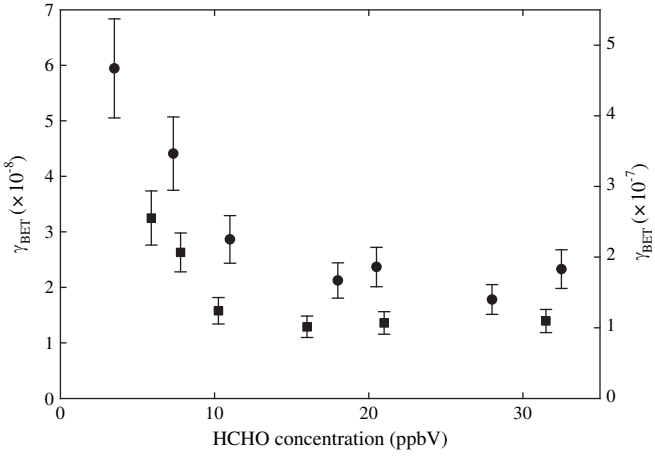

Fig. 4. Trend of uptake coefficient as a function of the introduced HCHO concentration ranging from 3.5 to 32.5 ppbv. Experiments were performed with 6% of RH, at 293 K in UV-light conditions (lamps irradiance = 2.7×10^{15} photons cm^{-2} s^{-1}). Squares (■) and circles (●) correspond to measurements performed with 5 %wt of TiO_2 diluted in SiO_2 and pure TiO_2 coatings respectively. The latter data are related to the right hand scale.

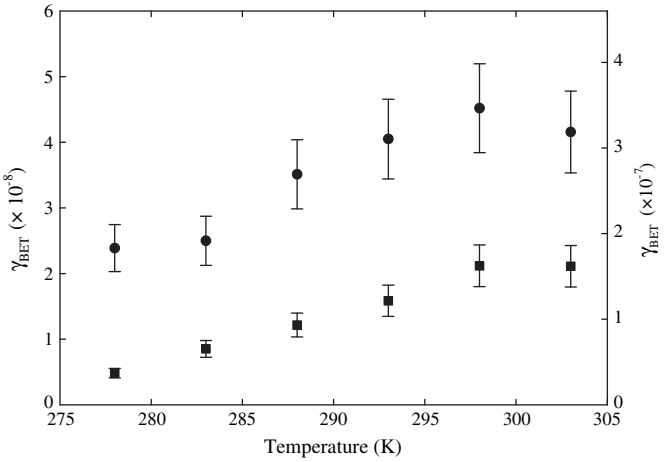

Fig. 6. Effect of Temperature on Uptake coefficient. Experiments were driven with coatings illuminated with 2.7×10^{15} photons cm^{-2} s^{-1} and exposed to 11 ppb of HCHO at 30% of RH. Squares (■) and circles (●) correspond to measurements performed with 5 %wt of TiO_2 diluted in SiO_2 and pure TiO_2 coatings respectively. The latter data are related to the right hand scale.

Please cite this article in press as: Sassine, M., et al., Kinetics of the tropospheric formaldehyde loss onto mineral dust and urban surfaces, Atmospheric Environment (2009), doi:10.1016/j.atmosenv.2009.07.044

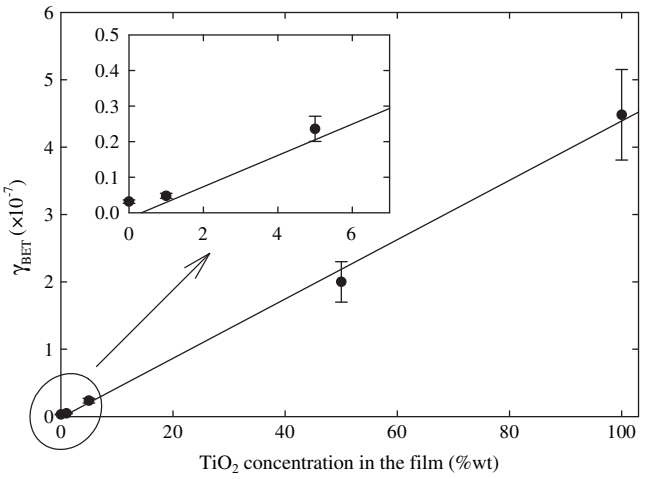

Fig. 7. Dependence of uptake coefficient with respect to TiO_2 content in the coatings. Experiments were performed with coatings irradiated with 2.7×10^{15} photons cm^{-2} s^{-1} and exhibited to 11 ppb of HCHO at 30% of RH and at 293 K.

4. Discussion and atmospheric implications

The data in this study show a strongly enhanced reactivity of synthetic surfaces containing TiO_2 and SiO_2, taken as proxies for atmospheric dust particles when irradiated with weak near-UV light using a coated flow tube reactor. Under dark conditions, the steady-state uptake BET coefficient (determined after 30 min of HCHO exposure time to the surface) is estimated as $(2.97 \pm 0.45) \times 10^{-9}$ onto SiO_2/TiO_2 (5 %wt) films and $(3.18 \pm 0.5) \times 10^{-9}$ onto pure TiO_2 coatings. Our results are smaller than those of Xu et al. (2006), who measured $\gamma_{BET} = (9.4 \pm 1.7) \times 10^{-9}$ on α-Al_2O_3 particles at 293 K (Xu et al., 2006). Initial dark uptake kinetics of HCHO onto pure mineral oxide surfaces (i.e., SiO_2, α-Fe_2O_3, α-Al_2O_3) measured by Grassian and co-workers at 295 K in a Knudsen-cell reactor operating at low pressure and under dry conditions (Carlos-Cuellar et al., 2003; Li et al., 2001) were much greater (γ_{BET} from 3×10^{-7} to 1×10^{-4}) than our values (γ_{BET} approx. 2×10^{-6} for pure illuminated TiO_2 coatings). One difference between the two studies is the low time resolution of the present study compared with the quasi-instantaneous response in the molecular flow reactor. Another difference is rapid surface deactivation observed in the Knudsen-cell study, in contrast to the sustained HCHO uptake during the 3.5-h exposure time measured in our work. In fact, water molecules and other trace gases can strongly interact with mineral oxide surfaces affecting the adsorption and reaction kinetics, thereby modifying HCHO uptake onto the surface. Given the atmospheric relevance of the conditions used in the current work, the photo-induced uptake coefficients reported herein may be useful in determining the global impact of mineral aerosol photochemistry in its role as a sink for HCHO in dust plumes. Assessing the global impact of such dust photochemistry is now facilitated by the photoinduced uptake coefficients reported in this study.

The dry deposition of HCHO is generally not considered as an efficient removal pathway. This was confirmed in the current study as the HCHO uptake rate on pure SiO_2 was very slow. However, adding TiO_2 to construction materials may add a new removal pathway close to the ground. The kinetics information obtained in this study can be used to assess whether and under which conditions HCHO removal through TiO_2-based construction materials may be significant. To do so, we assume an urban area in which TiO_2-based construction materials are deployed at a large scale, i.e., a city in which buildings are coated with a thin layer of TiO_2 (as has already been done in some locations). Let us assume that this TiO_2 layer covers between 0% (the case of most current cities) and 100% (a hypothetical futuristic case where all building are constructed using TiO_2-based construction materials). Using previous modelling studies for dense urban areas (Diamond et al., 2001; Kwamena et al., 2007; Theurer, 1999), which consider both the areas of occupied surface at the ground and shaped constructed surface, we estimate that the building surface exposed to HCHO deposition is 2.25 times the city surface at the ground. Current commercial TiO_2-based construction materials are covered by an approximately 10-nm-thick active TiO_2 layer (Abdullah et al., 2007) having an internal (BET) surface similar to the films explored in this study. This would expose a chemically active surface with a total area of 1.04×10^8 m^2 taking into consideration a ground surface of 46×10^6 m^2 (equivalent to the ground surface of Lyon, France).[1]

To assess if these processes may represent a significant HCHO sink, a simple approach is to compare the lifetimes due to photo-induced uptake on the buildings with those due to the main removal processes, i.e., photolysis or reaction with OH. The lifetimes associated with the main processes are readily available from the literature. Assuming an average OH concentration of 10^6 molecules cm^{-3}, the OH channel lifetime is calculated to be almost 26 h (Stief et al., 1980). Given a solar zenith angle of 30° and therefore an irradiance of 1.92×10^{17} photons cm^{-2} s^{-1} (Calvert, 1980; Finalyson-Pitts and Pitts, 2000), HCHO is photolysed with a lifetime of 6 h. The heterogeneous pathway (i.e., degradation at the surface of TiO_2-based construction materials) is evaluated using the uptake coefficient derived in this study.

To a first approximation, equation (4) can be used to calculate the HCHO lifetime by replacing the volume of the tube with the volume of air in the urban environment (simply defined as the ground surface times the mixing height) and the surface with the total surface of photocatalytically active material deployed in this virtual city. For these calculations, we used the uptake coefficient measured at 2 ppbv at 30% relative humidity and 293 K. Linear extrapolation of this value to realistic solar conditions ($I = 1.21 \times 10^{16}$ photons cm^{-2} s^{-1}) in the UV region (340–420 nm) gives an estimate of $(9.7 \pm 1.4) \times 10^{-6}$ for the uptake coefficient onto pure TiO_2 films.

Assuming a mixing height (h) between 50 and 500 m, the HCHO lifetime can be approximated as:

$$\tau_d(\mathrm{h}) = \frac{5.47 \times 10^6 \times h(\mathrm{m})}{S(\mathrm{m}^2)} \quad (6)$$

Fig. 8 compares all three estimated lifetimes as a function of the urban TiO_2 coverage. From this figure, it is apparent that HCHO loss increases significantly from high to low mixing heights where the deposition process is occurring. Compared to HCHO loss by means of $OH^{\cdot}$ reaction, deposition onto urban surfaces from heights ranging from 100 to 200 m is significant if 20 and 40% of the construction surface is covered by pure TiO_2. Moreover, we note that for the upper mixing heights, HCHO concentrations are estimated to be smaller, which implies faster kinetics deposition, according to Fig. 4. In this case, one may reconsider uptake coefficient values in the calculation of HCHO lifetime.

Hence, for low mixing heights, e.g., 50 m (or, in other words, in close vicinity of buildings), the removal by active depolluting material can compete with other homogeneous removal pathways if 10% or more of the building are covered with TiO_2. Moreover, if 40% of urban surfaces or more is activated then the heterogeneous removal may dominate over OH reaction and photolysis. Therefore, this hypothetical exercise suggests that implementing TiO_2-based

[1] http://www.lyon.fr/vdl/sections/en/vie_democratique/institutions/ville_lyon_1.

Please cite this article in press as: Sassine, M., et al., Kinetics of the tropospheric formaldehyde loss onto mineral dust and urban surfaces, Atmospheric Environment (2009), doi:10.1016/j.atmosenv.2009.07.044

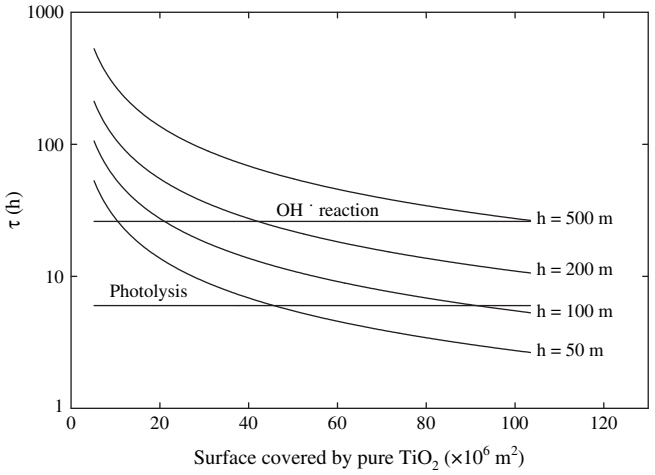

Fig. 8. Lifetimes of HCHO due to photolysis, reaction with $OH^{\cdot}$ and deposition process onto mineral surfaces. The latter trends are represented as a function of surface covered by TiO_2 coatings for different air mixing heights (ranging from 50 to 500 m).

construction materials can, for the specific case of HCHO, provide an additional sink that could contribute to the improvement of urban air quality.

5. Conclusions

This paper describes the kinetics of HCHO loss onto TiO_2/SiO_2 films to simulate the loss onto mineral aerosol and urban surfaces over atmospherically relevant conditions. The uptake kinetics of the HCHO heterogeneous reaction is explained using a Langmuir-Hinshelwood mechanism.

The measured uptake coefficients were used to estimate the lifetime of HCHO in a city where buildings are treated with TiO_2-active surfaces. It is estimated that this process may significantly reduce the HCHO level in the direct vicinity of the building surfaces.

Acknowledgments

We acknowledge the French Ministry for Environment for support from the Primequal2 grant PhotoBat and the ANR for support from the NeoRad grant. For support with the MS and and the HCHO analyzer, we acknowledge the region Rhône-Alpes (Cluster 5) and the French research ministry for the DALD grant through ACI.

References

Abdullah, H.Z., Taib, H., Sorrell, C.C., 2007. Coating methods for self-cleaning thick films of titania. Adv. Appl. Ceram. 106 (1/2), 105–112.

Andy, J.R., 2002. Dust in the Earth system: the biogeochemical linking of land, air and sea. Philos. Trans. R. Soc. A: Math. Phys. Eng. Sci. 360 (1801), 2905–2924.

Atkinson, R., 2000. Atmospheric Chemistry of VOCs and NO_x. Air Pollution Research Center, Department of Environmental Sciences, and Department of Chemistry, University of California, Riverside, CA, USA, pp. 7–14.

Basel, B., 2008. Paving for Leien Boulevard Antwerp, Belgium. Nano Mater., 116 (Part 14).

Beeldens, A., Van Gemert, D., 2005. Experimental investigation of efficiency of TiO_2-cement coating for self-cleaning and air purification. RILEM Proceedings PRO 41(RILEM International Symposium on Environment-Conscious Materials and Systems for Sustainable Development, 2004), pp. 353–359.

Behnke, W., George, C., Scheer, V., Zetzsch, C., 1997. Production and decay of $ClNO_2$ from the reaction of gaseous N_2O_5 with NaCl solution: bulk and aerosol experiments. J. Geophys. Res. 102, 3795–3804.

Calvert, J.G., 1980. The Homogeneous Chemistry of Formaldehyde Generation and Destruction Within the Atmosphere, pp. 153–190. Chemistry Department, Ohio State University, Columbus, USA.

Carlos-Cuellar, S., Li, P., Christensen, A.P., Krueger, B.J., Burrichter, C., Grassian, V.H., 2003. Heterogeneous uptake kinetics of volatile organic compounds on oxide surfaces using a Knudsen cell reactor: adsorption of acetic acid, formaldehyde, and methanol on α-Fe_2O_3, α-Al_2O_3, and SiO_2. J. Phys. Chem. A 107 (21), 4250–4261.

Clarisse, B., Laurent, A.M., Seta, N., Le Moullec, Y., El Hasnaoui, A., Momas, I., 2003. Indoor aldehydes: measurement of contamination levels and identification of their determinants in Paris dwellings. Environ. Res. 92 (3), 245–253.

Clifford, D., Donaldson, D.J., Brigante, M., D'Anna, B., George, C., 2008. Reactive uptake of ozone by chlorophyll at aqueous surfaces. Environ. Sci. Technol. 42 (4), 1138–1143.

Cooney, D.O., Kim, S.S., Davis, E.J., 1974. Analyses of mass-transfer in hemodialyzers for laminar blood-flow and homogeneous dialysate. Chem. Eng. Sci. 29, 1731–1738.

Dasgupta, P.K., Zhang, G., Poruthoor, S.K., Caldwell, S., Dong, S., Liu S.-, Y., 1998. High-sensitivity gas sensors based on gas-permeable liquid core waveguides and long-path absorbance detection. Anal. Chem. 70 (22), 4661–4669.

Dentener, F.J., Carmichael, G.R., Zhang, Y., Lelieveld, J., Crutzen, P.J., 1996. Role of mineral aerosol as a reactive surface in the global troposphere. J. Geophys. Res. 101 (D17), 22869–22889.

Derbyshire, E., 2007. Natural minerogenic dust and human health. Ambio 36 (1), 73–77.

Diamond, M.L., Priemer, D.A., Law, N.L., 2001. Developing a multimedia model of chemical dynamics in an urban area. Chemosphere 44 (7), 1655–1667.

Dibble, L.A., Raupp, G.B., 1990. Kinetics of the gas-solid heterogeneous photocatalytic oxidation of trichloroethylene by near UV illuminated titanium dioxide. Catal. Lett. 4 (4), 345–354.

Finalyson-Pitts, B.J., Pitts, J.N., 2000. Chemistry of the Upper and Lower Atmosphere. Academic Press, pp. 2–423.

Fujishima, A., Hashimoto, K., 1996. Self Cleaning and Antibacterial Effects of TiO_2 Containing and Coated Materials. Book of Abstracts, 211th ACS National Meeting, New Orleans, LA, 263 pp.

Fuller, E.N., Ensley, K., Giddings, J.C., 1969. Diffusion of halogenated hydrocarbons in helium. The effect of structure on collision cross sections. J. Phys. Chem. 73 (11), 3679–3685.

Grassian, V.H., 2001. Heterogeneous uptake and reaction of nitrogen oxides and volatile organic compounds on the surface of atmospheric particles including oxides, carbonates, soot and mineral dust: implications for the chemical balance of the troposphere. Int. Rev. Phys. Chem. 20 (3), 467–548.

Grosjean, D., 1991. Ambient levels of formaldehyde, acetaldehyde and formic acid in southern California: results of a one-year baseline study. Environ. Sci. Technol. 25 (4), 710–715.

Gueymard, C.A., Myers, D., Emery, K., 2002. Proposed reference irradiance spectra for solar energy systems testing. Solar Energy 73, 443–467. http://rredc.nrel.gov/solar/spectra/am1.5/#Gueymard2.

Hanisch, F., Crowley, J.N., 2001. Heterogeneous reactivity of gaseous nitric acid on Al_2O_3, $CaCO_3$, and atmospheric dust samples: a Knudsen cell study. J. Phys. Chem. A 105 (13), 3096–3106.

Iraci, L.T., Tolbert, M.A., 1997. Heterogeneous interaction of formaldehyde with cold sulfuric acid: implications for the upper troposphere and lower stratosphere. J. Geophys. Res. [Atmos.] 102 (D13), 16099–16107.

Jammoul, A., Gligorovski, S., George, C., D'Anna, B., 2008. Photosensitized heterogeneous chemistry of ozone on organic films. J. Phys. Chem. A 112 (6), 1268–1276.

Kieu, L., Boyd, P., Idriss, H., 2001. Modelling of the adsorption of formic acid and formaldehyde over rutile TiO_2(1 1 0) and TiO_2(0 1 1) clusters. J. Mol. Catal. A: Chem. 176 (1–2), 117–125.

Kwamena, N.-O.A., Clarke, J.P., Kahan, T.F., Diamond, M.L., Donaldson, D.J., 2007. Assessing the importance of heterogeneous reactions of polycyclic aromatic hydrocarbons in the urban atmosphere using the Multimedia Urban Model. Atmos. Environ. 41 (1), 37–50.

Li, P., Perreau, K.A., Covington, E., Song, C.H., Carmichael, G.R., Grassian, V.H., 2001. Heterogeneous reactions of volatile organic compounds on oxide particles of the most abundant crustal elements: surface reactions of acetaldehyde, acetone, and propionaldehyde on SiO_2, Al_2O_3, Fe_2O_3, TiO_2, and CaO. J. Geophys. Res. 106 (D6), 5517–5529.

Liu, H., Lian, Z., Ye, X., Shangguan, W., 2005. Kinetic analysis of photocatalytic oxidation of gas-phase formaldehyde over titanium dioxide. Chemosphere 60 (5), 630–635.

Lur'e, B.A., Mikhno, A.V., 1999. Adsorption and kinetics of oxidation of formaldehyde on powdered Fe_2O_3. Zh. Fiz. Khim. 73 (6), 1055–1061.

McNeill, V.F., Wolfe, G.M., Thornton, J.A., 2007. The oxidation of oleate in submicron aqueous salt aerosols: evidence of a surface process. J. Phys. Chem. A 111 (6), 1073–1083.

Michel, A.E., Usher, C.R., Grassian, V.H., 2003. Reactive uptake of ozone on mineral oxides and mineral dusts. Atmos. Environ. 37 (23), 3201–3211.

Mmereki, B.T., Donaldson, D.J., 2003. Direct observation of the kinetics of an atmospherically important reaction at the air–aqueous interface. J. Phys. Chem. A 107 (50), 11038–11042.

Ndour, M., D'Anna, B., George, C., Ka, O., Balkanski, Y., Kleffmann, J., Stemmler, K., Ammann, M., 2008a. Photoenhanced uptake of NO_2 on mineral dust: laboratory experiments and model simulations. Geophys. Res. Lett. 35 (5).

Ndour, M., Nicolas, M., D'Anna, B., George, C., Ka, O., 2008b. Photoreactivity of NO_2 on mineral dust originating from different locations of the Sahara desert. Phys. Chem. Chem. Phys.

Please cite this article in press as: Sassine, M., et al., Kinetics of the tropospheric formaldehyde loss onto mineral dust and urban surfaces, Atmospheric Environment (2009), doi:10.1016/j.atmosenv.2009.07.044

Obee, T.N., Brown, R.T., 1995. TiO_2 photocatalysis for indoor air applications: effects of humidity and trace contaminant levels on the oxidation rates of formaldehyde, toluene, and 1,3-butadiene. Environ. Sci. Technol. 29 (5), 1223–1231.

Poeschl, U., Letzel, T., Schauer, C., Niessner, R., 2001. Interaction of ozone and water vapor with spark discharge soot aerosol particles coated with benzo[a]pyrene: O_3 and H_2O adsorption, benzo[a]pyrene degradation, and atmospheric implications. J. Phys. Chem. A 105 (16), 4029–4041.

Saleh, J.M., Hussain, S.M., 1986. Adsorption, desorption, and surface decomposition of formaldehyde and acetaldehyde on metal films nickel, palladium, and aluminum. J. Chem. Soc. Faraday Trans. 82 (7), 2221–2234.

Sassine, M., Picquet-Varrault, B., Perraudin, E., Doussin, F., George, C. Development of a new HCHO analyzer for near-real time aldehydes measurements, in preparation.

Sawicki, E., Hauser, T.R., Stanley, T.W., Elbert, W., 1961. 3-Methyl-2-benzothiazolinone hydrazone test-sensitive new methods for the detection, rapid estimation, and determination of aliphatic aldehydes. Anal. Chem. 33, 93–96.

Stephan, D., Wilhelm, P., 2006. Innovative materials using titanium dioxide – self-cleaning and photocatalytically active building material surfaces. Cement Int. 4 (6) 76–82, 84–85.

Stief, L.J., Nava, D.F., Payne, W.A., Michael, J.V., 1980. Rate constant for the reaction of hydroxyl radical with formaldehyde over the temperature range 228–362 K. J. Chem. Phys. 73 (5), 2254–2258.

Theurer, W., 1999. Typical building arrangements for urban air pollution modelling. Atmos. Environ. 33 (24–25), 4057–4066.

Underwood, G.M., Li, P., Usher, C.R., Grassian, V.H., 2000. Determining accurate kinetic parameters of potentially important heterogeneous atmospheric reactions on solid particle surfaces with a Knudsen cell reactor. J. Phys. Chem. A 104 (4), 819–829.

Underwood, G.M., Li, P., Al-Abadleh, H., Grassian, V.H., 2001. A Knudsen cell study of the heterogeneous reactivity of nitric acid on oxide and mineral dust particles. J. Phys. Chem. A 105 (27), 6609–6620.

Usher, C.R., Michel, A.E., Grassian, V.H., 2003. Reactions on mineral dust. Chem. Rev. 103 (12), 4883–4940.

Van, B.K., Montgomery, D.G., 1998. Self-compacting concrete. A review. J. Australas. Ceram. Soc. 34 (2), 223–228.

Xu, B.-Y., Zhu, T., Tang, X.-Y., Ding, J., Li, H.-J., 2006. Heterogeneous reaction of formaldehyde on surface of alpha-Al_2O_3 particles. Gaodeng Xuexiao Huaxue Xuebao 27 (10), 1912–1917.

Yang, J., Li, D., Zhang, Z., Li, Q., Wang, H., 2000. A study of the photocatalytic oxidation of formaldehyde on $Pt/Fe_2O_3/TiO_2$. J. Photochem. Photobiol. A: Chem. 137 (2–3), 197–202.

Zhang, C., He, H., Tanaka, K.-i, 2006. Catalytic performance and mechanism of a Pt/TiO_2 catalyst for the oxidation of formaldehyde at room temperature. Appl. Catalysis B: Environ. 65 (1–2), 37–43.

Please cite this article in press as: Sassine, M., et al., Kinetics of the tropospheric formaldehyde loss onto mineral dust and urban surfaces, Atmospheric Environment (2009), doi:10.1016/j.atmosenv.2009.07.044

Nitrogen dioxide removal and nitrous acid formation on titanium oxide surfaces—an air quality remediation process?

Maria Eugenia Monge, Barbara D'Anna and Christian George*

Received 8th December 2009, Accepted 15th April 2010
DOI: 10.1039/b925785c

The reactivity of NO_2 on irradiated TiO_2/SiO_2 films was studied, with different TiO_2 contents, as proxies for NO_x de-polluting materials. The influence of the photocatalyst concentration, the role of molecular oxygen and the effect of nitrate on the reactivity of TiO_2 films were investigated. NO, HONO and nitrate anions are produced as a consequence of the NO_2 loss on UV-illuminated TiO_2 films. The photoinduced nitrate conversion into NO_x and HONO at the TiO_2 surface is discussed as being a renoxification process, which involves the NO_3 radical. The presence of O_2 in the carrier gas modifies the NO and HONO production yields in the heterogeneous reaction between NO_2 and TiO_2 as well as the products of the renoxification process. Depending on the nature of the surface, the interaction between NO_2 and nitrate with TiO_2 may generate HONO that may have a negative impact on air quality.

Introduction

Air pollution originating from traffic is an important problem in most urban areas. Nitrogen oxides (NO_x), volatile organic compounds (VOCs) and particulate matter (PM) are some of these pollutants. Not only are there strong associations between ambient air pollution levels and adverse health effects[1] but also their transformation within the atmosphere leads to photochemical air pollution.[2] As a result, several regulations have been implemented to reduce emissions from vehicles[3] and also a new approach has been applied in recent years by considering the use of self-cleaning and de-polluting materials to remove these pollutants.[4–7]

Titanium oxide, TiO_2, has become the material of choice in a variety of remediation processes due to its photocatalytic properties[8,9] and its favourable physical and chemical properties.[9] Besides, it is chemically inert in the dark, not expensive, non toxic and easy to handle. The self-cleaning properties of TiO_2 are ruled by the absorption of band gap light and the production of excited-state conduction-band electrons and valence-band holes, which can react with electron acceptors and electron donors adsorbed on the semiconductor surface.[8] The environmental relevance of TiO_2 is usually related to its overall capacity to deplete organic pollutants from aqueous and gaseous media. Many studies have recently focused on the development of environmentally friendly materials by adding TiO_2 to ordinary building materials such as concrete or by preparing TiO_2 film coatings.[4,5,7,10,11]Although various photocatalytic materials are already on the market, very little reliable information is available, except for limited technical data, regarding their impact on air quality considering the potential formation of harmful intermediates. This scenario motivates further studies in the field.[11]

Université de Lyon, Lyon, F-69626, France; université Lyon 1, Lyon, F-69626, France; CNRS, UMR5256, IRCELYON, Institut de recherches sur la catalyse et l'environnement de Lyon, Villeurbanne, F-69626, France. E-mail: christian.george@ircelyon.univ-lyon1.fr

Different works were focused on achieving the removal of NO_x from air by means of de-polluting surfaces containing TiO_2.[4,7,12–23] However, recent studies showed that UV-illuminated surfaces of pure TiO_2 aerosols can reduce NO_2 to HONO, together with the production of H_2O_2.[24,25] Besides the important impact of nitrous acid (HONO) as a free radical source in the atmosphere,[26] there are several mechanisms by which HONO may be harmful to health. Firstly, HONO is an acid, which may damage mucous membranes and surfaces of the respiratory tract. Secondly, in the reaction of HONO with amino groups of the nucleotides, the double helix of the DNA can be cross-linked[27–31] leading to mutagenic properties. In addition, in the reaction of HONO with amines, both in the atmosphere but also *in vivo*, nitrosamines are formed[32–35] which show carcinogenic and mutagenic properties.[36,37] Langridge *et al.* have just reported the formation of nitrous acid on a self-cleaning window glass coated by TiO_2.[38] In addition, the photoenhanced NO_2 uptake for real mineral dusts with HONO production was assigned to the chemistry occurring on the TiO_2.[39,40] In this process, nitrate anions are formed as a consequence of the photocatalytic oxidation of NO_2 on UV-illuminated TiO_2 surfaces.[16,24,41–44] Most of these studies argue that nitrate is the innocuous final product of the photocatalytic NO_x removal process. However, the photochemistry of nitrate doped mineral dust samples containing TiO_2 was proved to be a potential renoxification process of the atmosphere.[45] In addition, the photochemistry of adsorbed nitrate on aluminium oxide has been proved to give different yields of NO, NO_2 and N_2O according to the presence of water and molecular oxygen.[46,47]

In this study, we investigated the reactivity of irradiated TiO_2/SiO_2 films with different TiO_2 contents as proxies for de-polluting materials towards NO_2. The influence of the photocatalyst concentration was evaluated on the heterogeneous reaction with NO_2 using either pure N_2 or a mixture of O_2 (15%) and N_2 (85%) as carrier gases. The role of O_2 in the gas phase product distribution as well as the influence of nitrate on the reactivity of TiO_2 films were investigated. It was found that

O_2 plays a critical role in NO and HONO formation as well as on the products of the renoxification process that occurs on the TiO_2 films prepared with nitrate. A possible reaction mechanism is proposed to explain the results obtained.

Experimental

Samples

SiO_2 (Aerosil 130, Degussa) and TiO_2 powders (80% anatase, 20% rutile; Degussa P25) were used as purchased. A total mass of 2 g of TiO_2 and SiO_2 powder was dissolved in 20 ml of water. Different TiO_2 (x%)/SiO_2 films were prepared, varying the percentage between 10 and 100. This suspension was dripped uniformly into a Pyrex tube (20 cm length, 1.1 cm i.d.) and dried overnight in an oven at 100 °C. The resulting homogeneous film covered the entire inner area of the tube and was uniform in thickness.[48]

Flow reactor

The uptake experiments were conducted in a horizontal cylindrical coated-wall flow tube reactor made of Pyrex. The Pyrex tube containing the TiO_2/SiO_2 film was placed in the reactor, which was surrounded by 3 fluorescent lamps (OSRAM Sylvania TLD15W/08) with a continuous emission in the 340–420 nm range with a total irradiance of 1.5×10^{15} photons cm^2 s^{-1}. The spectral irradiance for the UV lamps reaching the inner surface of the reactor and its uniformity has been quantified using two methods as described by Jammoul *et al.*[49] NO_2 was introduced in the flow tube by means of a movable injector with radius 0.3 cm. Synthetic air as well as pure nitrogen were used as carrier gases with a total flow rate of 200 sccm in the flow tube reactor, ensuring a laminar regime. The NO_2 and NO concentrations were measured at the reactor exit as a function of the injector position along the tube. This position determined the exposure time of the film surface towards the gas. A THERMO 42C chemiluminescent analyzer was used for NO and NO_2 detection. The latter is based on the reaction between NO and O_3, which produces a characteristic luminescence with an intensity that is linearly proportional to the NO concentration. NO_2 is transformed into NO by means of a molybdenum converter in order to be measured with the chemiluminescent reaction. As HONO is detected by the instrument as NO_2, a denuder tube (9 cm × 0.95 cm i.d.) containing a mixture of K_2CO_3/Na_2CO_3 (Fluka) was introduced between the exit of the flow cell reactor and the detector. The denuder was either bypassed, leading to the detection of NO and NO_2 together with HONO; or it was switched into the sample line along the experiment, so that only NO and NO_2 species were measured after HONO removal from the gas stream. Therefore, HONO concentration was obtained as the difference of the detector signal without and with the carbonate denuder in the sampling line.[50]

Gas phase NO_2 concentration used in the experiments was fixed at 150 ppbv (3.8×10^{12} molecules cm^{-3}). The experiments were conducted at 298 ± 1 K by circulating temperature-controlled water through the outer jacket of the flow tube reactor and were performed under atmospheric pressure and 30% relative humidity. The temperature of the gas streams and the humidity were measured by using an SP UFT75 sensor (Partners BV). All gases were taken directly from cylinders without further purification prior to use. High purity synthetic air (99.999%), N_2 (99.0%) and NO_2 (1 ppmv in N_2; 99.0%) were purchased from Air Liquide. The gas flows were monitored before entering the reactor by mass flow controllers (Brooks).

Periodical calibrations of the NO_2 from the bottle were performed using the carbonate denuder. Only 3% of the total NO_2 (and possible contaminants) was trapped in the denuder. This value was then considered in the calculation of the uptake coefficients and product yields.

NO_2 photodissociates with unit quantum yield in the wavelength region emitted by the lamps (340–420 nm), but its loss in the gas phase is negligible for the residence time of 6 s used in our experiments. An estimation of the photolysis rate constant, $J = 4.75 \times 10^{-4}$ s^{-1} gives rise to a loss of 0.3% of the total NO_2 (g). Control experiments were performed to confirm the chemical inactivity of the Pyrex flow tube surfaces, and to evaluate the contribution of NO_2 photolysis. The empty tube (with no film) was filled with NO_2 and exposed to light. NO_2 photodissociation and loss at the Pyrex surface were negligible (below 3% of the total NO_2 loss) in comparison to the NO_2 loss observed in the presence of the TiO_2/SiO_2 film.

Uptake coefficient

The kinetic behaviour of the heterogeneous reaction between NO_2 and TiO_2/SiO_2 films under irradiation can be well described by assuming a pseudo first-order reaction with respect to the gas-phase NO_2 concentration. The derived first-order rate constant, k_{obs}, is related to the geometric uptake coefficient (γ_g) by:

$$\frac{d}{dt}\ln\frac{C_0}{C_i} = k_{obs} = \frac{\gamma_g \langle c_{NO_2}\rangle}{2r_{tube}} \quad (1)$$

where r_{tube}, γ_g, t, and $\langle c_{NO_2}\rangle$ are the flow-tube radius (0.547 cm), the geometric uptake coefficient, the exposure time, and the NO_2 average molecular velocity, respectively. C_0 is the NO_2 concentration when there is no contact between the film and the reagent; whereas C_i is the trace gas concentration when the contact with NO_2 is allowed. The uptake coefficient is defined as the fraction of effective collisions between a gas phase reagent and a reactive surface that lead to the loss of the gas phase reagent due to chemical reaction. γ_g is a mass dependent parameter for these substrates as diffusion and reaction of the trace gas take place at the internal surface of the films.[42] For that reason, a mass-independent uptake was derived by taking into account the entire BET surface area of the TiO_2/SiO_2 films.[39,51]

All experiments have been duplicated. The errors related to replicates are smaller than those associated with the variables involved in the calculation of γ.

Eqn (1) does not contemplate possible diffusion limitations caused by the formation of a radial concentration gradient in the gas phase, which would occur if the loss at the surface is too fast to be recovered with the reagent supply. As a consequence, the uptake coefficient was calculated by using

the Cooney-Kim-Davis (CKD) method,[52] which takes into account axial and lateral diffusion combined with a first order loss at the inner surface of a cylindrical tube under laminar flow conditions. An implementation of this method has been previously used.[53] The diffusion coefficient, D, was calculated using the formula proposed by Fuller *et al.*[54]

Results and discussions

Fig. 1 illustrates the behaviour of TiO_2 (10%)/SiO_2 films exposed to a continuous flow of 150 ppbv of NO_2 in the dark and under irradiation for a fixed length of the flow tube. Fig. 1a and b show the results obtained in pure N_2 and in the mixture of O_2 and N_2, respectively. An NO_2 concentration of 150 ppbv was chosen for these studies because it is representative of NO_2 concentrations found during intense photochemical pollution events in urban environments.[24,55] In addition, it allowed varying the TiO_2 content from 10 to 100% (as the observed rate is slower at higher gas phase concentrations). Once a constant initial NO_2 concentration was established, the injector was withdrawn to a certain distance to expose some fraction of the film to NO_2, indicated in the top of the figure with a black bar. The NO_2 was allowed to stabilize until it reached a plateau, returning to its initial concentration. The uptake in the dark was more important in absence of O_2 in the carrier gas for all residence times and for films with 10% and 100% of TiO_2. This behaviour may be related to the competition between NO_2 and O_2 for the adsorption sites on the film surface. When the lamps were turned on, a strong decrease of the NO_2 signal was observed (it must be remembered that without the alkaline denuder this signal corresponds to the sum of the NO_2 and HONO species) highlighting a light induced effective uptake on these surfaces introduced by a fast chemical reaction. The production of HONO was then verified under both conditions by passing the sample line through an alkaline denuder which trapped acidic species before detection. NO was produced both in absence and presence of O_2 in the carrier gas, the latter being in agreement with previous results.[44] When the lamps were turned off and the injector was moved forward to its original position, the NO_2 concentration returned to the initial value. Fig. 1 clearly shows that the NO_2 uptake on the samples, as well as the NO and HONO formation, were considerably enhanced under irradiation, both in the presence and absence of molecular oxygen in the carrier gas for films with 10 wt% TiO_2. The HONO yield was higher in presence of O_2 whereas the NO formation was favoured in the absence of O_2 (see Table 1).

The analytical procedure used here is not specific to HONO as the alkaline trap inserted periodically in front of the NO_x analyzer would trap any acidic gases. Therefore, only indirect detection of the produced HONO was made here by means of a NO/NO_x chemiluminescence detector, in combination with a sodium carbonate denuder tube for removing HONO from the gas stream. However, a direct HONO detection was made by using the HONO specific LOPAP device (long path absorption photometer) in a previous study on TiO_2 surfaces.[39] This product identification has also been independently confirmed by other studies also involving TiO_2 surfaces and different analytical devices.[25,38] We are therefore highly confident that the gaseous species escaping these surfaces is HONO (nitric acid would be trapped much more efficiently on the surface).

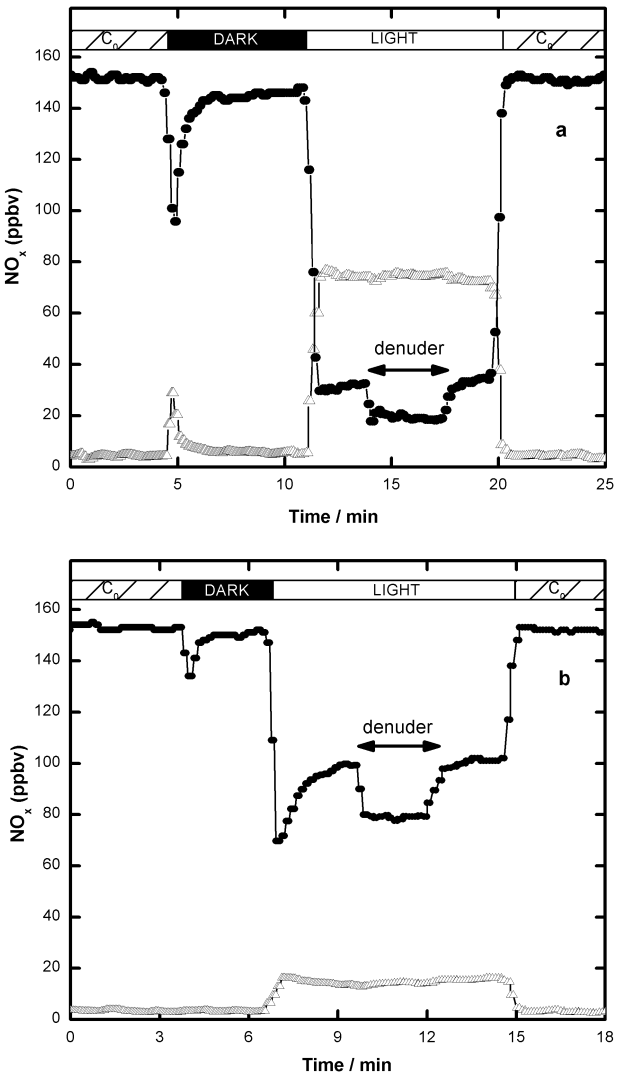

Fig. 1 NO_2 loss under irradiation of a TiO_2 (10%)/SiO_2 film when (a) only N_2 was used as carrier gas, and (b) when the O_2 (15%)/N_2 (85%) mixture was used as carrier gas. (●): NO_2 signal; (△): NO signal. The dashed bars correspond to the initial concentration of NO_2 which is not in contact with the film. The black and the white bars indicate the contact time between the NO_2 flow and a certain length of the film in the dark and under irradiation, respectively. The inclusion of the denuder into the sample line is indicated in the figure (see Experimental).

Regarding the heterogeneous reaction on irradiated 100% TiO_2 films, NO was only detected in absence of O_2 whereas HONO was mainly formed when O_2 was present in the carrier gas (Table 1). Indeed, the uptake coefficients (γ_{BET}) obtained for the NO_2 loss under irradiation were highly influenced by the presence of O_2, being one order of magnitude higher in pure N_2 for 100 wt% TiO_2 and two orders higher for the film prepared with 10 wt% TiO_2. This result suggests a competition between O_2 and NO_2 for scavenging the electrons at the surface of the photocatalyst.

The effect of the TiO_2 content on the NO_2 loss was determined for illuminated TiO_2/SiO_2 films (Fig. 2). As

Table 1 Effect of the carrier on the uptake coefficients, HONO and NO yields when exposing the films to 150 ppbv of NO_2. Errors are 2σ precision

Carrier	TiO_2 (*x*%)/SiO_2	γ_{BET}	HONO (%)	NO (%)
N_2	10	$(2.0 \pm 0.6) \times 10^{-7}$	8 ± 2	50 ± 10
O_2 (15%)/N_2 (85%)	10	$(2.2 \pm 0.8) \times 10^{-9}$	14 ± 4	26 ± 8
N_2	100	$(1.5 \pm 0.4) \times 10^{-6}$	3 ± 1	71 ± 8
O_2 (15%)/N_2 (85%)	100	$(1.1 \pm 0.2) \times 10^{-7}$	12 ± 4	—

expected, the uptake coefficients increased with increasing TiO_2 content in the films, which *a priori* would indicate that the higher the content of TiO_2 at the surface, the more efficient it should be as a de-polluting material.[4] As shown in Table 2 HONO was produced for all TiO_2 concentrations tested under irradiation, while NO was produced only on films containing between 10 and 55% of TiO_2. Furthermore, the HONO + NO yields on the different TiO_2/SiO_2 films were always lower than 100%. This result may be explained by the formation of nitrate during the heterogeneous reaction between TiO_2 and NO_2 under irradiation.[16,24,41–44] Rodriguez *et al.*[56] have proved by photoemission data and DF (density functional) calculations that surface NO_3 is formed through the disproportionation of NO_2 on Ti sites.

The influences of humidity and photon flux were reported previously[39] and were not repeated here as the high content of TiO_2 does not allow the use of a wide range of irradiance in our particular experimental set up in order to prevent the kinetics from being limited by the rate of gas phase diffusion, conditions in which heterogeneous kinetics cannot be measured.

After exposure to NO_2 under irradiation the films were flushed by a constant flow of synthetic air or pure N_2 (depending on the carrier gas used in each case) in order to promote molecule desorption from the surface. Once no further traces of NO and NO_2 were observed, lamps were turned on again and emission of nitrogen containing species from the surface was observed. Fig. 3 shows the formation of NO and NO_2 under irradiation for both carrier gases.

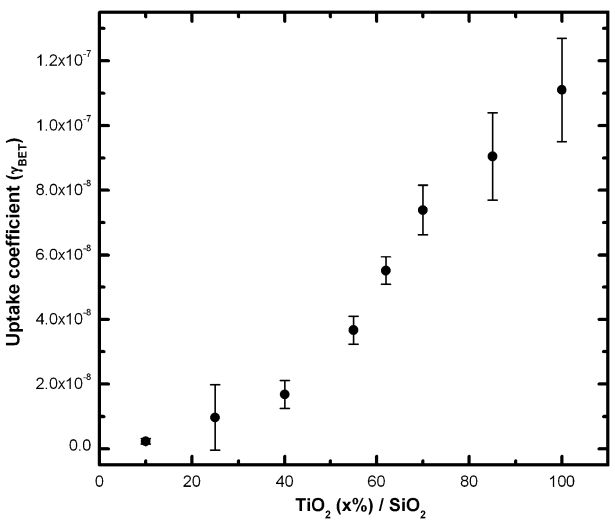

Fig. 2 Effect of TiO_2 content on the uptake coefficient when the films were exposed to 155 ppbv of gas phase NO_2 under irradiation using O_2 (15%) and N_2 (85%) as carrier. Error bars are 2σ precision.

Table 2 Effect of the TiO_2 content on the gas phase product yields when exposing the films to 150 ppbv of NO_2 under irradiation using O_2 (15%) and N_2 (85%) as carrier. Errors are 2σ precision

TiO_2 (*x*%)/SiO_2	HONO (%)	NO (%)
10	14 ± 4	26 ± 8
25	35 ± 2	16 ± 4
40	28 ± 7	42 ± 9
55	36 ± 20	49 ± 20
62	11 ± 5	3 ± 1
70	10 ± 6	2 ± 1
85	27 ± 7	—
100	12 ± 4	—

In agreement with the results presented in Fig. 1, NO was the major product in pure nitrogen (Fig. 3a). However, not only was NO_2 the major product when air was used as carrier gas, but also the production of another volatile compound was observed when passing the effluent flow through the carbonate denuder (Fig. 3b). This product was observed for films which had previously been exposed to NO_2 under illumination and contained between 40 and 100% TiO_2, and it was not observed when N_2 was used as carrier gas. We hypothesise that the signal observed when switching the carbonate denuder into the sample line may be due to N_2O formation, as previously observed by Rubasinghege and Grassian on aluminium oxide particle surfaces containing adsorbed nitrate.[46] While this is speculative, as our analytical system is not specific nor sensitive to N_2O, our results clearly suggest that nitrate ions produced during the heterogeneous reaction of NO_2 and illuminated TiO_2 films may be involved in a renoxification process (*i.e.* production of NO_x from reservoir compounds believed to be unreactive, such as the nitrate anions) as previously discussed by Ndour *et al.* for mineral dusts containing TiO_2.[45] The yield of NO (as shown in Fig. 3a) from an irradiated surface, previously exposed to 150 ppbv of NO_2 in N_2, is 20% of the nitrate produced on this surface and the yield of NO_2 is *ca.* 4%. In other words, 20–25% of nitrate anions deposited on these surfaces may be reprocessed into gaseous NO_x.

The proposed mechanism for the obtained gas phase products, which is consistent with that reported by Ohko *et al.*[44] is the following:

$$TiO_2 + h\nu \rightarrow h^+_{vb} + e^-_{cb} \quad (2)$$

$$H_2O + h^+_{vb} \rightarrow H^+ + HO^\bullet \quad (3)$$

$$NO_2 + e^- \rightarrow NO_2^- \quad (4)$$

$$NO_2 + HO^\bullet \rightarrow HNO_3 \quad (5)$$

$$NO_2^- + H^+ \rightleftarrows HONO \quad (6)$$

$$NO_2^- + h\nu \rightarrow NO + O^- \quad (7)$$

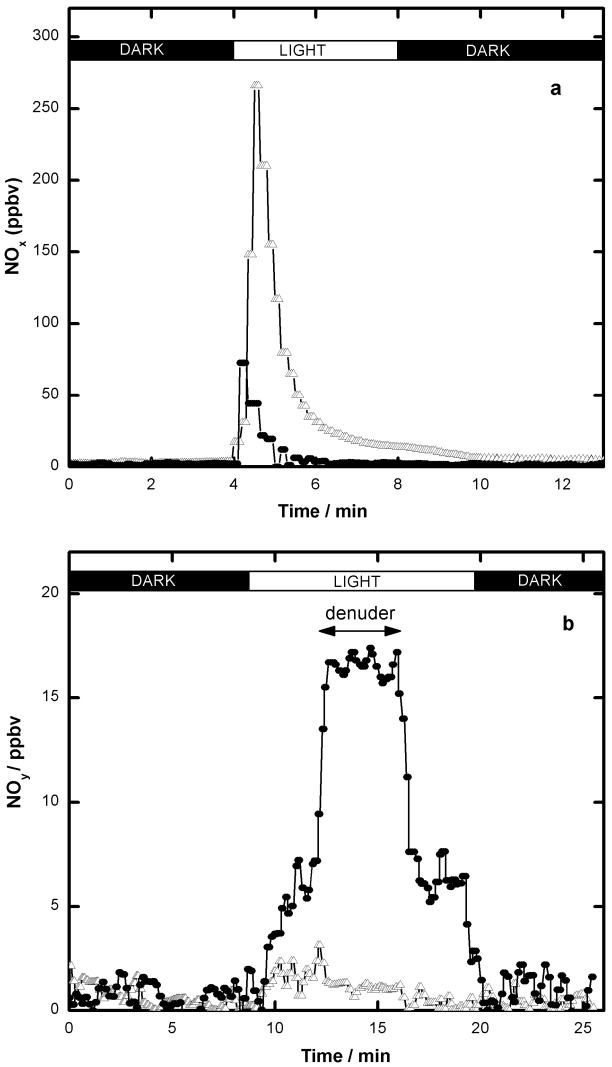

Fig. 3 Effect of light on pure TiO_2 films which were previously exposed to NO_2 and light using (a): N_2 as carrier gas; and (b): synthetic air as carrier gas. The black and the white bars indicate the contact time between the carrier flow and the total length of the film in the dark and under irradiation, respectively. The inclusion of the denuder into the sample line is indicated in the figure. (●): NO_2 signal; (△): NO signal.

In the presence of molecular oxygen, there is an electron transfer to O_2 that acts as the primary electron acceptor, leading to oxygen activated species[8,57,58] which can participate in the previous mechanism as follows:

$$O_2 + e^- \rightarrow O_2^{\bullet -} \quad (8)$$

$$NO_2 + O_2^{\bullet -} \rightarrow NO_2^{\bullet -} + O_2 \quad (9)$$

$$H^+ + O_2^{\bullet -} \rightarrow HO_2^{\bullet} \quad (10)$$

$$HO_2^{\bullet} + NO \rightarrow NO_2 + HO^{\bullet} \quad (11)$$

These pathways explain the higher HONO yield and the lower NO yield obtained from the heterogeneous reaction between NO_2 and illuminated TiO_2 films when O_2 is present in the carrier gas. The production of $HO_2^{\bullet}$ by reaction (10) leads to the formation of H_2O_2, which has been observed by Beaumont *et al.*[24] Indeed, no H_2O_2 is detected in absence of O_2.[8] Gerischer and Heller[59] have suggested that electron transfer to O_2 may be the rate-limiting step in semiconductor photocatalysis. Hirakawa *et al.* have proved that $O_2^{\bullet -}$ participates in the decomposition of alcohols.[60]

A second set of experiments was performed to verify the role of nitrate anions in the renoxification process, using TiO_2 films prepared with 50 wt% of KNO_3. Again, the role of molecular oxygen in the carrier gas was investigated. Fig. 4a shows that NO was the major product when pure N_2 was used as carrier gas, in agreement with the results from Fig. 3a, while NO_2 and HONO were the main products in the presence of the carrier gas with O_2. Similarly, Schuttlefield *et al.*[47] observed high NO_2 and low NO emission during the renoxification process of nitrate adsorbed on alumina surfaces in an atmosphere with oxygen. Rubasinghege and Grassian[46] suggested that oxygen vacancy sites may play a role in the photochemical process of adsorbed nitrate or on the chemistry of the photoproducts, as these sites may be binding sites for molecular O_2. Fig. 4 also shows that NO release in pure N_2 is faster than the release of NO_2 in air, which is also in agreement with the results shown in Fig. 3. This difference can also be explained considering the affinity of O_2 for the adsorption sites of TiO_2. Control experiments were carried out to determine whether nitrate photolysis was involved in the release of NO, HONO and NO_2. None of these products were observed on films without TiO_2; indeed irradiation of a SiO_2/KNO_3 50 wt% and KNO_3 film did not lead to any NO_y release, at least over our limit of detection. These control experiments indicate that nitrate photolysis was a negligible pathway in our experiments, in contrast to the mechanism proposed by Grassian and co-workers[46,47] on adsorbed nitrate on aluminium oxide particles. The proposed mechanism for the renoxification process has already been discussed by Ndour *et al.*[45] for dust samples irradiated in pure N_2.

$$NO_3^- + h_{vb}^+ \rightarrow NO_3^{\bullet} \quad (12)$$

$$NO_3^{\bullet} + h\nu \rightarrow NO + O_2 \quad (13)$$

$$NO_3^{\bullet} + h\nu \rightarrow NO_2 + O^{\bullet} \quad (14)$$

The ability of a TiO_2/KNO_3 50 wt% film to remove NO_2 ($\sim$170 ppbv) under irradiation in an atmosphere with O_2 was also investigated. Fig. 5 shows that the TiO_2 surface is active towards NO_2 removal with HONO production under irradiation even when the film was prepared with a high content of nitrate. The observed NO_2 loss ($\sim$35 ppbv) approximately balances the release of NO_2 ($\sim$50 ppbv) from the renoxification process (Fig. 4b) and the NO_2 loss ($\sim$85 ppbv) observed on a film of TiO_2 (55%)/SiO_2, shown in Fig. 6. These results are in disagreement with previous studies,[43,44] where the photocatalyst was deactivated by the nitrate ions produced during the photooxidation. But these previous investigations did not consider the renoxification process occurring at the surface of the TiO_2 film when nitrate ions are deposited. This result suggests that HONO would not only be produced during the heterogeneous

reaction between NO_2 and a clean irradiated TiO_2 surface, but also on a TiO_2 surface containing nitrate. As a consequence, special care should be taken in the development of an environmentally friendly material which contains TiO_2 in its matrix as undesired products may also be formed under irradiation.

Conclusions

The present paper suggests that de-polluting materials based on TiO_2 may contribute to the production of HONO, NO and NO_2. The NO, HONO and nitrate are produced as a consequence of the uptake of NO_2 on UV-illuminated TiO_2 films.

The presence of O_2 in the carrier gas modifies the NO and HONO production yields in the heterogeneous reaction between NO_2 and TiO_2. NO was the major product in an O_2 free atmosphere, whereas HONO formation was favoured in the presence of O_2. This difference can be elucidated by the presence of activated oxygen species, such as $O_2^{\bullet -}$ and $HO_2^{\bullet}$, in the reaction mechanisms.

A renoxification pathway that involves the photochemistry of the NO_3 radical leads to the release of NO, NO_2 and of HONO from the TiO_2 surface. The gas phase product distribution depends on the carrier gas used, in agreement with the uptake experiments.

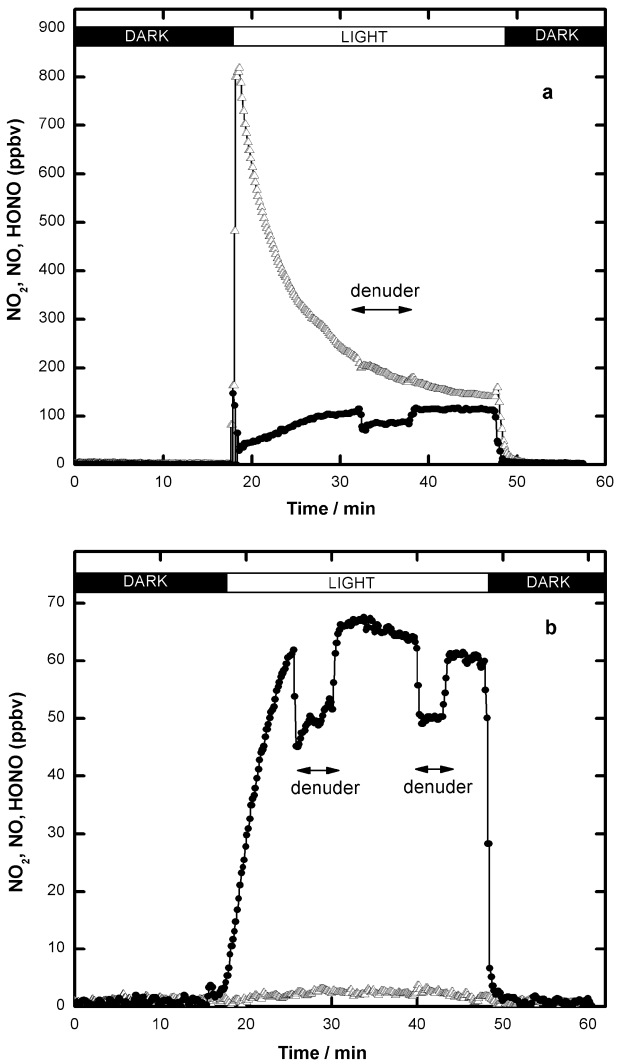

Fig. 4 Effect of light on a TiO_2/KNO_3 50 wt% film when (a): it is exposed to a flow of N_2; and (b): it is exposed to a flow of synthetic air. The black and the white bars indicate the contact time between the carrier flow and the film in the dark and under irradiation, respectively. The inclusion of the denuder into the sample line is indicated in the figure. (●): NO_2 signal; (△): NO signal.

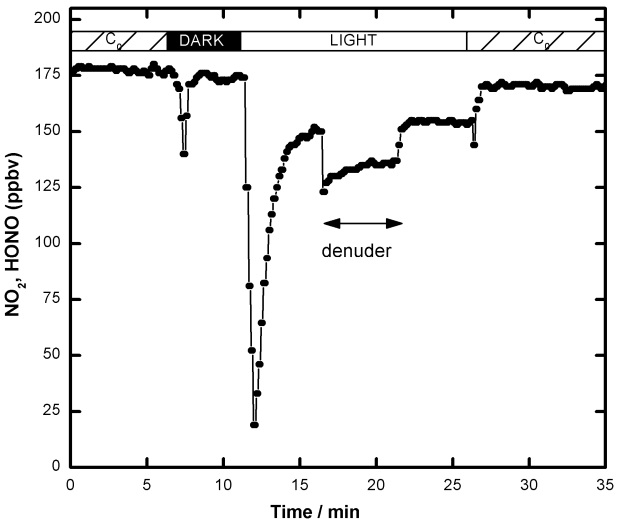

Fig. 5 Effect of the NO_2 exposure under irradiation after the renoxification process on the same film of TiO_2/KNO_3 50 wt% presented in Fig. 4b. The dashed bars correspond to the initial concentration of NO_2 which is not in contact with the film. The black and the white bars indicate the contact time between the NO_2 flow and the film in the dark and under irradiation, respectively. (●): NO_2 signal.

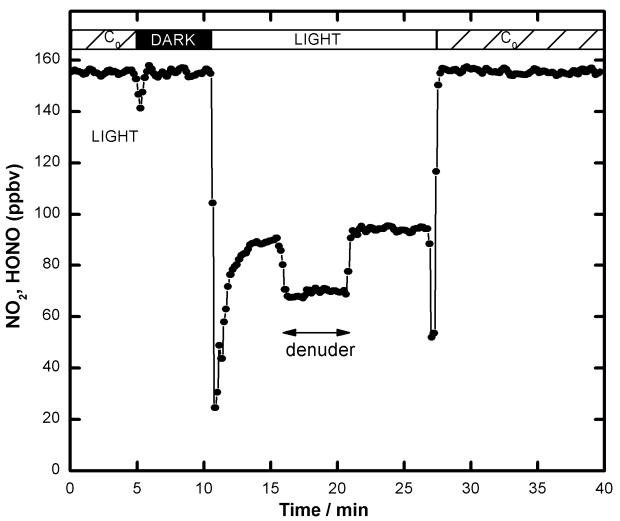

Fig. 6 Effect of the NO_2 exposure under irradiation on a film of TiO_2 (55%)/SiO_2. The dashed bars correspond to the initial concentration of NO_2 which is not in contact with the film. The black and the white bars indicate the contact time between the NO_2 flow and the film in the dark and under irradiation, respectively. (●): NO_2 signal.

The renoxification process carried out on the surface of TiO_2 containing materials questions their use for the improvement of air quality as it has been recently suggested. In the real atmosphere, different organic and inorganic compounds may compete for the TiO_2 sites and may be involved in different reactions, which may modify the product yields presented in this work. These processes need to be considered further as potentially important in polluted urban atmospheres, taking into account the role of buildings, roads and natural materials in promoting heterogeneous reactions.[61]

Consequently, these results suggest the need for field measurements of NO_y levels in locations where self-cleaning materials are already being used, as well as the need for further basic investigation into these new materials.

Acknowledgements

We acknowledge the French Ministry for Environment and Ademe for support from the Primequal2 grant PhotoBat and the ANR for support from the NeoRad grant.

References

1 B. Brunekreef and S. T. Holgate, *Lancet*, 2002, **360**, 1233–1242.
2 B. J. Finlayson-Pitts and J. N. Pitts, Jr., *Science*, 1997, **276**, 1045–1051.
3 http://europa.eu/legislation_summaries/internal_market/single_market_for_goods/motor_vehicles/interactions_industry_policies/l28186_en.htm.
4 A. Beeldens and D. Van Gemert, *RILEM Proceedings pro041 (RILEM International Symposium on Environment-Conscious Materials and Systems for Sustainable Development)*, 2004, 353–359.
5 F. Dehn, D. Bahnemann and B. Bilger, *RILEM Proceedings pro041 (RILEM International Symposium on Environment-Conscious Materials and Systems for Sustainable Development)*, 2004, 347–352.
6 N. Kashino, *RILEM Proceedings pro041 (RILEM International Symposium on Environment-Conscious Materials and Systems for Sustainable Development)*, 2004, 3–17.
7 F. Vallée, B. Ruot, L. Bonafous, L. Guillot, N. Pimpinelli, L. Cassar, A. Strini, E. Mapelli, L. Schiavi, C. Gobin, H. André, N. Moussiopoulos, A. Papadopoulos, J. Bartzis, T. Maggos, R. McIntyre, C. Lehaut-Burnouf, A. Henrichsen, P. Laugesen, R. Amadelli, D. Kotzias and P. Pichat, *RILEM Proceedings pro041 (RILEM International Symposium on Environment-Conscious Materials and Systems for Sustainable Development)*, 2004, 337–346.
8 M. R. Hoffmann, S. T. Martin, W. Y. Choi and D. W. Bahnemann, *Chem. Rev.*, 1995, **95**, 69–96.
9 I. P. Parkin and R. G. Palgrave, *J. Mater. Chem.*, 2005, **15**, 1689–1695.
10 J. Kasanen, M. Suvanto and T. T. Pakkanen, *J. Appl. Polym. Sci.*, 2009, **111**, 2597–2606.
11 K. Motohashi, T. Inukai and K. Toshimasa, *RILEM Proceedings pro041 (RILEM International Symposium on Environment-Conscious Materials and Systems for Sustainable Development)*, 2004, 27–34.
12 C. H. Ao, S. C. Lee, C. L. Mak and L. Y. Chan, *Appl. Catal., B*, 2003, **42**, 119–129.
13 S. Devahasdin, C. Fan, K. Li and D. H. Chen, *J. Photochem. Photobiol., A*, 2003, **156**, 161–170.
14 L. Frazer, *Environ. Health Perspect.*, 2001, **109**, A174–A177.
15 H. Hamada, K. Komure, R. Takahashi and T. Yamaji, *RILEM Proceedings pro041 (RILEM International Symposium on Environment-Conscious Materials and Systems for Sustainable Development)*, 2004, 361–366.
16 T. Ibusuki and K. Takeuchi, *J. Mol. Catal.*, 1994, **88**, 93–102.
17 T. Maggos, J. G. Bartzis, P. Leva and D. Kotzias, *Appl. Phys. A: Mater. Sci. Process.*, 2007, **89**, 81–84.
18 T. Maggos, J. G. Bartzis, M. Liakou and C. Gobin, *J. Hazard. Mater.*, 2007, **146**, 668–673.
19 T. Maggos, A. Plassais, J. G. Bartzis, C. Vasilakos, N. Moussiopoulos and L. Bonafous, *Environ. Monit. Assess.*, 2008, **136**, 35–44.
20 N. Moussiopoulos, P. Barmpas, I. Ossanlis and J. Bartzis, *Environ. Model. Assess.*, 2008, **13**, 357–368.
21 F. Nakajima and I. Hamada, *Catal. Today*, 1996, **29**, 109–115.
22 H. Wang, Z. Wu, W. Zhao and B. Guan, *Chemosphere*, 2007, **66**, 185–190.
23 H. Yumoto, S. Matsudo and K. Akashi, *Vacuum*, 2002, **65**, 509–514.
24 S. K. Beaumont, R. J. Gustafsson and R. M. Lambert, *ChemPhysChem*, 2009, **10**, 331–333.
25 R. J. Gustafsson, A. Orlov, P. T. Griffiths, R. A. Cox and R. M. Lambert, *Chem. Commun.*, 2006, 3936–3938.
26 J. Kleffmann, *ChemPhysChem*, 2007, **8**, 1137–1144.
27 E. F. Becker Jr, Bk Zimmerma and E. P. Geiduschek, *J. Mol. Biol.*, 1964, **8**, 377–391.
28 E. A. Harwood, P. B. Hopkins and S. T. Sigurdsson, *J. Org. Chem.*, 2000, **65**, 2959–2964.
29 J. J. Kirchner and P. B. Hopkins, *J. Am. Chem. Soc.*, 1991, **113**, 4681–4682.
30 J. J. Kirchner, S. T. Sigurdsson and P. B. Hopkins, *J. Am. Chem. Soc.*, 1992, **114**, 4021–4027.
31 R. Shapiro, S. Dubelman, A. M. Feinberg, P. F. Crain and J. A. McCloskey, *J. Am. Chem. Soc.*, 1977, **99**, 302–303.
32 D. Grosjean, *J. Air Waste Manage. Assoc.*, 1991, **41**, 306–311.
33 P. L. Hanst, J. W. Spence and M. Miller, *Environ. Sci. Technol.*, 1977, **11**, 403–405.
34 J. N. Pitts, *Environ. Health Perspect.*, 1983, **47**, 115–140.
35 J. N. Pitts, D. Grosjean, K. Vancauwenberghe, J. P. Schmid and D. R. Fitz, *Environ. Sci. Technol.*, 1978, **12**, 946–953.
36 O. G. Fahmy and M. J. Fahmy, *Cancer Res*, 1976, **36**, 5404–5412.
37 D. Shapley, *Science*, 1976, **191**, 268–270.
38 J. M. Langridge, R. J. Gustafsson, P. T. Griffiths, R. A. Cox, R. M. Lambert and R. L. Jones, *Atmos. Environ.*, 2009, **43**, 5128–5131.
39 M. Ndour, B. D'Anna, C. George, O. Ka, Y. Balkanski, J. Kleffmann, K. Stemmler and M. Ammann, *Geophys. Res. Lett.*, 2008, **35**, L05812.
40 M. Ndour, M. Nicolas, B. D'Anna, O. Ka and C. George, *Phys. Chem. Chem. Phys.*, 2009, **11**, 1312–1319.
41 J. S. Dalton, P. A. Janes, N. G. Jones, J. A. Nicholson, K. R. Hallam and G. C. Allen, *Environ. Pollut.*, 2002, **120**, 415–422.
42 V. H. Grassian, *Int. Rev. Phys. Chem.*, 2001, **20**, 467–548.
43 Y. M. Lin, Y. H. Tseng, J. H. Huang, C. C. Chao, C. C. Chen and I. Wang, *Environ. Sci. Technol.*, 2006, **40**, 1616–1621.
44 Y. Ohko, Y. Nakamura, A. Fukuda, S. Matsuzawa and K. Takeuchi, *J. Phys. Chem. C*, 2008, **112**, 10502–10508.
45 M. Ndour, P. Conchon, B. D'Anna, O. Ka and C. George, *Geophys. Res. Lett.*, 2009, **36**, L05816.
46 G. Rubasinghege and V. H. Grassian, *J. Phys. Chem. A*, 2009, **113**, 7818–7825.
47 J. Schuttlefield, G. Rubasinghege, M. El-Maazawi, J. Bone and V. H. Grassian, *J. Am. Chem. Soc.*, 2008, **130**, 12210–12211.
48 M. Sassine, L. Burel, B. D'Anna and C. George, *Atmos. Environ.*, DOI: 10.1016/j.atmosenv.2009.07.044.
49 A. Jammoul, S. Gligorovski, C. George and B. D'Anna, *J. Phys. Chem. A*, 2008, **112**, 1268–1276.
50 L. Gutzwiller, C. George, E. Rossler and M. Ammann, *J. Phys. Chem. A*, 2002, **106**, 12045–12050.
51 M. Nicolas, M. Ndour, O. Ka, B. D'Anna and C. George, *Environ. Sci. Technol.*, 2009, **43**, 7437–7442.
52 D. O. Cooney, S. S. Kim and E. J. Davis, *Chem. Eng. Sci.*, 1974, **29**, 1731–1738.
53 M. Ammann, E. Roessler, R. Strekowski and C. George, *Phys. Chem. Chem. Phys.*, 2005, **7**, 2513–2518.
54 E. N. Fuller, K. Ensley and J. C. Giddings, *J. Phys. Chem.*, 1969, **73**, 3679–3685.

55 S. K. Pandey, K.-H. Kim, S.-Y. Chung, S. J. Cho, M. Y. Kim and Z.-H. Shon, *Atmos. Environ*., 2008, **42**, 607–622.
56 J. A. Rodriguez, T. Jirsak, G. Liu, J. Hrbek, J. Dvorak and A. Maiti, *J. Am. Chem. Soc*., 2001, **123**, 9597–9605.
57 K. Hashimoto, K. Wasada, N. Toukai, H. Kominami and Y. Kera, *J. Photochem. Photobiol., A*, 2000, **136**, 103–109.
58 J. Shang, Y. Du and Z. Xu, *Chemosphere*, 2002, **46**, 93–99.
59 H. Gerischer and A. Heller, *J. Electrochem. Soc*., 1992, **139**, 113–118.
60 T. Hirakawa, T. Daimon, M. Kitazawa, N. Ohguri, C. Koga, N. Negishi, S. Matsuzawa and Y. Nosaka, *J. Photochem. Photobiol., A*, 2007, **190**, 58–68.
61 A. M. Rivera-Figueroa, A. L. Sumner and B. J. Finlayson-Pitts, *Environ. Sci. Technol*., 2003, **37**, 548–554.

J|A|C|S COMMUNICATIONS

Published on Web 05/28/2010

Ozone Formation from Illuminated Titanium Dioxide Surfaces

María Eugenia Monge,[†] Christian George,*[,†] Barbara D'Anna,[†] Jean-François Doussin,[‡] Adla Jammoul,[‡] Junnan Wang,[‡] Grégory Eyglunent,[§] Géraldine Solignac,[§] Véronique Daële,[§] and Abdelwahid Mellouki[§]

IRCELYON, Institut de recherches sur la catalyse et l'environnement de Lyon, CNRS UMR 5256, Université Lyon 1. 2, Av. Albert Einstein, F-69626 Villeurbanne Cedex, France, LISA Laboratoire interuniversitaire des systèmes atmosphériques, Universités Paris Est Créteil et Paris Diderot, CNRS UMR 7583, 61 Av. du Général de Gaulle, 94010 Créteil, France, and ICARE Institut de Combustion, Aérothermique, Réactivité et Environnement, CNRS - UPR3021, 1C, Av. de la recherche scientifique, 45071 Orléans Cedex 02, France

Received March 5, 2010; E-mail: christian.george@ircelyon.univ-lyon1.fr

Titanium dioxide, TiO_2, is used in a variety of remediation processes due to its favorable physical, chemical, and photocatalytic properties.[1–3] Possible removal of NO_x by means of depolluting surfaces containing TiO_2 has been previously reported.[4–13] Other recent studies[14–17] show that this process converts NO_2 to HNO_2 producing also H_2O_2[18] and nitrate anions[9,18–22] which are then involved in a renoxification process.[23] Similarly, the photochemistry of adsorbed nitrate on aluminum oxide has been proven to produce NO, NO_2, and N_2O.[24,25] However, the formation of non-nitrogen containing products in the NO_x reaction with illuminated TiO_2 surfaces has been largely unexplored.

Herein, we report the first investigation of such products from TiO_2 coated glasses exposed to nitrogen oxides (NO_x) in two simulation chambers using both artificial and natural illumination and from irradiated TiO_2/KNO_3 films using a coated-wall flow tube reactor. These studies demonstrate the formation of ozone from TiO_2 surfaces containing nitrate anions.

Chamber simulation experiments are performed in two different chambers (i) a stainless steel Multiphase Atmospheric Experimental Simulation Chamber (CESAM) equipped with artificial irradiation and (ii) a Teflon outdoor chamber (see Supporting Information for experimental details and Figures S1−S3). After introduction of synthetic air and NO into the CESAM chamber, the concentrations of NO, NO_2, HNO_2, and O_3 are monitored in the dark for 1 h. Then, the artificial illumination is turned on, and the gas mixture is again monitored for typically 90 min.

A similar procedure is adopted for the experiments conducted in the Teflon outdoor chamber using natural illumination. In the latter, known amounts of NO and NO_2 are injected after flushing with dry purified air, and the NO, NO_2, and O_3 concentrations are monitored for 30 min in the dark. The reactor is then exposed to natural light, and the gas mixture composition is monitored for 4 h. The results for a TiO_2 coated glass and for a standard glass studied with the CESAM and the outdoor chamber are displayed in Figures 1 and 2, respectively. An example of the NO, NO_2, and O_3 concentration−time profiles obtained in the absence of any surface using the outdoor chamber is shown in Figure S4.

Despite the different time scales and the chamber characteristics (i.e., irradiation type and chambers building material) the observed trace gas evolution is similar over a TiO_2 coated glass. In agreement with previous studies,[26] NO uptake on the TiO_2 coated glass is enhanced under irradiation increasing with time in both experiments. The NO_2 concentration profile exhibits a maximum under illumination, suggesting that it is formed from NO photocatalytic oxidation and then converted into HNO_3 and HNO_2 at the surface.[14–17,22] At the same time, a significant accumulation of ozone is observed. In agreement with previous studies,[14–16] HNO_2 production is enhanced under irradiation in the presence of TiO_2 (Figure 1). However, when a standard glass (i.e., TiO_2 free) is analyzed in both chambers, no O_3 formation is observed (Figures 1b and 2b). The NO_2 and NO concentration−time profiles obtained in the absence of glass samples are similar to those observed in the presence of standard glasses, with no evidence of any light effect (Figures 2b and S4). These results clearly suggest that O_3 formation cannot be explained by the gas phase chemistry occurring in the chambers. The differences between the O_3 profiles from the blank experiments and the coated glass indicate that TiO_2 should be involved in the reaction mechanism leading to O_3 formation probably via new surface reactions.

To further investigate the reason for O_3 production, a second type of experiment has been carried out using a flow tube reactor, where only air or N_2 was present in the gas phase. It is well-known

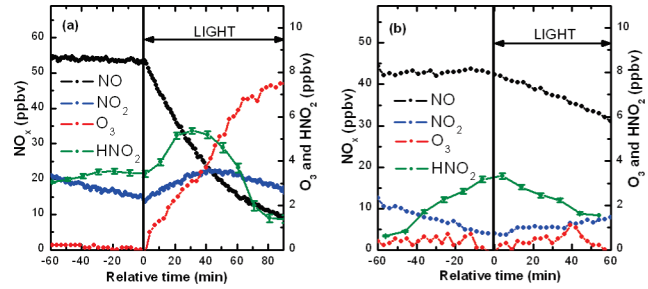

Figure 1. NO, NO_2, HNO_2, and O_3 concentration profiles over (a) a TiO_2 coated glass and (b) a standard glass (TiO_2 free) in the CESAM chamber. The vertical line indicates the start of the irradiation.

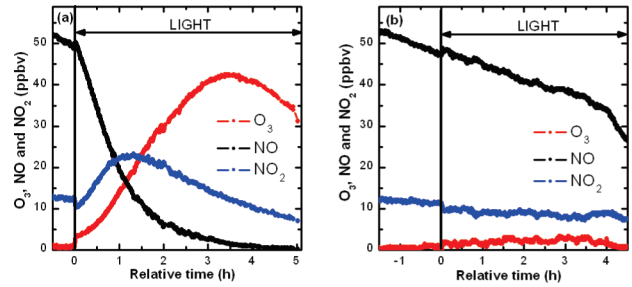

Figure 2. NO, NO_2, and O_3 profiles under natural irradiation in the presence of (a) a TiO_2 coated glass and (b) a standard glass in the outdoor chamber. The vertical line indicates the start of the irradiation.

[†] IRCELYON, Université Lyon 1.
[‡] LISA, Universités Paris Est Créteil et Paris Diderot.
[§] ICARE.

10.1021/ja1018755

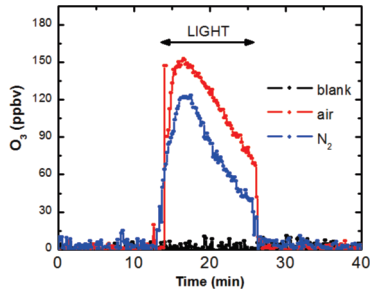

Figure 3. Effect of light (8 near-UV emitting lamps in the 300−420 nm wavelength range) on a TiO_2/KNO_3 (50% w/w) film using synthetic air and pure N_2 as carriers. The same blank signal was given by an empty tube and by a tube with a KNO_3 deposit using both carriers.

that nitrate anions are formed as a consequence of the photocatalytic oxidation of NO_2 on UV-illuminated TiO_2 surfaces.[9,18−22] Therefore a film of TiO_2/KNO_3 50% w/w has been exposed to near-UV irradiation (300−420 nm) using synthetic air or pure N_2 as a carrier gas with 30% RH under atmospheric pressure and at $T = 298 \pm 1$ K (Figure 3).

As described previously, a renoxification process occurs on illuminated TiO_2 films mixed with nitrate.[23] In contrast with the mechanism proposed by Grassian and co-workers[24,25] for the photochemistry of adsorbed nitrate on alumina, control experiments indicate that nitrate photolysis is negligible under the experimental conditions (Figure 3). NO_3^- reduction by conduction band electrons may lead to the release of NO_x, but it does not explain O_3 formation.[27] An alternative surface chemical pathway would involve the photochemistry of the NO_3 radical, produced by a charge exchange reaction between the nitrate anion and the solid surface, followed by photolysis of the radical (occurring at longer wavelength compared to the anion)[23] according to

$$TiO_2 + h\nu \rightarrow h^+_{vb} + e^-_{cb} \quad (1)$$

$$O_2 + e^-_{cb} \rightarrow O_2^{\bullet -} \quad (2)$$

$$NO_3^- + h^+_{vb} \rightarrow NO_3^\bullet \quad (3)$$

$$NO_3^\bullet + h\nu \rightarrow NO_2 + O^\bullet \quad (4)$$

$$NO_3^\bullet + h\nu \rightarrow NO + O_2 \quad (5)$$

$$O^\bullet + O_2 + M \rightarrow O_3 + M \quad (6)$$

TiO_2 band gap excitation (eq 1) produces excited-state conduction-band electrons and valence-band holes, which can then react with electron acceptors and electron donors adsorbed onto the semiconductor surface. According to Marcus theory,[28] the activation energy ($\Delta G^{\neq}$) for the oxidation of nitrate anion into nitrate radical by the holes can be calculated by eq 8:

$$\Delta G^{\neq} = \frac{\lambda}{4}\left(1 - \frac{F(E_{vb} - E_{NO_3^\bullet/NO_3^-})}{\lambda}\right)^2 \quad (7)$$

where λ is the reorganization energy necessary to transform the nuclear configurations in the reactant and the solvent to those on the product state; $E_{vb} = 3.25 - 0.06$pH V (vs NHE) is the valence band edge potential[29] in TiO_2 and $E = 2.3 - 2.5$ V (vs NHE) is the redox potential range for the $NO_3^\bullet/NO_3^-$ couple.[30,31] Assuming that the reorganization energy accounts for only the solvent contribution and that it is approximately 0.5 eV,[29] then $\Delta G^{\neq}$ approaches zero, so h^+_{vb} can directly oxidize NO_3^-.

New surface reactions occurring on illuminated TiO_2 surfaces are discussed, for the first time, as a possible source of O_3. Although O_3 has been recently proven to decompose on illuminated TiO_2 surfaces,[32] its formation is observed when TiO_2 treated surfaces are exposed to NO_x under illumination. Charge transfer reactions are taking place at the surface of TiO_2, producing nitrate radicals from the corresponding anions. The photochemistry of the NO_3 radical leads to O_3 formation, enhancing the oxidizing power of these surfaces.

Acknowledgment. We acknowledge the French Ministry for Environment and Ademe for support from the Primequal2 grant PhotoBat and the ANR for support from the NeoRad grant. This work was also supported by the European Community within the 7th Framework Program, through the EUROCHAMP-2 project.

Supporting Information Available: Experimental procedures, Figures S1−S4, and references. This material is available free of charge via the Internet at http://pubs.acs.org.

References

(1) Fujishima, A.; Rao, T. N.; Tryk, D. A. *J. Photochem. Photobiol. C* **2000**, *1*, 1–21.
(2) Malato, S.; Fernández-Ibáñez, P.; Maldonado, M. I.; Blanco, J.; Gernjak, W. *Catal. Today* **2009**, *147*, 1–59.
(3) Parkin, I. P.; Palgrave, R. G. *J. Mater. Chem.* **2005**, *15*, 1689–1695.
(4) Ao, C. H.; Lee, S. C.; Mak, C. L.; Chan, L. Y. *Appl. Catal., B* **2003**, *42*, 119–129.
(5) Beeldens, A.; Van Gemert, D. *RILEM Proceedings pro041 (RILEM International Symposium on Environment-Conscious Materials and Systems for Sustainable Development)* **2004**, 353–359.
(6) Devahasdin, S.; Fan, C.; Li, K.; Chen, D. H. *J. Photochem. Photobiol. A* **2003**, *156*, 161–170.
(7) Frazer, L. *Health Perspect.* **2001**, *109*, A174–A177.
(8) Ibusuki, T.; Takeuchi, K. *J. Mol. Catal.* **1994**, *88*, 93–102.
(9) Maggos, T.; Plassais, A.; Bartzis, J. G.; Vasilakos, C.; Moussiopoulos, N.; Bonafous, L. *Environ. Monit. Assess.* **2008**, *136*, 35–44.
(10) Moussiopoulos, N.; Barmpas, P.; Ossanlis, I.; Bartzis, J. *Environ. Model. Assess.* **2008**, *13*, 357–368.
(11) Nakajima, F.; Hamada, I. *Catal. Today* **1996**, *29*, 109–115.
(12) Vallée, F.; et al. *RILEM Proceedings pro041 (RILEM International Symposium on Environment-Conscious Materials and Systems for Sustainable Development)* **2004**, 337–346.
(13) Wang, H.; Wu, Z.; Zhao, W.; Guan, B. *Chemosphere* **2007**, *66*, 185–190.
(14) Gustafsson, R. J.; Orlov, A.; Griffiths, P. T.; Cox, R. A.; Lambert, R. M. *Chem. Commun.* **2006**, 3936–3938.
(15) Langridge, J. M.; Gustafsson, R. J.; Griffiths, P. T.; Cox, R. A.; Lambert, R. M.; Jones, R. L. *Atmos. Environ.* **2009**, *43*, 5128–5131.
(16) Ndour, M.; D'Anna, B.; George, C.; Ka, O.; Balkanski, Y.; Kleffmann, J.; Stemmler, K.; Ammann, M. *Geophys. Res. Lett.* **2008**, *35*, L05812.
(17) Ndour, M.; Nicolas, M.; D'Anna, B.; Ka, O.; George, C. *Phys. Chem. Chem. Phys.* **2009**, *11*, 1312–1319.
(18) Beaumont, S. K.; Gustafsson, R. J.; Lambert, R. M. *ChemPhysChem* **2009**, *10*, 331–333.
(19) Dalton, J. S.; Janes, P. A.; Jones, N. G.; Nicholson, J. A.; Hallam, K. R.; Allen, G. C. *Environ. Pollut.* **2002**, *120*, 415–422.
(20) Grassian, V. H. *Int. Rev. Phys. Chem.* **2001**, *20*, 467–548.
(21) Lin, Y. M.; Tseng, Y. H.; Huang, J. H.; Chao, C. C.; Chen, C. C.; Wang, I. *Environ. Sci. Technol.* **2006**, *40*, 1616–1621.
(22) Ohko, Y.; Nakamura, Y.; Fukuda, A.; Matsuzawa, S.; Takeuchi, K. *J. Phys. Chem. C* **2008**, *112*, 10502–10508.
(23) Ndour, M.; Conchon, P.; D'Anna, B.; Ka, O.; George, C. *Geophys. Res. Lett.* **2009**, *36*, L05816.
(24) Rubasinghege, G.; Grassian, V. H. *J. Phys. Chem. A* **2009**, *113*, 7818–7825.
(25) Schuttlefield, J.; Rubasinghege, G.; El-Maazawi, M.; Bone, J.; Grassian, V. H. *J. Am. Chem. Soc.* **2008**, *130*, 12210–12211.
(26) Lim, T. H.; Jeong, S. M.; Kim, S. D.; Gyenis, J. *J. Photochem. Photobiol. A* **2000**, *134*, 209–217.
(27) Ravishankara, A. R.; Longfellow, C. A. *Phys. Chem. Chem. Phys.* **1999**, *1*, 5433–5441.
(28) Marcus, R. A. *Rev. Mod. Phys.* **1993**, *65*, 599–610.
(29) Grela, M. A.; Brusa, M. A.; Colussi, A. J. *J. Phys. Chem. B* **1999**, *103*, 6400–6402.
(30) Thomas, K.; Volz-Thomas, A.; Mihelcic, D.; Smit, H. G. J.; Kley, D. *J. Atmos. Chem.* **1998**, *29*, 17–43.
(31) Venkatachalapathy, B.; Ramamurthy, P. *J. Photochem. Photobiol., A* **1996**, *93*, 1–5.
(32) Nicolas, M.; Ndour, M.; Ka, O.; D'Anna, B.; George, C. *Environ. Sci. Technol.* **2009**, *43*, 7437–7442.

JA1018755